DEVELOPMENT OF MICROWAVE SPECTROSCOPIC RESONANT SENSOR FOR APPLICATION IN EDIBLE AND WASTE OIL VERIFICATION

SALIFU BOGOSOGO OSMAN

A thesis submitted in partial fulfilment of the requirement of the Liverpool John Moores University for the degree of Doctor of Philosophy

January 2020

ABSTRACT

This work is a contribution and value addition to edible oil verification and the waste oil recovery process. It comprised the development of a sensing technique that will primarily enable the ability to probe different oils and establish their differences for authentication, and in addition test free fatty acid levels in waste cooking oils, and methanol levels in the oil recovery process. It does so in real time and in a cost-effective manner. Various techniques that have been applied to this so far, have proven to be either too sophisticated and require specialised trained persons to employ, or are too expensive for large scale implementation.

Microwave spectroscopy is used to develop the sensor. Experiments were carried out using samples of different edible oils to probe and verify their differences, as a result each sample presented different signal spectra. To verify the authenticity of extra virgin olive oil diluted with sunflower oil, samples were mixed in different percentages of concentration, 0 to 50% of sunflower in extra virgin olive oil. The results were regressed and attained a value of correlation coefficient of 0.9739. To probe the levels of free fatty acid and methanol in oil, 0 to 17.5% of free fatty acid was mixed with vegetable oil, and the results attained a regression coefficient value of 0.9942. Levels 0 to 17.5% of free fatty acid were mixed with methanol and attained 0.9944. Levels 30 to 50% mixed with methanol gave a value of 0.9846.

Using the results of the experiments, computer aided models were evolved, which were simulated using COMSOL Multiphysics software. The simulated work produced results that were favourably comparable to the laboratory experiments. The design of a new conceptual industry model of the microwave spectroscopic resonant sensor for waste oil recovery was carried out and scaled out of the laboratory model. Finally, the industry model with a Q-factor of 7856 and resonant frequency of 2.3562 GHz was attained as a result.

ACKNOWLEDGEMENT

First, I would like to show appreciation to Prof Hassan Al Nageim for initiating the thought of the programme to me on his visit to Ghana, as an adjunct Dean of the school of Engineering, without whom this dream could not have been possible. To Prof Ahmed Al-Shamma'a for facilitating the programme. To Prof Sylvester Achio for his contribution in providing the reference when I needed it.

My gratitude goes to Dr Nurudeen Iddrisu, Head of Forestry Commission London Office, for being there for me when I most needed it and making my stay in the UK less stressful. I appreciate his support given to me all these years.

To my supervision team, Prof Andrew Shaw, Dr Jeffrey Cullen and Dr Muhammad Ateeq for their help, guidance and advice. I herein acknowledge the invaluable time dedicated in helping shape my research work. To Prof David Phipps for his help and contribution to the research in the chemistry, without which I would be found wanting. To Dr Monserrat Ortoneda Pedrola for her help and advice in the use of the chemical lab. My thanks go to Dr Alex Mason and Dr Olga Korostynska for their contribution. To all my mates in Henry Cotton and Byrom Street, words cannot describe how much I enjoyed their company throughout the period.

My thanks go to all the supporting staff of the faculty, without their contribution none of this would have been possible. Special thanks to Elizabeth Hoare for her support over all the years. For those I have not mentioned, because the list is so long, thank you everyone for making this dream come true.

TABLE OF CONTENTS

LIST OF TABLES

LIST OF FIGURES

LIST OF ABREVIATIONS

AC	Alternating Current
ANOVA	Analysis of Variance
BEST	Built Environment and Sustainable Technology
C	Carbon
CPM	Cavity Perturbation Method
DC	Direct Current
DF	Degrees of freedom
EC	European Community
EHF	Extremely High Frequency
ELSD	Evaporative Light Scattering Detector
EVOO	Extra Virgin Olive Oil
F	F-Statistic
FAM	FFA in Methanol
FCC	Fluidic Catalytic Cracking
FFA	Free Fatty Acid
FFOO	Fruity Flavour Olive Oil
FO	FFA in Oil
FTIR	Fourier Transforms Infrared Spectroscopy
GC	Gas Chromatography
GHz	Gigahertz
GNO	Groundnut Oil
GPC	Gel Permeation Chromatography
GSO	Grape Seed Oil

HP	Hewlett Packard
HPLC	High Performance Liquid Chromatography
IDE	Interdigitated Electrode
IR	Infra-Red
KNN	K-Nearest Neighbour
LC	Liquid Chromatography
LDA	Linear Discriminant Analysis
LLL	Trilinilein
MFOO	Medium Flavour Olive Oil
M	Methanol
ME	Methyl Ester
MFOO	Medium Flavoured Olive Oil
MHz	Megahertz
MO	Methanol in Oil
MTO	Methanol to Olefins
MTP	Methanol to Propylene
MS	Mean square
NIR	Near Infra-Red
NMR	Nuclear Magnetic Resonance
OOO	Triolein
PCA	Principal Component Analysis
PDH	Propane Dehydrogenation
PLS	Partial Least Squares
PML	Perfectly Matched Layers
PPP	Tripalmitin

PVC	Polyvinyl Chloride
RF	Radio Frequency
ROO	Mixed Refined Olive Oil
SFC	Supercritical Fluid Chromatography
SFO	Sunflower Oil
SHF	Super High Frequency
SS	Sum of squares
SVM	Support Vector Machine
TOS	Toxic Oil Syndrome
TR	Transmission/Reflection line
UHF	Ultra-High Frequency
VNA	Vector Network Analyser
VO	Vegetable Oil
WCO	Waste Cooking Oil

LIST OF SYMBOLS

^{1}H   Hydrogen-1

^{13}C   Carbon-13

A   Amperes

A_{CH2} Integration value of the methylene protons

A_{ME} Integration value of the protons of the methyl ester

α Attenuation constant

B Magnetic field

∂ Flux

β Phase constant

C Capacitance

C   Percentages of conversion triglycerides

c Speed of light

D   Dissipation factor

μ_r Relative permeability

P_{nm} Value of the Bessel function for the TE or TM modes of a circular waveguide

ρ Conductivity, charge density

E_i Incident energy

E_r Reflected energy

ε	Complex permittivity
ε'	Dielectric constant
ε''	Dielectric loss factor
ε_r	Relative dielectric constant of the medium
ε_R^*	Complex permittivity in relation to air
μ_R^*	Complex permeability in relation to air
f	Frequency of oscillation
$F_{o\ (3dB)}$	3dB frequency bandwidth for empty cavity
$F_{s\ (3dB)}$	3dB frequency bandwidth for filled cavity
G	Conductance
g	Grams
H	Height of Cavity
k	Constitutive relations
L	Inductance
l	Lecher wire
mg	Milligram
mm	Millimetre
n	Normal point out of the domain
nm	Nanometre

λc	Cutoff Wavelength
λco	Cutoff wavelength of empty waveguide
λg	Guide Wavelength
μ	Permeability of material
μ_o	Magnetic constant
μ_r	Relative permeability of material
λ	Wavelength
σ	Electric conductivity of material
δ_p	Penetration depth
γ	Propagation
t	Time
S	Siemens
s	Seconds
S_{11}, S_{22}	Scattering parameters for reflected wave
S_{12}, S_{21}	Scattering parameters for transmitted wave
$tan\ \delta$	Tangent loss, dissipation factor
TE	Transient electric
TM	Transient magnetic
R	Resistance

Γ	Reflection coefficient
f	frequency of oscillation
ω	Angular frequency
Q	Quality Factor
Q_o	Quality factor for empty container
Q_s	Quality factor for filled container
R	Resistance
G	Conductance
Ω	Ohms
V	Voltage, volts
V_c	Volume of cavity
V_s	volume of test material
v	Velocity of propagation in free space
W	Watts
Y	Admittance
Y_0	Characteristic admittance
Z	Impedance
Z_0	Characteristic impedance
Z_{TE}	Waveguide impedance for TE

Z_{TM} Waveguide impedance for TM

1.0   INTRODUCTION

In the food industry, there has been the need to identify edible oils with the aim to establish their nature and most importantly to authenticate that they are fit for purpose. With the growing amount of food oil production, mainly from plant and seed sources, the ability to differentiate one kind from the other becomes essential, mainly for the purpose of quality control (Maggio et al., 2010). Many different approaches have been examined in this respect and have achieved some degree of success (Rohman and Man, 2010).

In the waste oil industry, the recovery of used oils from domestic sources and restaurants, is not only beneficial to the environment, but also a source of income for many as demonstrated in Badday et al., (2012). The ability to monitor this process is of importance, not only for the purpose of quality assurance but also to improve the efficacy of the final product (Demirbas, 2009).

In this work, an effort is being made to address the problem regarding the verification of edible and waste oil products, by researching into a technology that would facilitate the solution in real time and in a cost-effective manner. Microwave technology is found to provide versatile solutions to this sort of problem as indicated in many sources, including Korostynska et al., (2013). In this work the microwave sensor was able to show different spectra of some edible oils but not as far as to establish authentication (i.e. show concentration of contaminant oils). The work being undertaken in this thesis shows the difference between oils including the level of contamination.

Work carried out herein considered the use of a number of established tools, which include sensors and network analysers, in the lab environment to test numerous samples of oil sourced from the supermarkets. In addition to this, samples made of oil, free fatty acids and methanol were used to create a scenario similar to the waste oil recovery process. The samples were

measured principally for the process of determination of their dielectric properties. The tests were then subjected to quantifiable evaluation and verification and the results were used for the development of the microwave spectroscopic resonant sensor to be utilised for edible and waste oil verification.

1.1   Background

The verification of oil products of any sort has always proven challenging to researchers. Due to their nature, i.e. texture, colour, and volatility, etc, they tend to prove difficult in handling and measuring. The ability to find a suitable technique that has the potential to handle these products in real time and in a cost-effective manner is the essence of this work, which is to allow for the verification of oil types and to measure levels of free fatty acids and methanol in the waste oil recovery process.

The ability to differentiate edible oils apart from the labels they carry is mostly impossible by human senses. This allowed for possible adulteration of the products for the purpose of cheating and/or profiteering. Any technique that can make this happen in real time and in a cost-effective way will not only be solving a problem of oil adulteration but also contribute in a good way to enhancement of knowledge.

Edible oils also contribute to environmental issues, especially after use. These oils if not disposed of properly would run into sewers, and consequently into soils and rivers, therefore causing damage to the environment. One way of solving this problem is by what is termed as waste oil recovery. A process where the used oils are collected and processed into other forms of oils and/or fuels. This process does not only help to clean the environment from hazardous oils but also to bring back to life different kind of oils and it is linked to cleaner energy.

One of the main products of this waste oil recovery is biodiesel, which is known to be less harmful to the environment. A major part of this work includes the design of a sensor that is able to measure levels of some samples in the waste oil recovery process.

Currently the industry depends on sophisticated techniques, like gas chromatography (GC), high performance liquid chromatography (HPLC), nuclear magnetic resonance (NMR) and other related methods, as shown in the following literature review section (1.2), which rely on highly qualified and specialised personnel to operate. Moreover, the systems are, more often, located in dedicated laboratories, where samples have to be carried for tests and the results relayed back later for action to be taken, therefore lacking the real time effect and incurring handling and time penalties.

The work carried out here is the development of a sensor system based on microwave spectroscopy, capable of probing in real time, edible oils to establish their difference and identity leading to authenticity. To cater for the environment, it is linked to the after use of the oils, with the development of a sensor system that can monitor, in real time, the waste oil recovery process.

1.2   Literature Review

1.2.1   Vegetable oil verification

Vegetable oil production comes with numerous challenges. The toxic oil syndrome (TOS) epidemic (Europe, 1992) has long been known to have resulted from the consumption of rapeseed oil denatured with aniline, which caused mass food poisoning and many deaths in Spain during the 1980s. It necessitated researchers to look into the production of food oils in general and methods of their verification (Maggio et al., 2010).

The importance of olive oil as an economically important product with a fine aroma and a pleasant taste, and which is internationally appreciated for its nutritional value and health benefits was demonstrated in Aparicio and Harwood, (2013). Costs of virgin olive oil are high when compared to other commonly used vegetable oils, making it prone to adulteration with less expensive oils in order to increase profits. Firestone (2001) in his paper, 'Assuring the integrity of olive oil products', suggested that the most common adulterants found in virgin olive oil are seed oils, such as sunflower, soy, corn and rapeseed oils as well as nut oils, including hazelnut and peanut oils.

Several commercial categories of olive oil are legally defined by the European Community Council of Regulation (EC, 2001), which are marketed with different prices. Thus, there is also the possibility of mixing less expensive commercial categories such as refined olive oil and pomace oil with the highest quality product, extra virgin olive oil, for economic reasons. Detection of these two types of adulteration is often complicated with no single test available that can accomplish the task, especially when oils with chemical compositions similar to extra virgin olive oil are employed (Chester et al., 2007).

CHAPTER I INTRODUCTION

Detection and determination of the adulteration of extra virgin olive oil are not simple tasks; efforts to detect and determine adulteration traditionally demand monitoring of several organic compounds to establish a comparison with typical unadulterated oils in order to identify any change of composition that could be related to adulteration as demonstrated in Mueller, (2014).

Complementary analytical techniques devoid of such problems, could act as supporting tools for currently used methods, being very helpful to improve the detection of extra virgin olive oil adulteration. Among them, calorimetric techniques and the application of differential scanning calorimetry to make evident the adulteration of extra virgin olive oil was recently reported (Baranska, 2013). On the other hand, nuclear magnetic resonance coupled with multivariate statistical analysis was applied to detect extra virgin olive oil adulteration with lampante olive oil and refined olive oil (Ramesh, 2016).

Spectrofluorimetric methods also emerged as an alternative; excitation–emission fluorescence spectroscopy was reported for detecting adulteration of olive oil (Grimm et al., 2007). Fourier Transform Infrared (FTIR) has been also used to detect olive oil adulteration and freshness (Smith, 2011). The latter technique is often coupled with chemometrics methods such as principal component analysis (PCA), linear discriminant analysis (LDA), support vector machine (SVM) and K-nearest neighbour (KNN) that can be used to assign the measured spectrum to a category in a training set. In addition, quantitative chemometrics strategies have been used for analysis of complex mixtures as they enabled rapid and simultaneous determination of each component in a mixture without time-consuming separations and with minimum sample preparation (Maggio et al, 2010).

Among such methods, partial least squares (PLS) has been reported, and also a factorial multivariate calibration method, that decomposes spectral data into loadings and scores,

building the corresponding calibration models from new variables (Vinzi et al., 2010). The method, which requires analysts' compliance with Beer's Law, has been repeatedly coupled with FTIR spectroscopy and extensively used to obtain different quality parameters of edible oils (McDonald and Mossoba, 1997). Particularly, FTIR-PLS has been recently applied to the evaluation of the fatty acid composition and other quality parameters of virgin olive oil (Kiritsakis and Shahidi, 2017).

Near infrared spectroscopy (NIR), has also become popular in the analysis of vegetable oils because of its benefits, which include rapidity, directness, relative cost-effectiveness, and usually no need for sample preparation is demonstrated in (Siesler et al., 2008). In that report, NIR was used to indicate tocopherols in vegetable oils as an alternative to HPLC. Samples, similarly to liquid chromatography, were extracted with an organic solvent (in this case ethanol). The discussed technique, in connection with chemometric analysis, has also found application in the direct determination of acidity and peroxide index screening in vegetable oils (Ozaki et al., 2006)).

NIR, thanks to its low cost and short time of individual analysis, has also found application in the discovery of camellia oils adulterations with soybean oil (Singh, 2010), as well as at the differentiation and classification stages of vegetable oils (Li-Chan et al., 2011). Using mid-infrared spectroscopy, the detection limit of extra virgin olive oil adulteration was determined as 5 % for corn – sunflower binary mixture, cottonseed and rapeseed oils (Preedy and Watson, 2010).

The use of Raman's dispersion as a result of changes in polarization or the shape of the electron layout in the vibrating molecule, with the infrared radiation absorption requiring internal changes in the dipolar moment during the molecule's vibration was demonstrated in (Lewis and Edwards, 2001). Not only were oil samples analysed, but also the unsaponifiable

matter. Coupling the above-mentioned technique with a statistical analysis of the results obtained, makes it possible to determine an addition of over 8% of hazelnut oil or even 5% of sunflower, corn or soybean oil to olive oil (Weber and Merlin, 2000). Other techniques also allow for the classification as well as determination of purity and authenticity of other vegetable oils, such as corn, peanut, canola, soybean, sunflower and coconut oils (Kneipp et al., 2006).

Another important question in the analysis of oils is their oxidative stability developed from a respective method which is based on FTIR, and assumes that frequency changes in specific bonds allow for the differentiation of stages of the oxidation process and determination of the oxidation level of the analysed oil sample (Wilson and Lee, 2013). The proposed method is fast, easy and precise. Other studies to determine the influence of heating vegetable oils on the changes in oxidation levels and the emergence of trans-isomers of fatty acids were shown in Gunstone, (2004). Another study (Akoh, 2017) also determined the content of trans-isomeric fatty acids in vegetable oils, based on a method developed using the FTIR technique. They concluded that after applying two-dimensional correlation analysis, the fast and precise FTIR method for determining trans-isomers in fats and oils could compete with gas chromatography. For quantitative and qualitative determinations of trans-isomers undergoing the hydrogenation process in vegetable oils, a combination of Fourier transform and Raman spectroscopy technique was proved practical (Dijkstra et al., 2008).

Two-dimensional analysis connected with FTIR and FT-Raman was also used in order to trace the lipid oxidation process in vegetable oils (Lees, 2003). The FTIR technique enables the determination of the peroxide value. In the experiments, this method has been utilised to examine mixtures of extra virgin olive oil with sunflower adulterations from 10 to 50 percent.

Moreover, a combination of different antennas into a single system could be an option if a complex mixture of different vegetable oils needs to be precisely determined.

A new study published in Food Quality & Safety magazine, April/May 2014 demonstrated that a new form of this technique known as Supercritical Fluid Chromatography (SFC) in combination with evaporative light scattering detection (ELSD) is a valuable technique for the determination of the triglyceride composition of vegetable oils (Edwards, 2014).

Over the past fifty years, nuclear magnetic resonance spectroscopy, commonly referred to as NMR, has become the pre-eminent technique for determining the structure of organic compounds. Of all the spectroscopic methods, it is the only one for which a complete analysis and interpretation of the entire spectrum is normally expected. Although larger amounts of sample are needed for mass spectroscopy. NMR is non-destructive, and with modern instruments good data may be obtained from samples weighing less than a milligram (Keeler, 2011).

Adulteration of olive oil with poor quality hazelnut oils is a case of fraud. The main analytical challenge is that hazelnut and olive oils have a very similar chemical composition, and therefore, different NMR methodologies have been proposed (Jacobsen, 2007). The method included using mixtures of virgin olive oil with various percentages of hazelnut oil and was performed using hydrogen-1 proton nuclear magnetic (^{1}H NMR) spectroscopy. Another study using carbon-13 nuclear magnetic resonance (^{13}C NMR) has been also used for the detection of hazelnut oil in virgin olive oil (Knothe and Kenar, 2004).

An interesting method for rapid screening of olive oil adulteration with sunflower, soybean, hazelnut and peanut oils has been proposed (VIGLI et al., 2003). A high gradient diffusion NMR spectroscopy has been applied to measure diffusion coefficients of vegetable oil mixtures directly without any pre-treatment or solubilisation, to differentiate extra virgin olive

oil adulterated with 10% of sunflower or soybean oils, and with more than 30% of hazelnut oil.

There has not been a study beforehand that has demonstrated the use of microwave spectroscopy to completely verify the processes that culminate in oil identification on the one hand and also facilitate the monitoring of waste oil recovery process. However works carried out, as proposed in a study, and as part of this work, using microwave spectroscopy have shown the ability of this method to identify the differences in some vegetable oil samples (Osman et al., 2014, Osman et al., 2015). Supermarket oils were sourced of different types, namely sunflower, rapeseed, groundnut, mixed refined , medium flavoured fruity flavoured and extra virgin olive oils. Experiments were performed on these oils using an interdigitated, IDE sensor connected to a vector network analyser (VNA). As a result each oil displayed a unique signal spectra.

Additional works carried out herein and published as conference proceedings on authenticating vegetable oils, (Osman et al., 2015) using the cavity resonator connected to the VNA, saw mixtures of different oils analysed. Samples of different concentrations of sunflower oil (SFO) were used to adultrate extra virgin olive oil (EVOO) in 10, 20, 30, 40 and 50 percentages and measured using microwave. The same samples were again meassured using the HP spectrophotometer. The results were regressed and the correlation coefficient rated in the proximity of one.

1.2.2 Waste Oil Recovery Process

Some analytical methods developed for analysing mixtures containing fatty acids, esters and mono-, di- and tri-glycerides have been utilised for the trans/esterification of used oils.

Some of these are, Gas Chromatography, high performance liquid chromatography, gel permeation chromatography, ^{1}H NMR, and near infra-red (NIR) spectroscopy,

1.2.2.1 Gas Chromatography (GC)

A gas chromatographic method has been advanced for the determination of glycerol, mono-, di- and tri glycerides in vegetable oil methyl-esters. Tri-methyl-sialylation of glycerol, mono-, di-glycerides, followed by using GC. A capillary coated with a thin film of DB-5 allows for the determination of all evaluations with a single GC run (Meher et al., 2006). Most of the reports on the use of GC for biodiesel analysis employ flame–ionisation detectors.

The use of a microwave-spectrometric detector would eliminate uncertainties about the nature of eluting materials since the spectra attained is unique to the individual compounds.

1.2.2.2 High Performance Liquid Chromatography (HPLC)

The main advantage of HPLC compared to GC is that the time of analysis is reduced and analysis can be performed in a safer environment (GC works best with high temperature hydrogen as the carrier gas which presents serious risks). HPLC allows for the detection of mono-, di, and tri-glycerides as well as methyl esters as classes of compounds. The system is useful for the study of the degree of conversion of the transesterification reaction (Monteiro et al., 2008).

In a study (Holcapek et al., 1999) a reverse phase, high performance liquid chromatography was used for the determination of compounds occurring during the production of biodiesel from rapeseed oil with various detection methods. UV detection, ELSD and atmospheric pressure chemical ionisation mass spectroscopy were utilised. However, despite this being an accurate method of analysis, it still has a time impact (typically up to 30 minutes), hence its unsuitability for real-time analysis.

1.2.2.3 Gel Permeation Chromatography (GPC)

A method for concurrent analysis of transesterification reaction products-mono-glycerides, diglycerides, triglycerides, glycerol and methyl esters was studied using gel permeation chromatography together with refractive index detector (Knothe, 2006). The samples were then placed at 20ºC pending analysis. GPC has made the quantitation of methyl esters, mono-, di- and tri-glycerides and glycerol possible.

1.2.2.4 Nuclear Magnetic Resonance (NMR)

A report on spectroscopic determination of the yield of transesterification reaction utilised ^{1}H NMR showed its progressing spectrum (Knothe, 2001). The signal due to methylene protons adjacent to the ester group in triglycerides appears at 2.3 pulses per minute and after the reaction the methoxy protons of the methyl esters appear at 3.7 pulses per minute. The authors have used the areas of the signals of methylene and methoxy protons to monitor the yield of transesterification.

The authors gave the equation:

$$C = 100 \times \left(\frac{2A_{ME}}{3A_{CH_2}} \right) \tag{1.1}$$

where C, percentage conversion of triglycerides to matching methyl ester; A_{ME}, integration value of the protons of the methyl esters; and A_{CH2}, integration value of the methylene protons.

1.2.2.5 Near Infra-Red (NIR) Spectroscopy

NIR spectroscopy has been used to monitor the transesterification reaction (Knothe, 2000). The basis for quantitation of the turnover from triglyceride feedstock to methyl ester product is the differences in the NIR spectra of these classes of compounds. Using quantitation software, it was possible to develop a method for quantifying the turnover of triglycerides to

methyl esters. The mid range IR spectra of triglycerides and methyl esters of fatty acids were almost identical and offer no possibility for distinguishing.

NIR spectra were acquired with the aid of a fibre-optic probe coupled to the spectrometer, which renders their acquisition particularly easy and time-efficient, as denoted by Knothe, (1999). While the first NIR paper used a model system to describe monitoring of transesterification and for developing quantitation methods, a second paper applied the method to a transesterification reaction in progress on a 6L scale. Here spectroscopic results were obtained not only by NIR but also by ^{1}H-NMR and NIR. The results of both spectroscopic methods, which were correlated by simple equations, were in good agreement.

1.3 Aim and Objectives

The aim of this work is to develop a sensor system to offer a real time solution to the verification, and capable of rapidly differentiating, and authenticating edible oils, as well as determining the levels of free fatty acids and methanol in the waste oil recovery process using microwave spectroscopy.

In order to realise this aim, a number of objectives for the work have been set, which include:

- Critically evaluate the state-of-the-art techniques employed in the verification of edible and waste oils. Study of processes and procedures used to verify oils for the purposes of identification and authentication and of the formation of methyl-esters using vegetable oil, free fatty acids and methanol.

- Conduct experiments to determine the feasibility of using microwave spectroscopy to detect variability in different edible oils.

- Conduct experiments to determine levels of free fatty acids and methanol in oil. This is carried out to evaluate in percentage terms the amount of free fatty acids and methanol in oil for waste oil verification.

- Conduct simulations of the microwave reactor to verify the measured dielectric parameters and create a modified computer aided simulation for the waste oil recovery industry. The sensor is scaled out of the findings of experiments and simulations.

1.4 Novelty

The novelty of this work is mainly in the development of a method for the rapid verification of edible oils, and the monitoring of the waste oil recovery process.

Currently the industry lacks a solution, which can provide rapid indication of oil authenticity, or inline non-invasive monitoring of the industrial waste oil recovery process. Those that do exist are typically intrusive /destructive in nature, meaning that, the sampling and testing of many products is not practical. In most situations, samples must be carried to dedicated laboratories for testing and therefore incurring handling and time penalties.

In this work several oils were submitted to tests to establish a unique form of verification of type and identity. The ability to identify some supermarket oils was successfully probed, including the ability to verify the authenticity of extra virgin olive oil. The waste oil recovery process was probed with the development of a sensor capable of determining the levels of free fatty acids and methanol in oil.

A unique combination of several techniques involving optical and microwave and other permutations, such as cavity perturbation and transmission/reflexion methods were utilised. Computer aided methods (COMSOL) were utilised to model and simulate the sensor.

Furthermore, the solution as proposed herein offers a real-time, cost effective and low labour alternative to current techniques.

Microwave spectroscopy, which was utilised extensively in the work offers the following features:

- Non-invasive: input and output ports can be retro-fitted to outside of the sensing area.

- Non-destructive: samples remain the same and can be reused.

- Can be used for solids, liquids, gases and suspensions.

- Can be used with different coloured samples.

- Analyses whole samples and large volumes.

- Offers real time measurements.

1.5   Contribution to Knowledge

This thesis has contributed to addressing some of the pertinent issues surrounding the verification of oils. It has added a new method for oil type identification, in which different oils from the supermarket were tested and their differences were probed. A new method of oil authentication has been demonstrated by investigating the dilution of extra virgin olive oil with sunflower oil and opening the way to solving the problem of adulteration of oils. Using mixtures of vegetable oil, free fatty acid and methanol to portray the waste oil recovery process, facilitated the use of a simpler method over the handling of proper used oils. This allowed the achievement of the process avoiding the chemometrics involved.

Physical properties of materials were determined using two methods, both of which are in the application of microwave spectroscopy. The cavity perturbation and the transmission/ reflection line methods were applied to determine the permittivity of the sample materials. This helped to address the transfer of experiments into data, necessary for the modelling and simulation work. The simulation allowed for the testing and trial of the product by merely using a computer aided software, without which things would have resorted into trial and error.

An industry model of a resonant sensor was scaled out of the lab model. A new method based on old principles was realised to achieve this. The use of Bessel functions to scale the industry model is useful and is the basis for other applications towards this practical realisation.

In all, knowledge in science and technology has seen an addition in this work. Methods of doing things, such as identifying ways of testing oils for verification and for use with other mixtures leading to the recovery of waste were proven. Mathematics, physics, computer science and engineering were applied to create a model of a sensor, the application of which will go further to enrich posterity and advance other contributions.

1.6 Overview

Chapter 1 of the thesis presents the introduction, the literature review, the aim and objectives and the novelty. In here the problem is stated, as well as a brief description of the design consideration. Also featured are the sources from which the literature is derived. The aim of the work and the objectives to fulfil it are clearly outlined, and so is the novelty, i.e. what makes the work different from others.

Chapter 2 is dedicated to the methodology employed in the work and gives detail of the methods used. Tools and components used, as well as the sample preparations are explained in detail. Equipment and instruments employed in the lab are also featured in detail.

Chapter 3 captures the background of research in which microwave technology is featured broadly. The electromagnetic field and components, as well as the theoretical background of the work have been addressed, therefore paving the way for the much more practical elements to ensue afterwards. The theory and complete formulae for the determination of the complex relative permittivity and its components of the dielectric constant and the loss factor are also featured here.

The work on the design procedure is covered in detail in chapter 4. Measures taken to arrive at the design, including the determination of the physical properties of the sample materials. The realisation of the lab cavity modelling and simulation, leading to the scaling and modelling of the industry model are all featured.

Chapter 5 contains the results and the evaluation of the results to facilitate the quantification and understanding.

Chapter 6 covers conclusions and future work. Details of conclusive remarks and underlining vital points, as well as clarifications are pointed out. Successes and achievements

have been outlined in bullet points. The chapter also features work that is being considered to

be carried out in the future to complement this one.

2.0 BACKGROUND OF RESEARCH

2.1 Introduction

This chapter is dedicated to the theory of the techniques engaged in this work. Microwave spectroscopy is featured prominently here to complement the use of this technology in realising all the experiments. Theories and applications relating to this area have been explained and expanded in detail in the following pages to put emphasis on the place it occupies in the world of science and technology. Most of the mathematical expressions used in the thesis are explained exhaustively in this chapter.

In the earlier stages of development of radio techniques only the low-end (radio waves) of the frequency spectrum was utilised because not only was there a limited number of users of these techniques, but the number of applications was also limited (Sterling, 2004). As the number of scientists and technicians became more cognisant of the field of radio, and as its applications became more extensive, the lower range of the frequency became overpopulated, resulting in conflict in the areas of transmission and reception (Jensen, 1994). To solve this problem, international conventions had to be formed to allocate usable frequencies among the multitude of national and international researchers, industrialists, commercial users, and governmental services employing them, as explained in Kizer, (2013).

As techniques and components became more sophisticated, a wider bandwidth was essential for a full utilisation of these improvements, and the obvious direction was to reach for higher frequencies in the spectrum (Zhu et al., 2010). As a result, the bandwidth requirements for sophisticated communication and radar equipment became obvious in the microwave regions (Kharkovvsky and Zoughi, 2007). This further demonstrated that the increase in frequency meant the decrease in wavelength, and with that, the geometry of the

components used in the equipment became comparable to the wavelengths they use (Finkenzeller, 2003). Transmission line theory provides a solution to these problems in the microwave technology (Ida, 2015).

Microwaves are widely used in modern technology (Bryant and Engineers, 1993). The television industry is one of the major fields. Transcontinental transmission of programme material in the microwave range using complex transmitters, relays and receivers throughout the world is an example (Gupta, 2005). Microwaves are used in national and local security applications, such as early warning radar, missile guidance systems and to control the speed of vehicles (RAO, 2015). Microwave communication networks and relay stations are used for routine multichannel communication transmissions in both local and long distance (Strobel, 2016). Air and sea navigation are much more reliable since microwave technology has been applied to that area. Satellite communication and technology is another area where microwave is widely being applied (MITRA, 2005). These are just some of the everyday uses of microwaves, not forgetting the kitchen (Sobey, 2010). The field is progressively growing very fast (White, 2016).

2.2   Electromagnetic field

An electromagnetic field is a natural field shaped by electrically charged objects. The field expands indefinitely throughout space and is the combination of electrical and magnetic fields (Marcuvitz, 1951). The electrical field is a product of stationary charges and the magnetic field of moving charges (currents). The way in which charges and currents interact is defined by Maxwell equations (Huray, 2011).

2.2.1 Microwave Spectrum

The microwave spectrum forms part of the electromagnetic spectrum (Figure 3.1). Microwaves constitute an electromagnetic wave form of radiation that have wavelengths with

a range of one meter as the longest (100 cm long) and one millimetre as the shortest (0.1 cm short); and a range of frequencies between 300 MHz and 300 GHz (Bagad, 2009). This definition broadly includes both UHF and EHF, and in literature, various other sources use different boundaries. Nonetheless, in all cases, microwave includes the entire SHF band (between 3 and 30 GHz, or 10 and 1cm) at minimum, with RF engineering often restricting the range between 1 and 100 GHz (300cm and 3 mm) (Sorrentino and Bianchi, 2010). Figure 2.2 illustrates the microwave region of the electromagnetic spectrum.
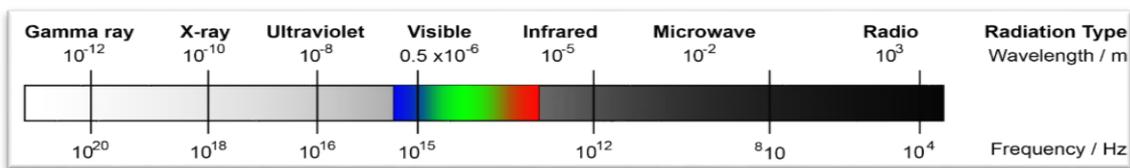
Figure 2-1: Electromagnetic wave spectrum
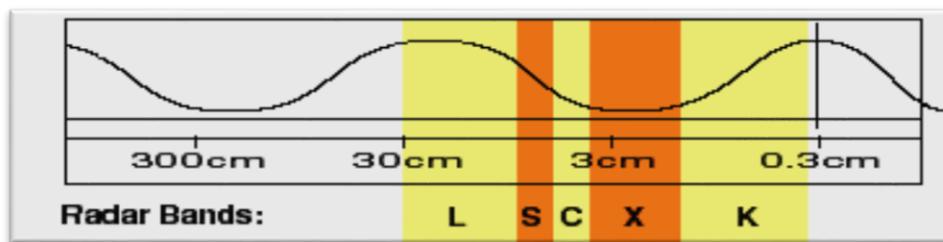
Figure 2-2: Microwave region of the electromagnetic spectrum

Microwaves can generate heat in any material composed of mobile charges in a molecular solvent or a solid material (Ringle, 1974). The solvents produce heat due to a force that rotates with the field of the molecular component and they collide with each other (Meredith, 1998).

2.3   Maxwell equations

Maxwell equations are critical for understanding electromagnetic waves (Huray, 2011). They are a set of four equations that govern the behaviour of electric and magnetic fields (Fleisch, 2008). They stipulate that the flow of an electric current will produce a magnetic field and if the current flow varies with time, then the magnetic field will give rise to an electrical field (Stewart, 2001).

The three components of Maxwell equations are Gauss's, Faraday's and Ampere's laws.

2.3.1 Gauss's law

If there exists an electric charge, somewhere, then the deviation of E at that point is non-zero, otherwise it is equal to zero. The deviation of the electrical field over any region of space is exactly equal to the net amount of charge in that region (Miller et al., 2009).

$$\nabla \times E = \frac{\rho}{\varepsilon_0} \tag{2.1}$$

where

$\nabla \times E$ = divergence of electric field

ρ = charge density

ε_0 = electric constant

The electric flux leaving is proportional to the change inside. Opposite charges attract and negative charges repel.

2.3.2 Gauss's law for magnetism

The Gauss's law for magnetism stated that the deviation in the magnetic field is zero in any volume (Miller et al., 2010), and expressed as:

$$\nabla \times B = 0 \tag{2.2}$$

where

$\nabla \cdot B$ = divergence of magnetic field

This expression supported the option that there are no magnetic monopoles and the total flux in a closed circuit is zero.

2.3.3 Faraday's law

Faraday's law states that a changing magnetic field within a loop gives rise to an induced current, which is due to a force or voltage within that circuit. Electric Current gives rise to magnetic fields. Magnetic fields around a circuit give rise to electric current. A Magnetic field changing in time gives rise to an E-field circulating around it. A circulating E-field in time gives rise to a Magnetic field changing in time (Fleisch, 2008).

$$\nabla \times E = -\frac{\partial B}{\partial t} \qquad (2.3)$$

Where

B = magnetic field

t = time

The voltage induced in a closed loop is proportional to the rate of change of the magnetic flux that the loop encloses.

2.3.4 Ampere's law

Ampere's law states that a flowing electric current gives rise to a magnetic field that encircles the current. A time-varying electric flux density gives rise to a magnetic field that circles the electric field (Stewart, 2001).

$$\nabla \times B = \mu_0 \left(J + \varepsilon_0 \frac{\partial E}{\partial t} \right) \qquad (2.4)$$

Where

μ_0 = magnetic constant

The magnetic field induced around a closed loop is proportional to the electric current plus the displacement currents that the loops enclose.

2.4   Transmission line theory

As the uses of the electromagnetic spectra increase, the equipment must be designed for much higher frequencies (Welton, 2011). As the frequency increases, the value of the components used in the network decreases (Caloz and Itoh, 2005). As the frequency of operation gets so high, the wavelength on the device or transmission system is generally comparable with its size (Rachidi and Tkachenko, 2008). Transmission line theory has been applied to analyse the behaviour of the device or transmission system (Voldman, 2005).

A transmission line is essentially a system of material boundaries forming a continuous path from one place to another and capable of directing the transmission of electromagnetic energy along this path. If there is a change in the geometry at any point, there will be an interruption in the line (Wadell, 1991).

2.4.1   Travelling waves

When a sinewave is applied to an infinitely long transmission line, the wave will propagate along the line (da Silva and Bak, 2013). The voltage wave on a uniform, lossless transmission line is always accompanied by a current wave of similar shape, and regardless of the shape, the two waves will be propagated without any change in magnitude or shape (Van Bladel, 2007). The length of the wave, λ is defined as the distance between sequential points with the same electrical phase (Fusco, 2005). The wavelength depends upon the frequency of the variation of the wave and the dielectric constant of the medium through which the wave is travelling (Pankov, 2005). Figure 2.3 shows travelling waves at three successive instants in time.
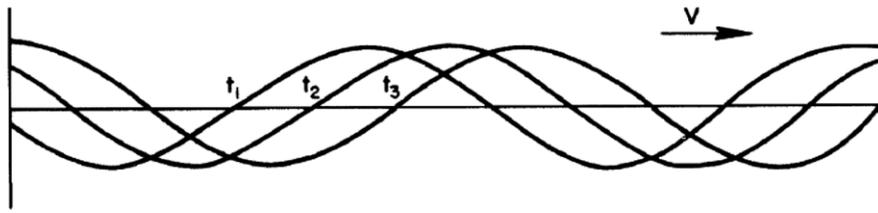
Figure 2-3: Travelling waves

The following equation shows the relationship between the factors that determine the wavelength:

$$\lambda = \frac{1}{\sqrt{\epsilon_r}} \cdot \frac{v}{f} \qquad\qquad (2.5)$$

where

v is the velocity of propagation in free space,

f is the frequency of oscillation,

ϵ_r is relative dielectric constant of the medium the wave is travelling in.

The wavelength can also be defined as the distance in which the phase changes by 2π radiance, where $2\pi \; radian = 360^o$.
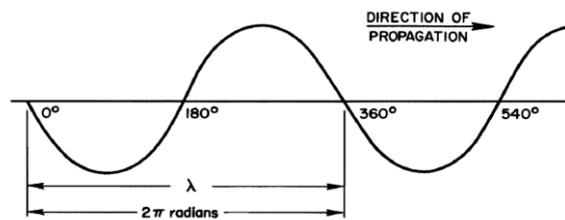
Figure 2-4: wavelength and phase change.

To comprehend fully the performance of signal propagation on a transmission line, it is not enough to understand the voltages between the conductors and the currents carried inside the conductors. If a signal is applied to an infinitely long, uniform transmission line, electromagnetic waves will be carried along its path. Voltage exists between the conductors and current flows through them. Electric and magnetic fields are formed between and around

the conductors and their behaviour and field, configurations are very important (Bewley, 1963).

2.4.2 Equivalent circuit

2.4.3 Transmission line parameters

The four components of the equivalent circuits of a uniform transmission line are divided into series and parallel groups defining the impedance and admittance of the transmission line (Bakshi, 2008). Two parameters can be divided using impedance and admittance expressions. The propagation constant is expressed as

$$\gamma = \sqrt{ZY} = \sqrt{(R + j\omega L)(G + j\omega C)} \qquad (2.6)$$

Since the square root of the product of two complex numbers is also complex, the propagation is expressed as

$$\gamma = \alpha + j\beta \qquad (2.7)$$

where

α is the attenuation constant and

β is the phase constant.

By definition, the other parameter is the characteristic impedance:

$$Z_0 = \sqrt{\frac{Z}{Y}} = \sqrt{\frac{R + j\omega L}{G + j\omega G}} \ \Omega \qquad (2.8)$$

Considering if R and G are negligible in size, that is if there is no absorptive loss on the transmission line, then

$$Z_0 = \sqrt{\frac{L}{C}} \ \Omega \qquad (2.9)$$

The characteristic impedance then becomes a real number that is independent of frequency changes (if $R = G = 0$, $j\omega$ $will$ $cancel$).

The reciprocal characteristic impedance is defined as the characteristic admittance:

$$Y_0 = \frac{1}{Z_0} \; \Omega \tag{2.10}$$

2.4.4 Reflections on transmission lines

If a signal is applied to a uniform, practically lossless transmission line and if that transmission line is terminated with an impedance unequal to the characteristic impedance of the line, that impedance will not be able to absorb all the energy, and part of the signal will be reflected (White, 2016). Figure 2.5 shows a transmission line with terminated impedance different from the characteristic impedance.
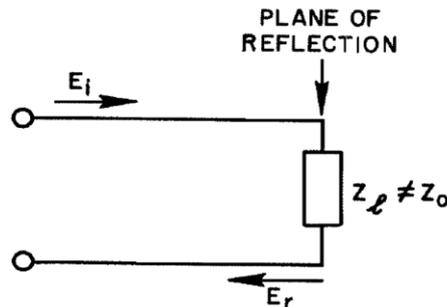
Figure 2-5: Transmission line with terminated impedance

E_i is the incident signal travelling toward the termination and E_r is the reflected signal travelling in the opposite direction. The ratio of these two voltages gives the reflective index, Γ.

$$\frac{E_r}{E_i} = \Gamma \tag{2.11}$$

The reflective index is a vector, since it has magnitude and phase information. Both the incident and the reflected waves are travelling on the same transmission line but in opposite directions. Their relative phases are dependent on the terminating impedance and the distance

from the termination to the point of measurement. The magnitude of the reflected voltage depends on how much mismatch there is in terminating impedance. That is why the reflection coefficient serves as a Figure of merit for the termination at the end of any particular transmission line (Kumar, 2003). The absolute value of the reflection coefficient is

$$\left|\frac{E_r}{E_i}\right| = |\Gamma| = \rho \tag{2.12}$$

2.4.5 Coaxial transmission lines

The preceding discussions are based on parallel wire transmissions; another name for them is Lecher wire and this has very serious limitations as far as radiation and losses are concerned. Coaxial transmission lines consist of a centre conductor with another conductor around it (Kogure et al., 2011).

To analyse the coaxial transmission line, the equivalence of parameters has to be determined: the series inductance, the series resistance the parallel capacitance and the parallel conductance. The following equation describes these parameters.

$$l = 0.4605\,\mu_r \left(\log\frac{b}{a}\right) \times 10^{-8} \tag{2.13}$$

This equation neglects the current penetration into the conductor. μ_r stands for relative permeability factor.

$$C = \frac{0.241\mathcal{E}_r}{\log\frac{b}{a}} \times 10^{-12} \tag{2.14}$$

where $\mathcal{E}_r$ stands for the relative dielectric constant compared to air or air.

$$R = \frac{\rho}{2\pi\delta}\left(\frac{1}{b}+\frac{1}{a}\right) = \sqrt{\frac{f\mu_r\rho}{10^9}}\left(\frac{1}{b}+\frac{1}{a}\right) \tag{2.15}$$

where δ stands for skin depth, f is frequency and ρ is the resistivity.

If a coaxial transmission line is air insulated, there is practically no parallel loss conductance involved. In most of the cables used for coaxial transmission lines, the dielectric loss involved corresponds to conductance loss. The following equation gives the equivalent parallel conductance equivalent circuit for coaxial transmission line (Dyson et al., 1970).

$$G = \omega C \ \tan \delta \tag{2.16}$$

Where C is the capacitance, $\tan \delta$ stands for the dielectric loss tangent and is equal to $2\pi f$ (f is the operating frequency).

2.4.6 Waveguide transmission line

If one makes a waveguide slotted line, one would find out that, for a particular frequency, the equivalent waveguide wavelength would be longer than the so-called free space wavelength because the effective velocity measured would be the phase velocity (Bartiromo and De Vincenzi, 2016). The waveguide wavelength relates to the cut-off frequency and to the free space wavelength. The relationship is

$$\lambda_g = \frac{\lambda}{\sqrt{1-\left(\frac{\lambda}{\lambda_c}\right)^2}} \tag{2.17}$$

Where λ_g stands for the guide wavelength, λ is the free space wavelength and λ_c is the cut-off wavelength. It can be seen that if the free space wavelength approaches the cut-off wavelength the guide wavelength gets very long.

If a waveguide filled with low loss dielectric constant is ϵ_r, the waveguide expression will be

$$\lambda_g = \frac{\lambda}{\sqrt{\epsilon_r-\left(\frac{\lambda}{\lambda_{co}}\right)^2}} \tag{2.18}$$

where λ_{co} is the cut-off wavelength of the empty waveguide, not the dielectric filled guide.

2.4.7 Waveguide impedance

The characteristic waveguide impedance is analogous to the characteristic impedance of two-wire and coaxial lines. The characteristic waveguide impedance represents the ratio of the electric and magnetic field, since the electric field is analogous to current (Olyslager, 1999). There is little practical use for the characteristic waveguide impedance, but it can be determined from the following expressions:

$$Z_{TE} = \frac{\eta}{\sqrt{1-\left(\frac{\lambda}{\lambda_c}\right)^2}} \tag{2.19}$$

$$Z_{TM} = \sqrt{1-\left(\frac{\lambda}{\lambda_c}\right)^2}\,(\eta) \tag{2.20}$$

where η is the intrinsic impedance of the medium (377 Ω for free space).

Because there are no unique currents and voltages, the characteristic waveguide impedance cannot be determined as easily for waveguides as for a coaxial line. This is not really a problem, since the process of normalisation eliminates characteristic impedance as a requirement for calculations (Cheremisinoff, 1997). The basic quantities for waveguides work are reflection coefficient, standing wave ratio and propagation constant. From these the normalised impedance at any point can be determined, and the complete waveguide system can be described in terms of performance and characteristics.

2.4.8 Waveguides

Waveguides are structures that guide electromagnetic waves or sound, with minimum loss of energy by restricting expansion to limited dimensions. There are different types of waveguides for each type of wave. The geometry of waveguides reflects in their function. The frequency of

transmission of wave also dictates the shape of a waveguide. As a rule of thumb, the width of a waveguide is of the same order of magnitude as the wavelength of a guided wave (Mahmoud, 1991).

A propagation mode in a waveguide is one answer to the wave equations, or, in other terms, the structure of the wave. Due to the limitations of the boundary conditions, there are only narrow frequencies and forms for the wave function, which can propagate in the waveguide. The lowest frequency in which a selected mode can propagate is the cut-off frequency of that mode. The mode with the smallest cut-off frequency is the underlying mode of the waveguide, and its cut-off frequency is the cut-off frequency of the waveguide (Olyslager, 1999).

2.4.9 Rectangular waveguides

Rectangular waveguides have been utilised as resonators to carry out experiments on the determination of properties of materials. The experiments using CPM and TR were both realised using waveguides of this nature.

2.4.9.1 TM Modes for Rectangular waveguides

The TM modes are the transverse magnetic modes where the magnetic field component of the electromagnetic waves vanishes along the waveguide. This amounts to $B_z = 0$ everywhere inside the guide (Bakshi, 2009).

Using Dirichlet boundary condition, $Ez = 0$

$$E_z(0, y) = E_z(a, y) = E_z(x. 0) = E_z(x. b) = 0 \qquad (2.21)$$

$$E_z(x. 0) = E_z(x. b) = 0 \qquad (2.22)$$

$$E_z(0. y) = E_z(a. y) = 0 \qquad (2.23)$$

A solution can be

$$E_z(x. 0) = E_0 \sin(m\pi x/a) \sin(n\pi y/b), \qquad (2.24)$$

To satisfy boundary conditions, with $m, n = 1,2,3 \ldots$ and such a solution is called a TM$_{mn}$ mode if

$$k^2 = (\omega/c)^2 - \left(\frac{m\pi}{a}\right)^2 - (n\pi/b)^2 \tag{2.25}$$

$$k^2 = k_0^2 - \left(\frac{m\pi}{a}\right)^2 - (n\pi/b)^2 \tag{2.26}$$

$$(2\pi/\lambda)^2 = (2\pi/\lambda_0)^2 - (2\pi/\lambda_c)^2 \tag{2.27}$$

$$\frac{1}{\lambda^2} = \frac{1}{\lambda_0^2} - \frac{1}{\lambda_c^2} \tag{2.28}$$

where λ_c is

$$\frac{1}{\lambda_c} = \frac{1}{2}\sqrt{\left(\frac{m}{a}\right)^2 + \left(\frac{n}{b}\right)^2} \tag{2.29}$$

The cut-off wavelength, λ and λ_0 are the effective wavelength inside and the guide and free space respectively. $\lambda_c > \lambda_0$ condition for any propagation of the electromagnetic wave through the waveguide. The other way around and the square of the effective wavelength will be negative and becomes a complex number.

E_x and E_y are calculated using the expressions:

$$E_x(x,y) = \frac{ikE_0}{(w/c)^2 - k^2}\left(\frac{m\pi}{a}\right)\cos(m\pi x/a)\sin(n\pi y/b) \tag{2.30}$$

$$E_y(x,y) = \frac{ikE_0}{(w/c)^2 - k^2}\left(\frac{n\pi}{b}\right)\sin(m\pi x/a)\cos(n\pi y/b) \tag{2.31}$$

The components B_x and B_y are obtained by:

$$Bx(x,y) = \frac{ikE_0}{(w/c)^2 - c^2 k^2}\left(\frac{m\pi}{a}\right)\cos(m\pi x/a)\sin(n\pi y/b) \tag{2.32}$$

$$By(x,y) = \frac{ikE_0}{(w/c)^2 - c^2 k^2}\left(\frac{n\pi}{b}\right)\sin(m\pi x/a)\cos(n\pi y/b) \tag{2.33}$$

therefore

$$B_z(0, y) = B_z(a, y) = B_z(x. 0) = B_z(x. b) = 0 \qquad (2.34)$$

The above conditions satisfy $Bx(0, y) = Bx(a, y) = 0$ and $By(x, 0) = By(x, b) = 0$, i.e. $B = 0$ on the boundary condition.

2.4.9.2   TE Modes for Rectangular Waveguides

The transverse electric or TE modes have $E_z = 0$ everywhere inside the waveguide. The solution for this becomes

$$B_z = B_0 \cos(m\pi x/a) \cos(n\pi x/b) \qquad (2.35)$$

The solution denotes TE$_{m,n}$, in which case either m or n can be zero but not both.

On the boundary $x = 0 \& a$ the normal direction is x and on the boundary $y = 0 \& b$ the normal direction is y.

$$B_z(0, y) = B_z(a, y) = B_z(x. 0) = B_z(x. b) = 0 \qquad (2.36)$$

Boundary conditions

$$Bx(x, y) = \frac{ikE_0}{(w/c)^2 - k^2}\left(\frac{m\pi}{a}\right) \sin(m\pi x/a) \, \cos(n\pi y/b) \qquad (2.37)$$

$$By(x, y) = \frac{ikE_0}{(w/c)^2 - k^2}\left(\frac{n\pi}{b}\right) \cos(m\pi x/a) \, \sin(n\pi y/b) \qquad (2.38)$$

2.4.10 Cylindrical waveguides

2.4.10.1 TM Modes for Cylindrical Waveguides

The equation of cylindrical co-ordinates

$$\frac{\partial^2 E_z}{\partial \rho^2} + \frac{1}{\rho}\frac{\partial E_z}{\partial \rho} + \frac{1}{\rho^2}\frac{\partial^2 E_z}{\partial \emptyset^2} + \left(\frac{\omega^2}{c^2} - k^2\right)E_z = 0 \qquad (2.39)$$

Assuming $E_z = \xi(\rho)\Phi(\phi)$ and substituted. Dividing by E_z and multiplying by ρ^2

The following arrangement is arrived at

$$\frac{\rho^2}{\xi}\frac{\partial^2 \xi}{\partial \rho^2} + \frac{\rho}{\xi}\frac{\partial \xi}{\partial \rho} + \rho^2\left(\frac{\omega^2}{c^2} - k^2\right) = -\frac{1}{\Phi}\frac{\partial^2 \Phi}{\partial \phi^2} \qquad (2.40)$$

In this way, the variables are separated from dependents.

$$\Phi(\phi) = Acos(p\phi) \text{ or } Bcos(p\phi) \qquad (2.41)$$

Where p^2 is the separation constant in the equation, since electric and magnetic fields are measurable quantities, a single value of $\Phi(\phi)$ demands ps integer.

The equation reduces to

$$\rho^2\frac{\partial^2 \xi}{\partial \rho^2} + \rho\frac{\partial \xi}{\partial \rho} + \left(\rho^2\frac{\omega^2}{c^2} - k^2\right) - p^2\xi = 0 \qquad (2.42)$$

Cylindrical Bessel differential equation

The solution for Bessel function:

$$\xi(\rho) = J_p\left(\sqrt{(\omega/c)^2 - k^2}\rho\right) \qquad (2.43)$$
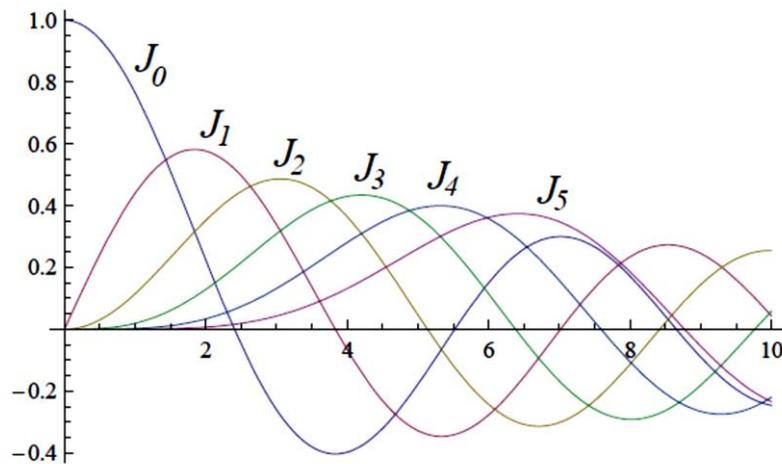
Figure 2-6: Cylindrical Bessel functions

Two solutions for each non-zero integer

$$E_{z(\rho,\phi)} = AJ_p\left(\sqrt{(\omega/c)^2 - k^2}\,\rho\right)\cos(p\phi) \qquad (2.44)$$

and

$$E_{z(\rho,\phi)} = AJ_p\left(\sqrt{(\omega/c)^2 - k^2}\,\rho\right)\sin(p\phi) \qquad (2.45)$$

For $p = 0$ there is only one solution,

$$E_{z(\rho,\phi)} = AJ_p\left(\sqrt{(\omega/c)^2 - k^2}\,\rho\right) \qquad (2.46)$$

Imposing boundary conditions, $Ez(R, \phi) = 0$ (*tangential component*),

$$\sqrt{(\omega/c)^2 - k^2}\,R = \rho_{n,m}, \qquad (2.47)$$

where $\rho_{n,m}$ is the nth zero of the pth order Bessel function Jp. The first few zeros of Bessel function are:

$$\rho_{0,1} = 2.4048, \rho_{1,1}=3.8317, \rho_{2,1} = 5.1356, \rho_{0,2} = 5.5201, \rho_{3,1} = 6.3802, \text{etc...}$$

Then

$$k^2 = (\omega/c)^2 - \left(\rho_{p,n}/R\right)^2 \qquad (2.48)$$

$$k^2 = k^2 - \left(\rho_{p,n}/R\right)^2 \qquad (2.49)$$

$$(2\pi/\lambda)^2 = (2\pi/\lambda_0)^2 - (2\pi/\lambda_c)^2 \qquad (2.50)$$

$$\frac{1}{\lambda^2} = \frac{1}{\lambda^2} - \frac{1}{\lambda^2} \qquad (2.51)$$

where the cut-off λ_c is defined as

$$\lambda_c = \frac{2\pi R}{\rho_{p,n}} \qquad (2.52)$$

The modes are designated by $TM_{p,n}$, such as TM_{01}, TM_{12} etc..

2.4.10.2 TE Modes for Cylindrical Waveguides

For TE modes of cylindrical waveguide, analysis is similar to that of the TM case, in which case B_z and E_z are the fields and the boundary condition is Neeumann.

$$EB_{z(\rho,\phi)} = AJ_p\left(\sqrt{(\omega/c)^2 - k^2}\rho\right)cos(p\phi) \tag{2.53}$$

and

$$B_{z(\rho,\phi)} = AJ_p\left(\sqrt{(\omega/c)^2 - k^2}\rho\right)sin(p\phi) \tag{2.54}$$

For non-zero integer

$$B_{z(\rho,\phi)} = AJ_p\left(\sqrt{(\omega/c)^2 - k^2}\rho\right) \tag{2.55}$$

Imposing boundary conditions, $p = 0$ (*tangential component*),

$$\sqrt{(\omega/c)^2 - k^2}\,R = \rho_{n,m}, \tag{2.56}$$

where $\rho_{n,m}$ is the nth zero of the pth order Bessel function Jp. The first few zeros of Bessel function are:

$$\rho'_{1,1} = 1.8412, \rho'_{2,1} = 3.0542, \rho'_{0,1} = 3.8317, \rho'_{3,1} = 4.2012, \rho'_{1,2} = 5.3312$$

etc..

$$\lambda_c = \frac{2\pi R}{\rho'_{p,n}} \tag{2.57}$$

The modes designated by $TE_{p,n}$ are TE_{11}, TE_{02} etc...

2.5   Microwave Cavity

Microwave cavities are widely used as means of material property characterization. A cavity is formed usually when the two ends of a segment of a waveguide are shortened. A cavity is therefore said to resonate when it has been excited at a corresponding frequency. Resonant mode is said to happen when the electric and magnetic fields form a standing wave, which depends on the internal dimensions of the cavity and the dielectric properties of the material under test (Yeh and Shimabukuro, 2008).

Air-filled microwave cavities confine electric and magnetic fields to the air spaces between their walls. Electric losses in such cavities are almost exclusively due to currents flowing in cavity walls. While losses from wall currents are small, cavities are frequently silver plated to increase their electrical conductivity and reduce these losses even further. Copper cavities may frequently oxidise, which increases their electric loss. Silver or gold plating prevents oxidation and reduces electrical losses in cavity walls. Even though gold is not quite as good a conductor as copper, it still prevents oxidation and the resulting deterioration of Q factor over time. Microwave cavities act as a resonant circuit with extremely low loss at their frequency of operation, with quality factors (Q factors) up to the order of 10^6, and are used in place of resonant circuits at microwave frequencies (Jerinic, 1966).

Therefore, the relative permittivity (ε_r) of the said material will change. The resonant frequency for *TE$_{nml}$* and *TM$_{nml}$* modes in a circular waveguide can be calculated using equation (Paillet et al.).

$$f_{nml} = \frac{c}{2\pi\sqrt{\mu_r \varepsilon_r}} \sqrt{\left[\left(\frac{P_{nm}}{R}\right)^2 + \left(\frac{l\pi}{H}\right)^2\right]} \qquad (2.58)$$

Where:

c - Speed of light

μ_r - Relative permeability

ε_r - Relative permittivity

P_{nm} - Value of the Bessel function for the TE or TM modes of a circular waveguide

R - Radius of the cavity

H - Height of the cavity

From the equation, it can be said that all *TE* and *TM* modes are proportionally dependant on $\sqrt{\varepsilon_r}$, so when the range of frequencies excite the waveguide, the highest signal spectrum is reached and the peaks of resonance of the modes will shift to lower frequencies with the increase of the permittivity.

The cylindrical cavity has the advantage of high-Q factors, and has been utilised as the resonant cavity sensor for the experiment. Two holes in opposite sides of the midsection of the cylindrical waveguide provide room for inserting the feed source antennas terminated with SMA connectors. Dielectric constant

A material is categorised as "dielectric" if it has the capability to store energy when an exterior electric field is applied. If a DC voltage source is positioned across a parallel plate capacitor, more charge is accumulated when a dielectric material is connecting the plates than if air is connecting the plates. The dielectric material increases the storage capacity of the capacitor by neutralizing charges at the electrodes, which ordinarily would contribute to the

external field. The capacitance with the dielectric material is directly linked to dielectric constant (Lododa et al., 2000).

The dielectric material increases the loading capability of the capacitor by counterbalancing charges at the electrodes, which generally would add to the external field. When complex permittivity is depicted as a simple vector schema (Figure 2.7) the real and imaginary components are 90° out of phase. The vector sum forms an angle δ with the real axis (ε'). The relative loss of a material is the ratio of the energy lost to the energy stored (Singh, 2000).
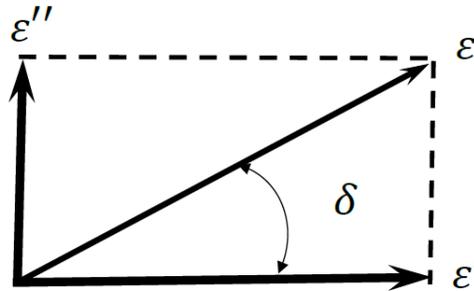
Figure 2-7: Simple vector schema

$$\tan \delta = \frac{\varepsilon''}{\varepsilon'} = D = \frac{1}{Q} = \frac{Energy\ Lost\ per\ Cycle}{Energy\ Stored\ per\ Cycle} \qquad (2.59)$$

The loss tangent or tan δ is expressed as the ratio of the imaginary part of the dielectric constant to the real part. D represents dissipation factor and Q is quality factor. The loss tangent, $tan\ \delta$ is termed *tan delta*, tangent loss or dissipation factor. Occasionally the phrase "quality factor or Q-factor" is used regarding an electronic microwave material, which is equal to the loss tangent. For very low loss materials, since $tan\ \delta \approx \delta$, the loss tangent can be expressed in angle units, milli-radians or micro radians (Case et al., 1998).

2.5.1 Permeability

Permeability, μ, defines the interaction of a material with a magnetic field. A comparable analysis can be done for permeability using an inductor with resistance to characterise core losses in a magnetic material. If a DC current source is located across an inductor, the inductance with the core material can be linked to permeability (Paillet et al., 1990).

If an AC sinusoidal current source is located across the same inductor, the subsequent voltage will be formulated out of an induced voltage and a loss voltage that is linked to permeability. The complex permeability (μ) consists of a real part (μ') that represents the energy storage term and an imaginary part (μ") that represents the energy loss term (Cheremisinoff, 1997). Relative permittivity μ_r is the permittivity relative to free space:

$$\mu_r = \frac{\mu}{\mu_0} = \mu'_r - j\mu''_r \tag{2.60}$$

Where

$\mu_0 = 4\pi \; x \; 10^{-7}$ H/m   is permeability of free space.

Some materials such as iron (ferrites), cobalt, nickel, and their alloys have substantial magnetic properties; however, many materials are non-magnetic, making the permeability very close to the permeability of free space ($\mu_r = 1$). All materials, on the other hand, have dielectric properties, so the focus of this discussion will mostly be on permittivity measurements (Amiet et al., 2003).

2.6   Cavity Perturbation Technique

The perturbation technique is a method for finding an approximate solution to a problem by starting from the exact solution of a related, simpler problem. The main feature of this technique is a middle step that breaks the problem into perturbation parts (Wiesel and

Technology, 2003). Perturbation methods start with a simplified form of the original problem, which is simple enough to be solved exactly.

Cavity perturbation theory is a derived form of the perturbation formulae for performance changes of a cavity resonator (Li et al., 1981b). The cavity perturbation technique is mostly used to measure properties of homogenous biochemical materials because of simplicity, easy data reduction and accuracy. The resonant cavities are designed in the standard mode of propagation, TM (transverse magnetic) or TE (transverse electric) of the electromagnetic fields (Meng et al., 1995). This is based on the resonant frequency shift and the change in the characteristics of absorption of a tuned resonant cavity, due to insertion of a sample of a material under test. The measurement is carried out by placing the sample into the centre of a circular or rectangular waveguide made into cavity (Linfeng Chen et al., 1999). Changes that occur in the centre frequency and the width due to the insertion of the sample provide information used to calculate the dielectric constant. The ratio of the energy stored to the energy dissipated is known as the Q-factor, and changes in this are used to estimate the dielectric loss (Kumar and Sharma).

2.6.1 Filled or partially filled resonant system

When a rectangular waveguide or cylindrical cavity filled or partially filled with a test material is used for an applicator, the resulting system is called the filled or partially filled (perturbation) cavity resonant system (Lin et al., 2005). The ε of the test material is calculated by taking note of the change in the resonant frequency, and the quality factor of the cavity when it is empty and when filled with the test material (Sheen, 2009). If fo and fs Qo and Qs are the resonant frequencies and the quality factors before and after filling with test material, then the permittivity, ε can be calculated by:

(a) Filled

$$\varepsilon' = \left(\frac{fo}{fs}\right)^2 \tag{2.61}$$

$$\varepsilon'' = \left(\frac{1}{Q_s} - \frac{1}{Q_o}\sqrt{\frac{f_o}{f_s}}\right)\left(\frac{f_o}{f_s}\right)^2 \tag{2.62}$$

in which:

$$Q_0 = \frac{f_0}{f_{s(3dB)}} \tag{2.63}$$

$$Q_S = \frac{f_S}{f_{s(3dB)}} \tag{2.64}$$

(b) Partially filled

$$\varepsilon' = \frac{1}{2}\left(\frac{f_o}{f_s} - 1\right)\frac{V_c}{V_s} - 1 \tag{2.65}$$

$$\varepsilon'' = \frac{1}{4}\left(\frac{1}{Q_s} - \frac{1}{Q_0}\right)\frac{V_c}{V_s} \tag{2.66}$$

where subscripts o and s indicate without and with sample respectively, and:

Q	=	quality factor,
$F_{o(3dB)}$	=	3dB frequency bandwidth for empty cavity,
$F_{s(3dB)}$	=	3dB frequency bandwidth for filled cavity,
V_s	=	volume of test material, and
V_c	=	volume of cavity.

2.7   Transmission / Reflexion line method

The transmission/reflection (TR) method has been known for its relative simplicity and is mostly used for broadband measurement. Using the TR method, a sample has been placed in a section of a waveguide to measure the two port scattering parameters by a VNA. The measured scattering parameters have then been related through the scattering equation to the

permittivity and permeability of the material. A system of equations with the complex permittivity and permeability as unknown has been utilised (Baker-Jarvis et al., 1990). The scattering equations are products of analysis of the electric fields E_I, E_{II} and E_{III}, in the regions I, II and III (Figure 2.8).
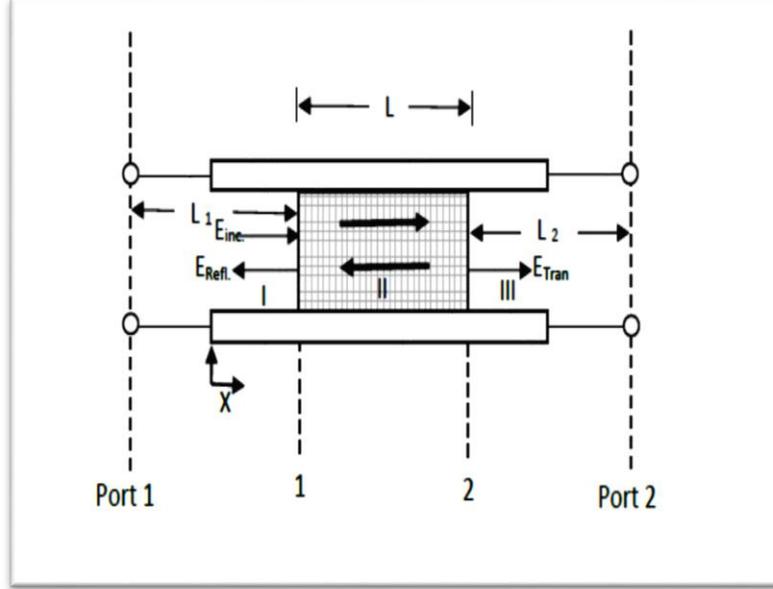
Figure 2-8: Dielectric sample in a transmission line waveguide

The spatial distribution of the electric field with electric field incident equal to one can be expressed as:

$$E_I = \exp(-\gamma_0 x) + C_1 \exp(\gamma_0 x) \tag{2.67}$$

$$E_{II} = C_2 \exp(-\gamma x) + C_3 \exp(\gamma x) \tag{2.68}$$

$$E_{III} = C_4 \exp(-\gamma_0 x) + C_5 \exp(\gamma_0 x) \tag{2.69}$$

where

$$\gamma = j\sqrt{\frac{\omega^2 \mu_R^* \epsilon_R^*}{c_{vac}^2} - \left(\frac{2\pi}{\lambda_c}\right)^2} \tag{2.70}$$

$$\gamma_0 = j\sqrt{\left(\frac{\omega}{c_{lab}}\right)^2 - \left(\frac{2\pi}{\lambda_c}\right)^2} \tag{2.71}$$

$$\varepsilon = [\varepsilon_R' - j\varepsilon_R'']\varepsilon_0 = \varepsilon_R^* \varepsilon_0 \tag{2.72}$$

$$\mu = [\mu_R' - j\varepsilon\mu_R'']\mu_0 = \mu_R^* \mu_0 \tag{2.73}$$

where $j = \sqrt{-1}$, C_{vac} and C_{lab} are the speed of light in air and air respectively, ω, angular frequency, λ_c, cut-off wavelength, ϵ_0 and μ_0 , permittivity and permeability respectively of air, ε_R^* and μ_R^*, the complex permittivity and permeability in relation to the air, and γ and γ_0 are constants of the material and air respectively. The boundary condition on the electric is the continuity of the tangential component of the magnetic field. The boundary condition on the magnetic field assumes that no surface current is generated (Li et al., 1981a).

The expressions for the measured scattering parameters follow the solution of equation (3.1) to (3.3), for a two-port device. Considering S matrix symmetrical, $S_{12} = S_{21}$. Hence the following expressions

$$S_{11} = R_1^2 \left[\frac{\Gamma(1-z^2)}{1-\Gamma^2 z^2} \right] \tag{2.74}$$

$$S_{22} = R_{12}^2 \left[\frac{\Gamma(1-z^2)}{1-\Gamma^2 z^2} \right] \tag{2.75}$$

$$S_{21} = R_1 R_2 \left[\frac{z(1-\Gamma^2)}{1-\Gamma^2 z^2} \right] \tag{2.76}$$

where

$$R_1 = \exp(-\gamma_0 L_1) \tag{2.77}$$

$$R_2 = \exp(-\gamma_0 L_2) \tag{2.78}$$

and where L_1 and L_2 are the distances from the reference planes to the sample ends, and R_1 and R_2 are the transformation expressions for the reference planes. The definition of reflection coefficient is hereby

$$\Gamma = \frac{\frac{\gamma_0}{\mu_0} - \frac{\gamma}{\mu}}{\frac{\gamma_0}{\mu_0} + \frac{\gamma}{\mu}} \tag{2.79}$$

By the transmission line theory, the transmission coefficient S_{21} is expressed by

$$S_{21} = \frac{4\Gamma_1 \Gamma_0}{(\Gamma_1 + \Gamma_0)^2 e^{\Gamma_1 L} - (\Gamma_1 + \Gamma_0)^2 e^{-\Gamma_1 L}} \tag{2.80}$$

where

$$\Gamma_0 = j\beta_0 \tag{2.81}$$

and

$$\Gamma_1 = \alpha_1 + j\beta_1 \tag{2.82}$$

The propagation of air-filled waveguide is

$$\beta_0 = \frac{2\pi}{\lambda_0}\left[1 - \left(\frac{2\lambda_0}{\lambda_c}\right)^2\right]^{1/2} \tag{2.81}$$

The propagation coefficient of loaded waveguide is

$$\alpha_1 + j\beta_1 = \frac{2\pi}{\lambda_0}\left[\left(\frac{\lambda_0}{\lambda_c}\right)^2 - \varepsilon_r\right]^{1/2} \tag{2.82}$$

λ_0 and λ_c are the wavelengths of free space and cut-off of the waveguide for the TE_{10} mode.

2.8   Properties of Materials

When microwaves are directed from a source towards a material under test (MUT), part of the resultant energy is reflected, some part of it is transmitted through the surface, and a third part of this quantity is absorbed. The proportions of energies that fall into these three categories are known to form the dielectric properties of the material (Venkatesh M S, 2005). The fundamental property of electrical nature through which the interactions manifest is referred to as the complex relative permittivity, ε. The mathematical expression is as follows:

$$\varepsilon = \varepsilon' - j\varepsilon'' \tag{2.83}$$

where

$\varepsilon' = dielectric\ constant$, and

$\varepsilon'' = dielectric\ loss\ factor.$

Whereby the absolute permittivity in air, ε_0 is expressed by:

$$C_o \mu_o \varepsilon_o = 1 \tag{2.84}$$

where

C_o = speed of light, and

μ_o = magnetic constant.

Using this formula, the value is $\varepsilon_o = \dfrac{1}{C_0^2 \mu_0} = \dfrac{1}{35\ 950\ 207\ 149.4727}\ F/m \approx 8.854 \times 10^{-12}$

F/m

The relative permittivity of a material, $\varepsilon_r = \varepsilon_{abs}/\varepsilon_o$, where ε_{abs} is the absolute permittivity of the material.

Materials that do not contain magnetic components, respond only to the electric field. The depth of penetration, d_p is known as the depth into which the microwave power is dropped 1/e or 36.8% of its transmitted value in a sample. Sometimes, d_p has the definition of the distance where the microwave power attenuation is 50% of the power transmitted, (P_{trans}).

$$\delta_p = \frac{\lambda_0 \sqrt{\varepsilon'}}{2\pi \varepsilon''} \tag{2.85}$$

Permittivity, in general is not a constant, and varies with the position occupied in the medium, the frequency of the electromagnetic field applied, humidity, temperature, and other parameters. The permittivity can also depend on the strength of the electric field in a non-linear medium. Permittivity as a function of frequency takes the form of real or complex values. The unit of permittivity is farad per meter, F/m.

Materials can be classified based on permittivity (YU and Cardona, 2005) as follows:

$$\frac{\varepsilon''}{\varepsilon'} = 0, \text{ perfect dielectric (lossless medium)}$$

$$\frac{\varepsilon''}{\varepsilon'} \ll 1, \text{ low conductor and good dielectric (low loss medium)}$$

$$\frac{\varepsilon''}{\varepsilon'} \approx 1, \text{ lossy conductor, lossy propagation medium}$$

$$\frac{\varepsilon''}{\varepsilon'} \gg 1, \text{ good conductor, high loss medium}$$

$$\frac{\varepsilon''}{\varepsilon'} = \infty, \text{ perfect conductor}$$

There are several measurement techniques employed for the determination of the permittivity of materials (Chen et al., 2004). In this study the perturbation and transmission line methods have been applied to determine the permittivity of the materials used in the experiments.

2.9   Waste cooking oil (WCO)

Waste cooking oils and fats from domestic and commercial handlers constitute a bulk of everyday commodities societies deal with as part of necessity. There are a number of interests in WCO recovery from restaurant chains and other entities who produce them (Rinco et al., 2005). Organisations dedicated to this have ways of collecting used cooking oil from their clients. One way is to distribute containers made specifically to handle this type of material and arrange for their collection (Rincon et al., 2007).

WCO is contaminated with a variety of contaminants that include, lead, magnesium, copper, zinc, chromium, arsenic, chlorides, cadmium, and chlorinated compounds (Abo-Dief et al., 2014). A gallon of waste oil if mal handled can spoil a million gallons of potable water. The recycling of WCO for the purposes of reuse in other ways is therefore essential to promote

environmental cohesion and cleanliness. Used oils may contain impurities such as water, food residues, and high free fatty acids (FFA) concentration, depending on the cooking process and successive storage (Rinco et al., 2005). Figure 2.9 illustrates three-phase recovery process of waste cooking oil from the drains. Phase 1 is the transportation to a depository, followed by phase 2 of classification into hazardous or non-hazardous and then phase 3, the treatment process.
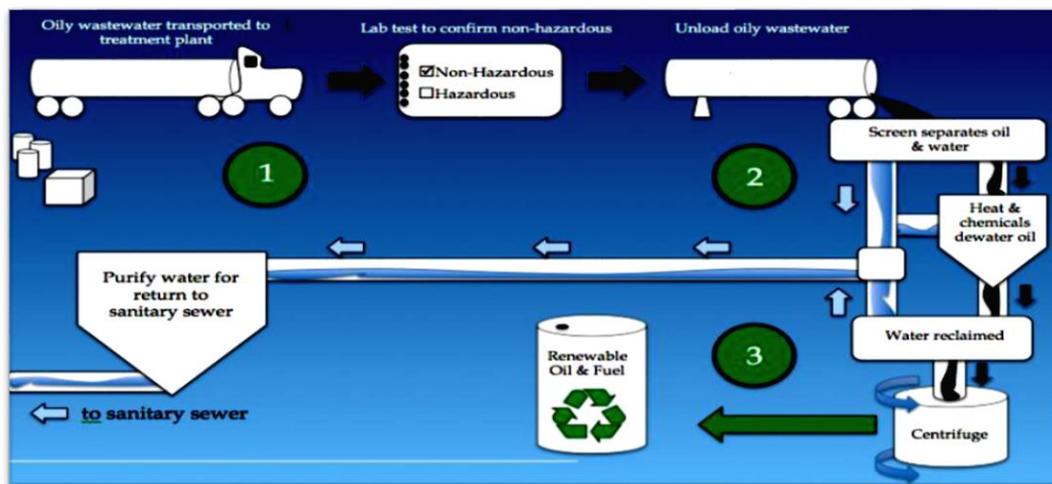
Figure 2-9: Some waste cooking oil recovery. Source: Advance Waste Services

Methanolysis is one form of recycling WCO (Tomasevic and Siler-Marinkovic, 2003). It consists of placing used frying oil into a dry reaction flask equipped with reflux condenser and magnetic stirrer. The blended reaction mixture at a temperature of 25° C is then separated into layers. The ester layer is separated from the glycerol layer in a separating funnel. Crude ester layer forms methyl-ester (ME), which is then refined and washed with hot water, until the washings are neutral. The ester layer is allowed to dry over sodium sulphate and then filtered.

Used frying oils (UFO) are useful ingredients for the preparation of biodiesels. The main issues with these is how to adjust their acidity and water content primarily to achieve the required values, they then are transformed into ME in a similar way as in the case of fresh

oils and fats, and the properties of ME are equivalent in both cases (Cvengroš and Cvengrošová, 2004).

2.10 Methanol

Methanol is the simplest alcohol and is the only methyl group related to the hydroxyl group. It is a low weight, volatile, colourless, combustible liquid with a characteristic smell very comparable to that of ethanol. However, unlike ethanol, methanol is extremely toxic and unhealthy for consumption. At room temperature, it is a polar liquid, and can be used as an antifreeze, solvent, fuel, and to denature ethanol. It can also be used for biodiesel production via transesterification reaction (Cheng, 1994).

Methanol is used primarily as a raw material for the manufacture of chemicals, and as a fuel for specialized vehicles. As mentioned above, it is a commonly used as a denaturing agent. As a common laboratory solvent, is useful for application in HPLC, UV/VIS spectroscopy, and LC-MS due to its low UV cut-off (de Reuck and Craven, 1993).

In the chemical industry methanol is primarily used in making other chemicals. About 40% of methanol is transformed into formaldehyde, and from there into more products like plastics, plywood, paints, explosives, and permanent press textiles (Sheldon, 2013).

Condensation of methanol molecules to produce hydrocarbon chains and even aromatic systems has been demonstrated with loss of water, carbon monoxide, and/or carbon dioxide. An aromatisation reaction, which generated hex methylbenzene as a minor product with a mixture of mostly aliphatic hydrocarbons directly from methanol, using zinc chloride as catalyst, has been demonstrated (Chang, 1983).

Other chemical derivatives of methanol include acetic acid and dimethyl ether (DME), the latter of which has replaced chlorofluorocarbons as an aerosol spray propellant. Dimethyl ether can also be blended with liquefied petroleum gas (LPG) for home heating and cooking, and can be used as a replacement for transportation diesel fuel (Bajpai and Chandrasekhar, 2016).

Of high interest to the petrochemical marketplace, methanol is an important component in new and lower-cost methods for producing propylene, which is much in demand. Such methods include methanol-to-olefins (MTO), methanol-to-propylene (MTO/MTP), metathesis, propane dehydrogenation (PDH), high severity FCC, and olefins cracking (Bao and Xu, 2004).

Methanol is sometimes used to fuel internal combustion engines. Pure methanol is mandatory to be used in sprint cars and other dirt track series, mainly because, in the event of an accident, methanol does not generate an opaque cloud of smoke. Since the late 1940s, Methanol has also been used as the main fuel ingredient in the power plants for radio control, control line, free flight airplanes, cars and trucks; such engines use a platinum filament glow plug that fires the methanol vapour via a catalytic reaction (Lee, 1989).

Methanol burns in oxygen, including open air, forming carbon dioxide and water (Masterton and Hurley, 2015):

$$2\,CH_3OH\ +\ 3\,O_2\ \rightarrow\ 2\,CO_2\ +\ 4\,H_2O \tag{2.86}$$
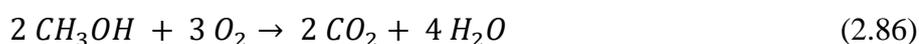
One problem with high concentrations of methanol in fuel is that alcohols corrode some metals, particularly aluminium. An acid, even though weak, methanol damages the oxide coating that normally protects the aluminium from corrosion (Behrens, 1991):

$$6\,CH_3OH\ +\ Al_2O_3\ \rightarrow\ 2\,Al(OCH_3)_3\ +\ 3\,H_2O \tag{2.87}$$
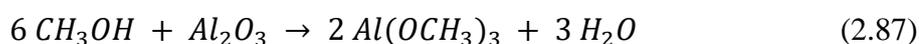
CHAPTER II – BACKGROUND OF RESEARCH

The resulting methoxide salts are soluble in methanol, resulting in a clean aluminium surface, which is readily oxidised by dissolved oxygen. Also, the methanol can act as an oxidiser (Garverick, 1994):

$$6\,CH_3OH \;+\; 2\,Al \;\rightarrow\; 2\,Al(OCH_3)_3 + 3\,H_2 \qquad\qquad (2.88)$$
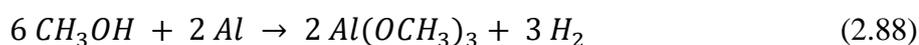
This reciprocal process in effect fuels corrosion until either the metal is eaten away or the concentration of CH_3OH is negligible. Methanol's tendency to corrosiveness has been addressed with methanol-compatible materials and fuel additives that serve as corrosion inhibitors (Carroll, 2014).

Organic methanol, produced from wood or other organic materials (bio-alcohol), has been suggested as a renewable alternative to petroleum-based hydrocarbons. Low levels of methanol can be used in existing vehicles with the addition of solvents and corrosion inhibitors (Kuznetsov, 2013).

Methanol fuel has been proposed for ground transportation. The main advantage of a methanol economy is that it could be adapted to gasoline internal combustion engines with minimum modification to the engines and to the infrastructure that transports and stores liquid fuel (Boshier and Moy, 1982).

The European Fuel Quality Directive allows up to 3% methanol with an equivalent amount of solvent to be mixed together with gasoline sold in Europe. China uses above one billion gallons of methanol per year as a transportation fuel in low level blends for normal vehicles and high level blends in vehicles intended for methanol fuels (Folkson, 2014).

Stoichiometry for methanol production of syngas requires the ratio of H_2 / CO to equal 2. The partial oxidation process yields a ratio of 2, and the steam reforming process yields a ratio of 3. The H_2 / CO ratio can be lowered to some extent by the reverse water-gas shift reaction (Stuart and El-Halwagi, 2012),

$$CO_2 + H_2 \rightarrow CO + H_2O, \qquad\qquad (2.89)$$

to provide the suitable stoichiometry for methanol synthesis.

Methanol is freely biodegradable in both aerobic and anaerobic environments. Methanol will not persist in the environment. The half-life for methanol in groundwater is just one to seven days, while many common gasoline components have half-lives in the hundreds of days. Since methanol is miscible with water and biodegradable, it is unlikely to accumulate in groundwater, surface water, air or soil (Clary, 2013).

2.11   Biodiesel

Biodiesel refers to diesel fuel that is animal fat or vegetable oil based and consists of long-chain alkyl   esters (ethyl,   methyl   or propyl).   Biodiesel   is   made   by   chemically reacting triglycerides, animal fat (tallow), and vegetable oil with alcohol, which produce fatty acid esters. The major advantage of biodiesel is that it enhances the life of the engine, and unlike petroleum, it does not pollute the environment (Sarin, 2012).

The global biodiesel market is mainly motivated by escalating apprehension of energy security and fossil fuel costs. Biodiesel is a direct alternative to fossil fuel, and notwithstanding the ongoing misunderstanding in the biofuels sector concerning the sustainability, quality of raw materials, and significant slowdown in financing, the global biodiesel market will continue to grow at a steady rate (Luque et al., 2016). The top five-biodiesel producers in the world are the U.S., Germany, France, Argentina and Brazil. Australia is the largest producer of biodiesel in the Asia Pacific region, followed by China and India (Luque and Melero, 2011).

Since Rudolf Diesel, a German inventor, introduced the diesel engine (Bryant, 1965), there has been a great deal of research and development in the design area of finding appropriate fuel to use for these engines. For over the years, readily available petroleum products did not

do much to incentivise this area of research. It was the crisis of the 1970s and the subsequent rise of petroleum prices that ignited the need for alternative fuels. Also, with the advent of climate concerns, many have proposed an environmentally friendly alternative to the fossil fuel-based products that we are used to so far. The use of vegetable oils and other biodegradable fats for biodiesel production then became prominent. The cost and conflict with farmers, who would prefer the use of land for food crops, then became evident (Romano and Sorichetti, 2010).

The production of biodiesel is the result of the conversion of triglycerides (vegetable oils or animal fats) to alkyl or methyl esters. The consequence is an alternative diesel with a high level of viscosity, around 10 to 17 times greater than that of the conventional diesel (Rachmanto et al., 2014). It is therefore inconvenient to utilise directly in a diesel engine designed to operate with common diesel. Working with the alkyl or methyl ester-based fuel as prescribed can lead to increased carbon deposits, injector coking, oil ring sticking, and the possibility of lubrication oil degradation caused by contamination with vegetable oil. The main technical challenge of using biodiesel from low quality used oil is the pre-treatment of FFA.

Numerous methods have been anticipated to try to reduce the viscosity of vegetable oils and fats to meet diesel fuel standards. One of which is transesterification, a technique widely used for the production of biodiesel.
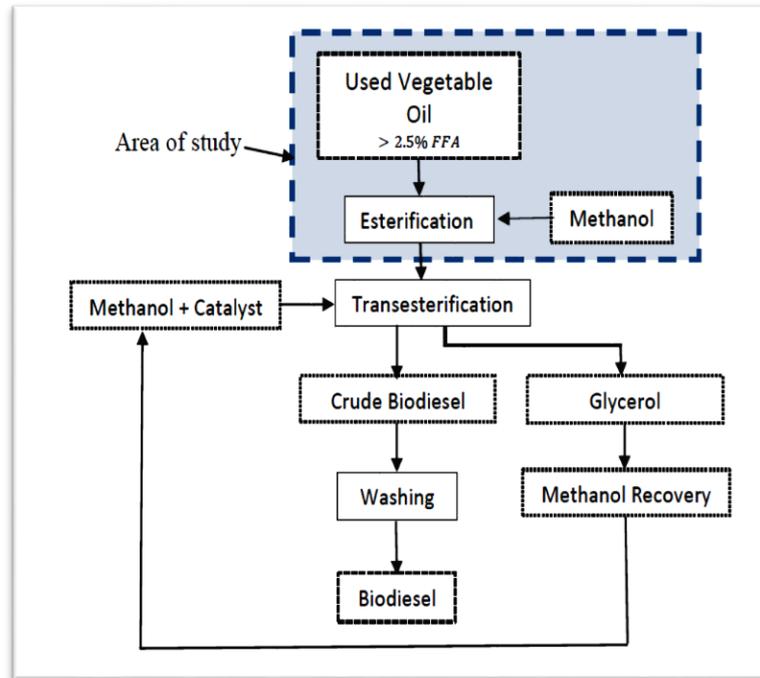
Figure 2-10: Biodiesel production process chart showing area of study

The processes involved in biodiesel production as shown in Figure 2.10, are esterification, transesterification, methanol recovery and washing. The WCO is to possess free fatty acids in excess of 2.5% and the reaction with methanol is to be used for the process (Scragg, 2009).

In this work, 3 to 10 percent of FFA was utilised in the experiments. The other processes, such as transesterification, are not touched in detail in this work and may require other expertise to be performed. The area of study is highlighted in Figure 2.10.

2.11.1 Esterification

The presence of FFA in the oil is detrimental during the alkali transesterification process due to the possible materialisation of soap, yield loss and increased difficulty in product separation. The acid catalysed transesterification can straightforwardly transform both FFA and oil into biodiesel. Conversely, this has not been much practised by biodiesel producers due to the much longer reaction time and low yield (Chai et al., 2014). Instead, a two-step conversion process made of an acid catalysed esterification pre-treatment to first lower the FFA content, followed by the traditional alkali-catalysed transesterification is widely used

both in laboratory and industry. The acid-catalysed esterification requires additional acid and methanol usage, but the majority of the methanol is recovered through a system that has commonly been installed by the manufacturers.

The elimination of FFA uses a well-known esterification reaction:

$$R_1 - COOH - COO - R_2 + H_2O \qquad (2.90)$$
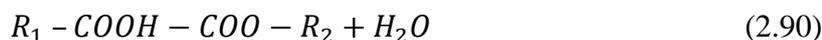
which is catalysed by acids. R_1 is a linear chain of carbon atoms containing a variable number of unsaturation, which depends in particular to the origin of the material and R_2 is methyl related radical (Berrios et al., 2007). The reaction is heterogeneous, since methanol is only sparsely soluble in vegetable oil and therefore requires agitation to avoid mass transfer in the process.

The goal of this study is to evaluate the amount of FFA in the oil by combining from zero up to 20% in vegetable oil (VO) and try to assimilate a system of monitoring of this process in the laboratory environment. The same FFA combinations added to methanol (M) allow for monitoring using the same process. Further combinations were carried out to evaluate the saturation of M in higher percentages of 50, 60 and 70 in oil (VO).

2.11.2 Transesterification

Triglycerides and free fatty acids go through a reversible reaction with alcohol, out of which they form glycerol and fatty acid alkyl/methyl esters. During the reactions, monoglycerides and diglycerides are made and as final products are glycerol and methyl ester (De Boni and Lima da Silva, 2011). This process is with or without catalyst; however, alkali or acid catalyst is mostly used in commercial applications. A catalyst free reaction is achieved under critical conditions. Equations (2.91), (2.92) and (2.93) show different combinations of transesterification reaction processes without the use of catalyst.

$$
\begin{array}{llll}
\text{CH}_2\text{-O-CO-R}_3 & & \text{CH}_2\text{-OH} & \\
| & & | & \\
\text{CH-O-CO-R}_2 & + \quad \text{CH}_3\text{OH} \quad \leftrightarrows & \text{CH-O-CO-R}_2 & + \quad \text{CH}_3\text{+OCO-R}_1 \\
| & & | & \\
\text{CH}_2\text{-O-CO-R}_3 & & \text{CH}_2\text{-O-CO-R}_3 & \\
\textbf{Triglycerides} & \textbf{Methanol} & \textbf{Diglycerides} & \textbf{Methylester}
\end{array}
\tag{2.91}
$$

$$
\begin{array}{llll}
\text{CH}_2\text{-OH} & & \text{CH}_2\text{-OH} & \\
| & & | & \\
\text{CH-O-CO-R}_2 & + \quad \text{CH}_3\text{OH} \quad \leftrightarrows & \text{CH-O-CO-R}_2 & + \quad \text{CH}_3\text{+OCO-R}_1 \\
| & & | & \\
\text{CH}_2\text{-O-CO-R}_3 & & \text{CH}_2\text{-OH} & \\
\textbf{Diglycerides} & \textbf{Methanol} & \textbf{Monoglycerides} & \textbf{Methylester}
\end{array}
\tag{2.92}
$$

$$
\begin{array}{llll}
\text{CH}_2\text{-OH} & & \text{CH}_2\text{-OH} & \\
| & & | & \\
\text{CH-O-CO-R}_2 & + \quad \text{CH}_3\text{OH} \quad \leftrightarrows & \text{CH-OH} & + \quad \text{CH}_3\text{+OCO-R}_1 \\
| & & | & \\
\text{CH}_2\text{-OH} & & \text{CH}_2\text{-OH} & \\
\textbf{Monoglycerides} & \textbf{Methanol} & \textbf{Monoglycerides} & \textbf{Methylester}
\end{array}
\tag{2.93}
$$
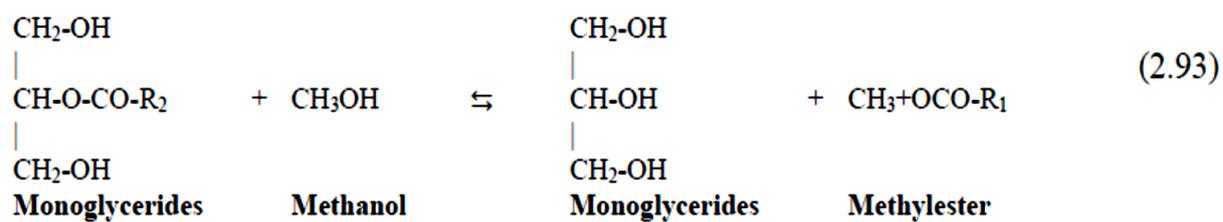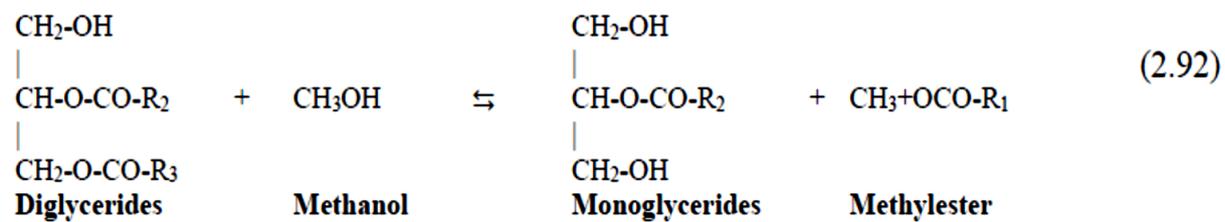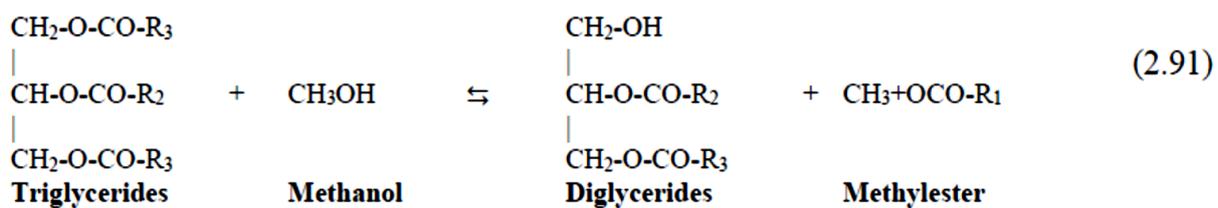
3.0   METHODOLOGY

3.1   Introduction

Work started with the probing of the difference in edible oils sourced from supermarkets. The simple aim was to use the sensor to identify and establish the difference in the oils. The next experiments were carried out on mixtures with the aim of authenticating extra virgin olive oil (EVOO), for which sunflower oil (SFO) was used as adulterant in the tests.

The physical properties, especially the complex permittivity of the samples of materials were determined, with the aim of using those parameters to design a model of the sensor. Experiments were carried out using the rectangular waveguide cavity to set up the perturbation method. In addition, the other method used to determine the properties is the transmission/reflection line where the tape sealed cavity experiment was utilised.

Experiments relating to waste oil recovery were realised using the cylindrical cavity resonator. Sample preparation for the experiments are herein explained in detail. Computer modelling and simulation was carried using COMSOL software.

3.2   Experiments on Oil Type Differentiation

Tests were carried out with the intent to verify the differences in the types of edible oils. Nine different oils were sourced from the commonplace supermarkets (Table 3.1, Figure 3.1) for the experiments. Samples were prepared and labelled out of these and each sample submitted to tests. The goal was to compare them and establish the differences between them using their microwave generated signal spectra, results shown in 5.2.1.

Table 3.1: Oils from the Supermarket

ITEM	PRODUCT
1	Sunflower oil
2	Grape seed oil
3	Groundnut oil
5	Mixed refined olive oil (ASDA)
4	Mixed refined olive oil (Felippo Berrio)
6	Medium flavour olive oil (Napolina)
7	Fruity flavour olive oil (Napolina)
8	Extra virgin olive oil (ASDA)
9	Extra virgin olive oil (Felippo Berrio)

Figure 3-1: Edible oils sourced from supermarket

Seven samples were finally tested for the differentiation of oil types. Table 3.2 shows the exact samples used for the oil type verification experiments.

Table 3.2: Samples for Oil Type Verification Experiment

SAMPLES	DESCRIPTION
1	Sunflower Oil (SFO)
2	Grape seed Oil (GSO)
3	Groundnut Oil (GNO)
4	Olive Oil (Mixed Refined) (ROO)
5	Olive Oil (Medium Flavour) (MFOO)
6	Olive Oil (Fruity Flavour) (FFOO)
7	Olive Oil (Extra Virgin) (EVOO)

The seven samples were prepared and labelled in test tubes for the realisation of the experiments. The IDE sensor (Figure 3.2) was connected to port 1 of the VNA to read the reflection coefficient, S_{11}. S_{11} is part of scattering parameters ($S_{11}, S_{21}, S_{12}, S_{22}$) that helps to determine what happens to the signal applied to the sensor port when interacting with the material, i.e. describe the flow of the signal. It measures the input reflection coefficient of the device in the form of reflected microwave signal. S_{21} on the other hand defines the transmission coefficient in the case of a two-port sensor device. The sensing area, or antenna, of the sensor was adequately cleaned and dried with nonabrasive wipes and the samples of oil applied to the area, using pipettes and making sure the small squared area ($0.16cm^2$) fencing the digitated platform is covered with the oil sample (50 µl). Figure 3.2 shows the IDE sensor as used for the experiment and described by Korostynska et al., (2013).
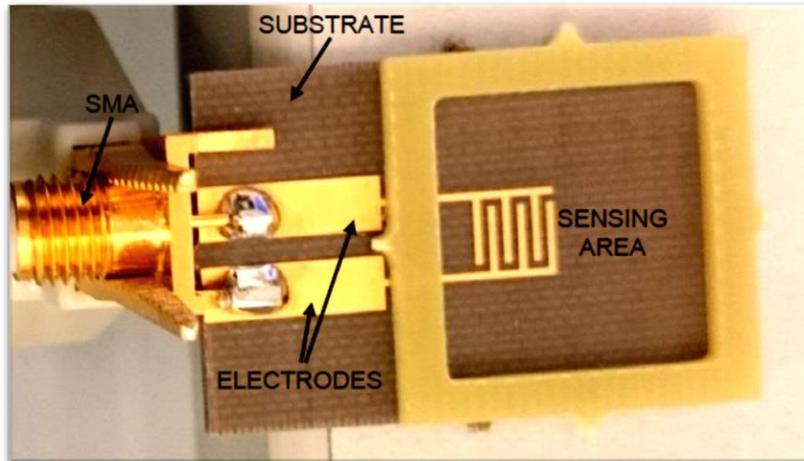
Figure 3-2: The interdigitated electrode sensor (IDE) used for oil type differentiation

The Rohde and Schwarz, ZVL 6 GHz was used for the set-up of the experiment. Figure 3.3 illustrates the setup of the experiment to verify the difference in the oils.
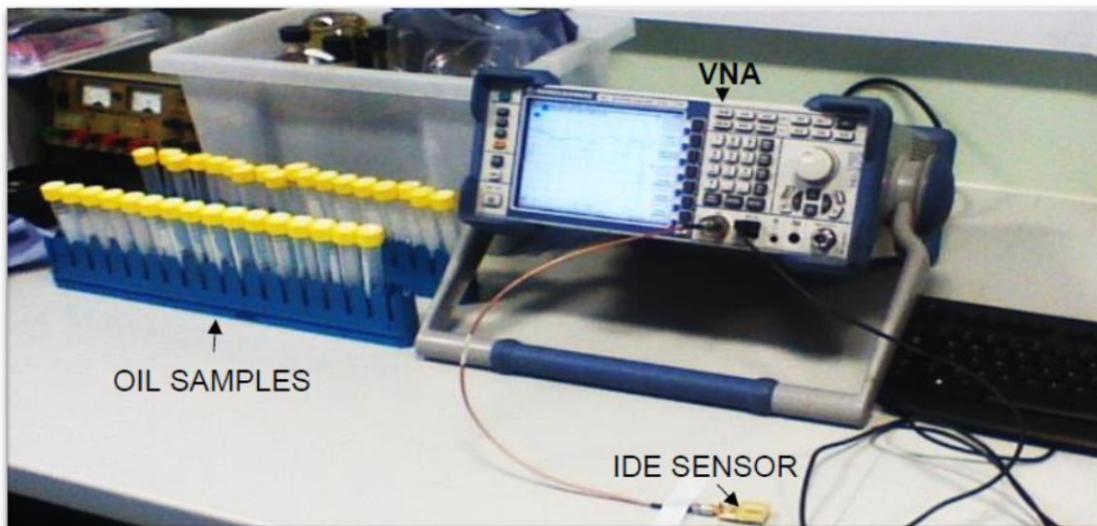

Figure 3-3: Set-up for oil type verification test showing samples, VNA and sensor

Readings from the VNA were taken and saved in a formatted form to the computer. Each cycle was repeated (n=10) for each sample. All 10 readings were aggregated together, and an average chart was used for analyses. Data processing was carried using Microsoft Excel platform. The results for these experiments can be found in section 5.2.1.

3.3   Experiments on Dilution of EVOO

Tests were carried out to establish the adulteration of extra virgin olive oil using sunflower oil (SFO) as the adulterant. An extra virgin olive oil (EVOO) was mixed with 10%, 20%, 30%, 40%, and 50% of sunflower oil (SFO), as a form of dilution. These percentages were selected purposely and primarily to test the ability of the sensor to verify the percentages of concentration of SFO in EVOO. The reason the tests were limited to 50 percent is that adulteration beyond this limit begins to shift pigmentation and lose the intensity of the EVOO. The dominance of the SFO then becomes obvious. Since most adulterations are for profit, becoming too obvious could raise suspicion and deter buyers from patronising. Samples have been prepared according to table 3.3.

Table 3.3: Sample of Mixtures of SFO and EVOO

SAMPLES	SFO/EVOO
1	SFO 10% / EVOO 90%
2	SFO 20% / EVOO 80%
3	SFO 30% / EVOO 70%
4	SFO 40% / EVOO 60%
5	SFO 50% / EVOO 50%

For best results, samples were prepared using weight to compensate for the difference in densities of the materials under test. Samples were weighed using KERN scale, with maximum range of 100g (shown in Figure 3.6). Ten grams was adequate for maximum sample weight, owing to the fact that it is enough to be pipetted into the NMR tubes for the measurements. Table 3.4 shows the distribution of the mixtures by weight and percentages.

Table 3.4: Sample Preparation of SFO in EVOO

SAMPLES	MIXTURE	WEIGHT
1	SFO0% / EVOO 100%	0:10g
2	SFO 10% / EVOO 90%	9g:1g
3	SFO 20% / EVOO 80%	8g:2g
4	SFO 30% / EVOO 70%	7g:3g
5	SFO 40% / EVOO 60%	6g:4g
6	SFO 50% / EVOO 50%	5g:5g

3.3.1   Set-up of Authentication of EVOO using Microwave.

Tests were carried out on samples of extra virgin olive oil diluted with sunflower oil of 0 to 50% in 10% intervals using weight. The pancake cavity sensor (Figure 3.4), expected to operate here within the range of 4 to 6GHz, has an internal diameter of 13cm and a height of 2cm, connected to two ports (to read the transmitted, S_{21} and reflected, S_{11} parameters/signals) of the Rohde & Schwarz ZVA24. Samples were pipetted into NMR tubes and labelled and were inserted one by one into the pancake cavity resonator for tests. The test cycle was repeated (n=10) for each sample. The sum of all 10 readings were accumulated and an average chart used to process the data. Data processing was carried out using Microsoft® Excel platform. The results for these experiments can be found in section 5.2.2.
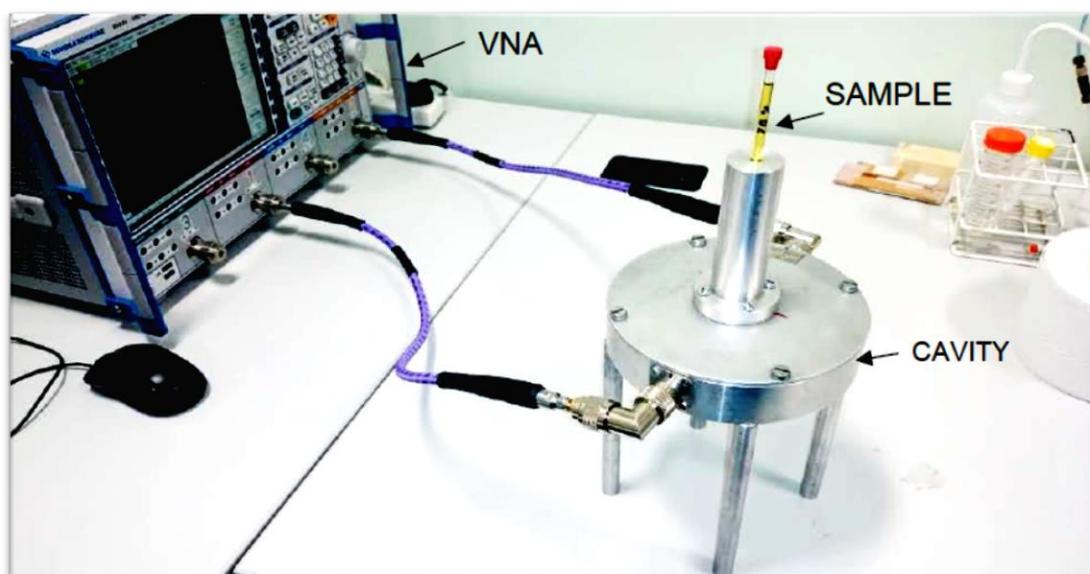
Figure 3-4: Set-up for microwave spectroscopic tests using the pancake cavity sensor

3.3.2 Set-up of Authentication of EVOO using Spectrophotometer

The spectrophotometric readings were carried out using the HP spectrophotometer (Figure 3.5). Samples were pipetted into cuvettes and labelled and were each slotted into the spectrophotometer for measurement. In the beginning air, water, sunflower and extra virgin oil were each trialled as *blank*, leading to the realisation that air (empty cuvette) provided the best blank for the best readings. Samples used were prepared according to table 3-4. All 10 readings were added together, and an average chart used for the analyses. Data processing was carried out using Microsoft® Excel platform. Figure 3.5 illustrates the HP spectrophotometer used for the experiments. The results for these experiments can be found in section 5.2.2.
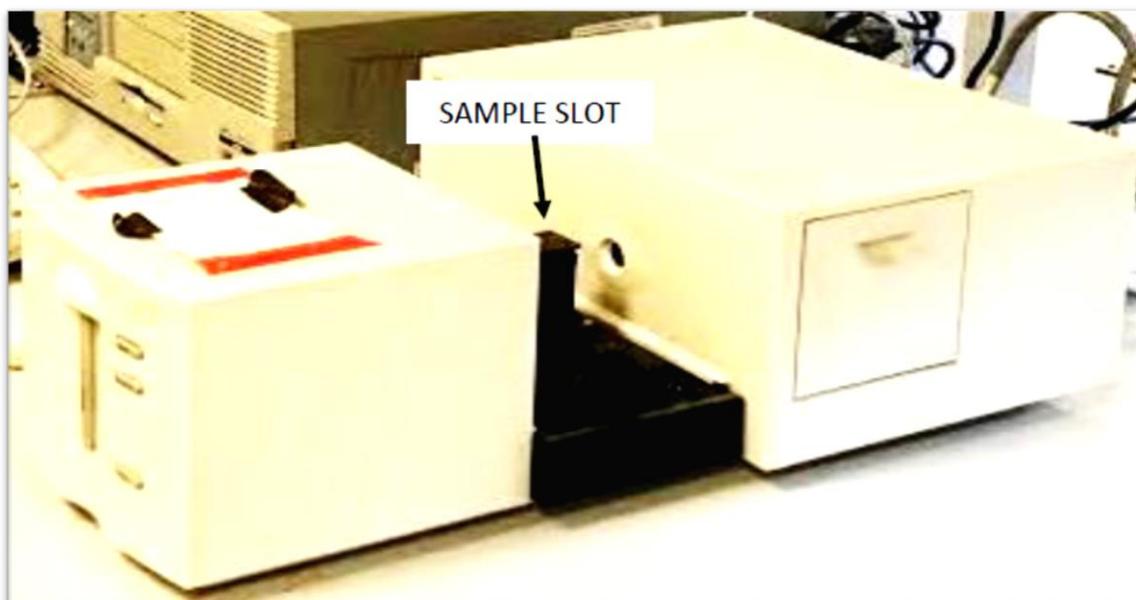
Figure 3-5: HP spectrophotometer used for tests

3.4   Experiments on Waste Oil Recovery Process

The aim of this experiment is to assimilate the process leading to waste oil recovery by combination in various preparations of mixtures of vegetable oil (VO), free fatty acids (FFA) and methanol (M) in a way that would mimic the samples as applied in the industry. A laboratory scale was utilised to measure samples by weight instead of just relying on volume of the mixtures. Mixing substances with different densities by volume has its own challenges, for which reason it is advisable to use weight. The type of measurements, as carried out here, which is to determine the properties of the materials, also rely on the conditions under which they are measured. Figure 3.6 shows the laboratory scale as used to weigh the samples for the experiment, a product of KERN brand, with maximum range of 100g, read out of 0.001g, reproducibility of 0.001g and linearity of ±0.003g.

Figure 3-6: Laboratory scale for measurements

VO, M and FFA were prepared as samples and placed in 15 millilitre test tubes and labelled (as shown in Figure 3.7). Mixture pairings were prepared of methanol and vegetable oil (denominated MO), FFA and VO (denominated FO), and FFA and M (denominated FAM). For the purposes of these experiments, all mixture samples were prepared in the same day and at the same temperature in an air-conditioned environment (at room temperature of 20^0C).

3.4.1 FFA in Vegetable Oil (FO)

The aim of this experiment is to identify the changes occurring in the variation of the percentages of mixture concentration of FFA in the oil using microwave technology. This would lead to the measurement of the stages of occurrences during the processes needed to reduce FFA in the oil. VO mixture with FFA is to identify the presence of fatty acids in the oil during esterification. The fact is that waste oil is most likely to contain a large amount of FFA, and it is key to reduce it in the process to an adequate level (about 2.5%). Figure 3.7 illustrates the labelled test tubes containing the samples as used for the measurements.

Figure 3-7: Test tubes containing samples for measurements

The mixture of Vegetable oil with FFA was realised to trace the amount of fatty acids present in the oil during the process. The allocation of these percentages of 2.5 to 17.5 of FFA in VO represent the tests to ascertain the traces of free fatty acids in the vegetable oil during the esterification process. The levels of FFA at this stage should prevail at this range to give meaning to the process. Table 3.5 shows the distribution of mixtures by weight and percentages of FFA vegetable oil.

Table 3.5: Sample measurement by weight of FFA in oil

VO (g)	FFA (g)	VO (%)	FFA (%)
40	0	100	0
39	1	97.5	2.5
38	2	95	5
37	3	92.5	7.5
36	4	90	10
35	5	87.5	12.5
34	6	85	15
33	7	82.5	17.5

3.4.2 FFA in Methanol

The mixture of FFA in methanol (FAM) was realised to trace the amount of fatty acids in methanol. Adding 0 to 17.5 percent of FFA to methanol would allow for the tests of detecting the amount of FFA in methanol, vital for monitoring the presence of the substance in the alcohol during the esterification process. It is important to note that at the temperature at which this is being carried out (20^c), shaking is vital for this type of mixture since the substances tend to separate if allowed in time. It is therefore important to vigorously shake the mixture just before any measurement is realised. Table 3.6 shows the distribution of mixtures of FFA in methanol.

Table 3.6: Sample measurement by weight of FFA in methanol

M (g)	FFA (g)	M (%)	FFA (%)
40	0	100	0
39	1	97.5	2.5
38	2	95	5
37	3	92.5	7.5
36	4	90	10
35	5	87.5	12.5
34	6	85	15
33	7	82.5	17.5

3.4.3 Methanol in Vegetable Oil

The mixture of methanol in vegetable oil (MO) was realised to detect the concentration of the alcohol present in the oil. In the waste oil recovery process, a large amount of methanol is utilised to leach out FFA from the oil. The ability to test the presence of large amounts of

methanol saturated in vegetable oil was realised in this experiment by mixing 50 to 70% of

MO. It is important to note also that at the temperature at which this is being carried (20° C),

shaking is necessary to maintain the composition of the mixture, which tends to decompose

if allowed, in time. It is therefore important to consistently shake the mixture just before any

measurement is realised. Table 3.7 shows the distribution of mixtures of VO and methanol.

Table 3.7: Sample measurement by weight of methanol in oil

VO (g)	VO (%)	M (g)	M (%)
20	50	20	50
19	47.5	21	52.5
18	45	22	55
17	42.5	23	57.5
16	40	24	60
15	37.5	25	62.7
14	35	26	65
13	32.5	27	67.5
12	30	28	70

Initially all measurements were carried out in a larger container that is capable of

containing the 40g of the mixture of the liquid samples, in this case a 100ml *beak*er before

later transferring into the 15 millilitre test tubes that were used for the measurements.

3.5   Set-up of Experiments on Waste Oil Recovery

To set up the experiment for the waste oil recovery process, the Rohde and Schwarz, ZNB20 Vector Network Analyser was utilised. The VNA was set to read both the S_{11} and S_{21} parameters respectively at frequencies ranging from 100 kHz to 20GHz (full range). A cylindrical cavity resonator, as the sensor, expected to operate within 2 to 5GHZ range, was connected to the ports 1 and 2 of the VNA. Figure 3.8 illustrates the experimental set-up of the waste oil recovery process verification using 1. VNA, 2. Cylindrical cavity resonator and 3. Samples in test tubes.
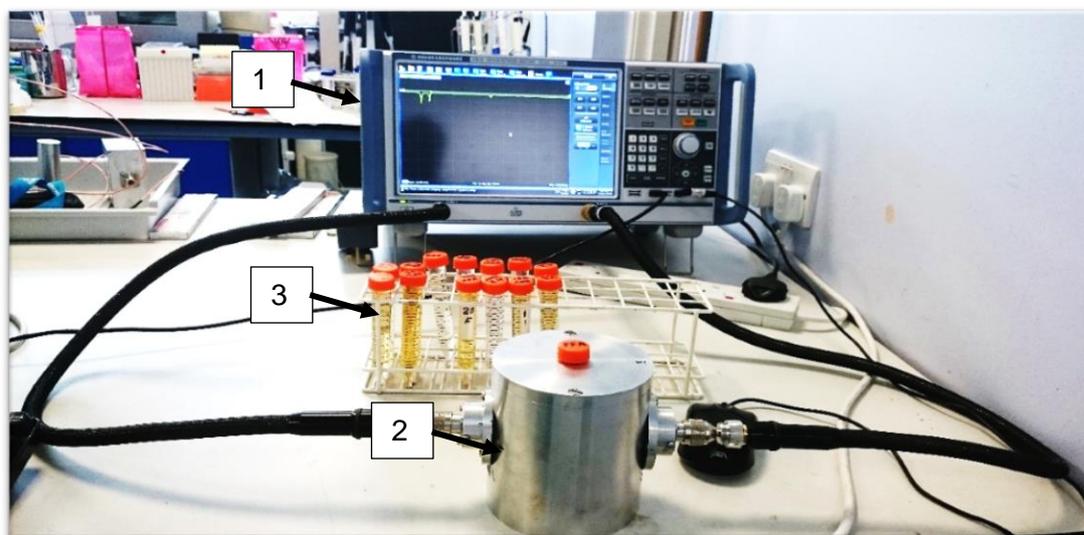
Figure 3-8: Experimental set-up for FFA, M and VO verification.

[1. VNA, 2. Cavity Resonator (Sensor) and 3. Samples]

The sample-filled test tubes (3 in picture) were inserted one by one into the cavity sensor (2 in picture) and the readings were taken by the VNA (1 in picture). Reading cycles were realised (n=10) and recorded in complete format (both real and imaginary) for analyses. It is important to allow for a complete sweep before reading is started and up to three sweeps during the reading period before recording is carried out. Recorded readings were exported for data processing using Microsoft Office Excel. All 10 times readings were summed

together, and a determined average chart was utilised for the processing. Processed data was analysed for regression using Curve Expert software

3.6   Experiments on Determining Properties of Materials

Two distinct methods were utilised for the purpose of determining the properties of the materials used in the experiments. The cavity perturbation method (CPM) was used to determine the complex relative permittivity of all the materials with the exception of methanol. For the determination of the complex permittivity of methanol, the transmission/reflection line method (TR) was suitably utilised as Methanol is a high loss material and the cavity perturbation method is suitable for low loss materials at high frequencies.

3.6.1   Experiments using the CPM

The cavity perturbation method was utilised to determine the properties of most of the materials used in the experiments. To realise this experiment, a specially designed rectangular waveguide cavity was utilised as the sensor. The NMR tube containing each sample of the material was inserted into the middle slot of the waveguide cavity (Figure 3.9) connected to the VNA, which was purposely set to read the transmission coefficient, S_{21}. Readings of the full spectra were then narrowed to a single resonant peak for processing by visually looking at the spectrum alongside the VNA signal processing capability to identify the resonant frequencies. At each reading a snapshot of the peak was taken in a way to preserve the recordings.
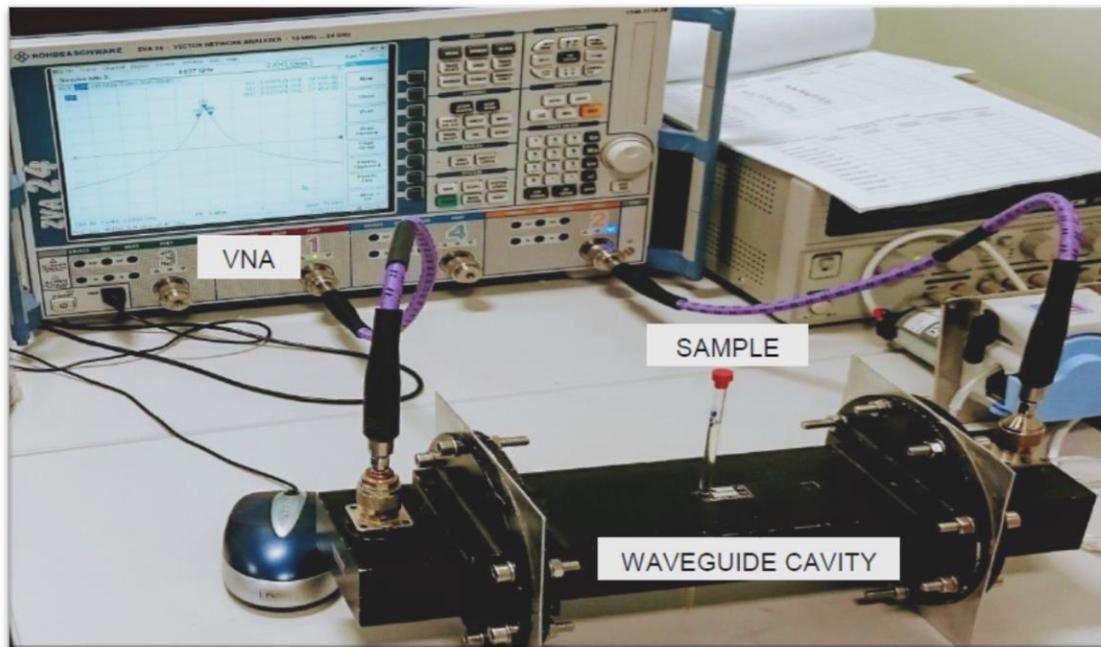
Figure 3-9: Set-up for Cavity Perturbation Experiments

The main active peak of the spectra was selected, and the frequency associated with this was marked alongside the associated amplitude. Then the frequencies corresponding to $\mp$3dB shift from the peak to the left and right sides and their amplitudes were also marked. These marked frequencies and amplitudes, alongside the overall dimensions of the cavity are useful for the tabulation of the dielectric constant, ε' and the loss factor, ε'' using the CPM.

3.6.2 Experiments using TR

Another method used to determine the permittivity of materials, used here purposely to determine the complex relative permittivity of methanol, is the transmission/reflection line method. Due to its volatile nature, a new approach has to be used (please see 3.7). A sample of approximately 100 millilitres of methanol is placed in a container, the bottom of which is sealed with a light duct tape to prevent leakage. The container is fastened with nut and screws and sandwiched between two separate waveguides and connected to the input and output ports of ZVB20 (Figure 3.10).
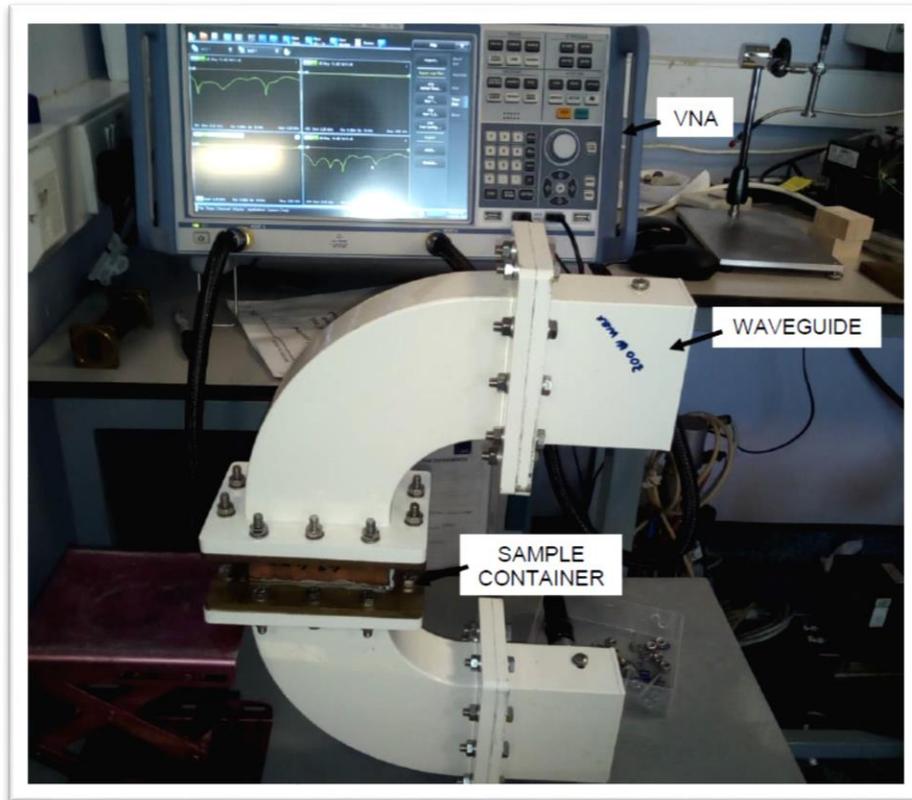
Figure 3-10: Set-up for experiment on transmission/reflection line method

The S-parameter readings were taken and exported for data processing using the Microsoft Excel platform. Data processing here included a series of spreadsheet calculations to determine the dielectric constant, ε' and the loss factor, ε''.

4.0   DESIGN PROCEDURE

4.1   Introduction

The design procedure is different from the methodology and as such does emphasize more on the process of developments leading to the creation of the model of the dielectric spectroscopic sensor. This chapter takes into account the procedure utilised in arriving at the preferred design of the microwave spectroscopic sensor for use in the industrial waste oil recovery system. Figure 4.1 illustrates the flowchart for the design procedure.
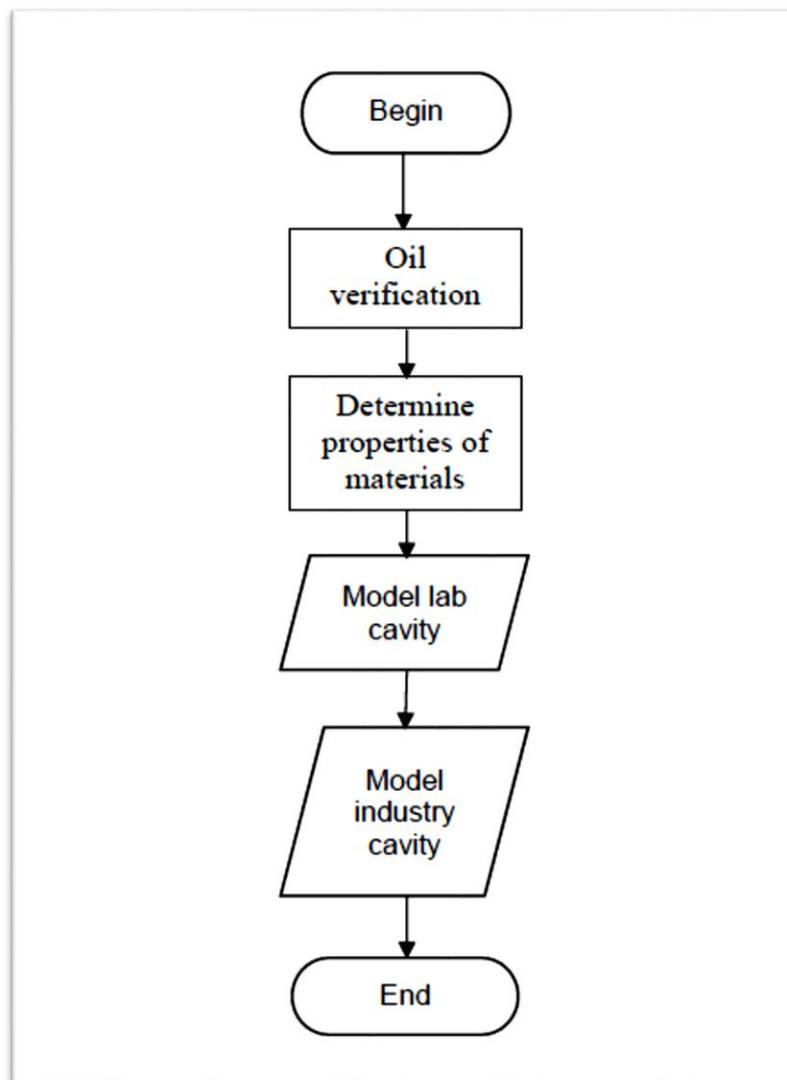

Figure 4-1: Flowchart of design procedure

The process begins with the verification of the oil samples, which are the main materials under test. Determining the electrical properties of the samples used in the lab experiments set the process off and is the way to transfer the physical properties of the laboratory samples into numbers. These numbers are used to represent the samples mathematically in order to model the sensor. They then are also used to facilitate the computer aided simulation of the model.

The modelling of the laboratory work was carried by recreating the geometry of the cylindrical cavity resonator, used for the experiments, as a model that has all the dimensions of the real cavity. The model, which would be translated into physics and numbers and in combination of the determined electrical properties of the sample materials are utilised for the simulation. Furthermore, the values attained in the lab model are scaled up physically and through mathematical formulae to attain the dimensions of the targeted sensor, which is for the industrial waste oil recovery process.

4.2   Determining the Properties of the Materials

The physical properties of the sample materials, such as the relative complex permittivity form part of the design process. The aim here is to determine the physical properties of the samples as used in the experiments and use those for the computer aided simulation. Simulated results would tell us whether the lab experiments are according to expectations.

The dielectric properties of materials used in the lab work were determined by using microwave spectroscopy. Two techniques were essentially applied for that, namely the cavity perturbation and the transmission / reflection line methods.

4.2.1 Application of Cavity Perturbation Method

The cavity perturbation method (detailed in section 3.6) was utilised to determine the complex relative permittivity of the sample materials used in the realisation of the experiments. The main feature of the CPM is the rectangular waveguide cavity resonator (shown in Figure 4.2). The waveguide works under the principles as subscribed in section 3.4.8.

The rectangular waveguide cavity resonator (Figure 4.2), which has two slots (one in the middle and one offset) is used in this work to realise these experiments relating to the CPM.
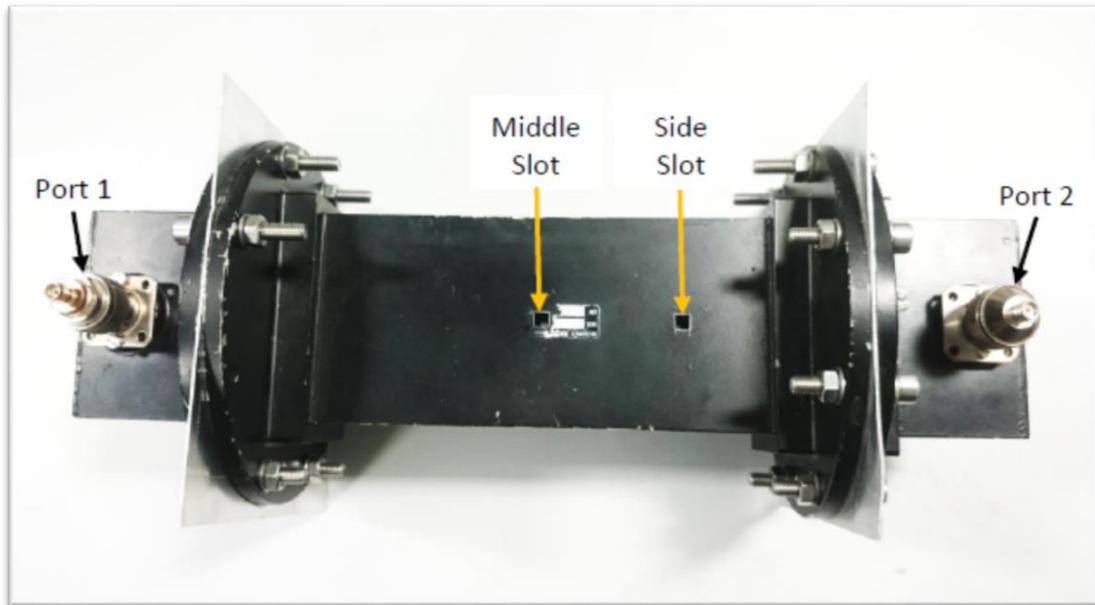
Figure 4-2: The waveguide cavity used for the perturbation method

The transmitted signals in this rectangular waveguide follow the principles as displayed in the transmission line theory (section 3.4). The waveguide is connected to ports 1 and 2 of the VNA. The material under test, consisting of the sample in an NMR tube, is placed in the middle slot for the test to be carried. The spectra generated by the sample material are used for the process data as follows. The full range is worked on by observing the peaks with significant amplitudes and this is further narrowed to a single most active peak.

The frequency and the amplitude of the peak is located and marked, and so are the frequencies corresponding to -3dB and +3dB to the left and right of the peak. The snapshot of each display is taken to preserve the data (Figure 4.3). The complex relative permittivity is determined using the formulae displayed in section 2.6.1. The following section shows an example of the determination of the permittivity, using air sample as an example. Other samples were treated using similar pattern. Figure 4.3 illustrates the snapshot of the peak of the marked frequencies and amplitudes for the determination of permittivity of air sample.

4.2.2 Permittivity of air (Empty tube)
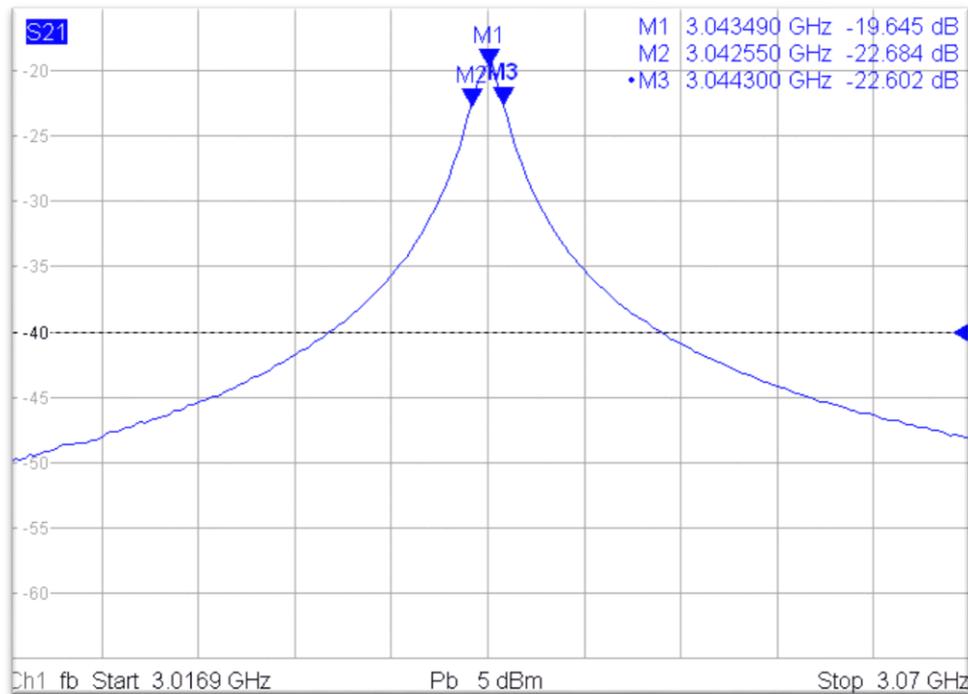
Figure 4-3: Selected peak for permittivity determination of air sample

The permittivity of an empty NMR tube (air) was determined using the CPM. An empty NMR tube was inserted into the sample slot. Then the waveguide cavity was connected to the VNA, which has been set to read the transmission coefficient, S_{21}. The range of the spectra was reduced to a single peak at 3.0435GHz and at -19.645dB. The first marker, M1 has been set on the centre of the peak, the second marker; M2 set to 3dB lower at approximately - 22.684dB corresponding to 3.0425GHz and the third marker, M3, set to 3dB higher at approximately – 22.6023dB and at 3.0443GHz. This enables calculations of quality factor and subsequently the permittivity of the material as discussed in section 4.2.3 below.

4.2.3 The complex permittivity of the sample materials

This method was applied to determine the complex relative permittivity of all the remaining sample materials, namely VO, FFA, ROO and EVOO. Table 4.1 shows the peak data of the frequencies and amplitudes as used for the calculations of the permittivity of the sample materials.

Table 4.1: Peak data for material samples used for the calculations

SAMPLE	ANOTATION	LEFT	CENTRE	RIGHT
AIR	Frequency	3.0425 GHz	3.0435 GHz	3.0425 GHz
	Amplitude	-22.684dB	-19.645dB	-22.6023dB
VO	Frequency	3.0340GHz	3.0354GHz	3.0370GHz
	Amplitude	-27.801dB	-24.772dB	– 27.762dB
FFA	Frequency	3.0374GHz	3.0362GHz	3.0351GHz
	Amplitude	– 25.213dB	-22.179dB	-25.296dB
ROO	Frequency	3.0340GHz	3.0354GHz	3.0370GHz
	Amplitude	-27.788dB	-24.725dB	– 27.717dB
EVOO	Frequency	3.03395GHz	3.03565GHz	3.0371GHz
	Amplitude	-27.709dB	-24.743dB	– 27.632dB

The complex permittivity of the materials was arrived at using the values obtained from the air and also using the dimensions of the containers, the waveguide and the NMR tube. The volume of the rectangular waveguide, V is $4.9104 \times 10^6 \, mm^3$, whilst that of the NMR tube, v is $4.5817 \times 10^2 \, mm^3$. Using equation (3.6) and (3.7) the Q factor values were determined, and finally with (3.8) and (3.9) the dielectric constant, ε' and loss factor, ε'' were determined. As a result, the dielectric constant and loss factors of the following materials were attained. Table 4.2 displays the determined relative complex permittivity of the sample materials.

Table 4.2: The relative complex permittivity of materials as determined

Material	Dielectric Constant, ε'	Loss factor, ε''	Permittivity, ε
VO	2.3859	0.1151	2.3859+j0.1151
FFA	2.2708	0.0445	2.2708+j0.0445
ROO	2.3947	0.1151	2.3947+j0.1151
EVOO	2.5536	0.1108	2.5536+j0.1108

4.2.4 Application of Transmission/Reflection Line Method

Applying the TR method (section 3.7) allows for determination of the complex permittivity of the sample of methanol. The parameterisation of the dielectric properties of methanol using the single Debye function can only be valid over a limited frequency and temperature range, for which reason careful attention has to be given to the use of the liquid. Safety standards and guidelines are therefore to be adhered to at all times.

A container was filled with the liquid, methanol, of approximately 100 millilitres. A tiny flexible tape (with not much influence on the material) was used to seal the bottom of the cavity to prevent leakage. The container was then fastened with nuts and screws and tightened with the aid of spanners to the mid-section of the waveguide between ports 1 and 2. The signal was transmitted through the liquid to read the transmitted and reflected powers. Figure 4.4 illustrates the sketch of the cross section of the waveguide containing the sample, using adhesive tape to seal the bottom.
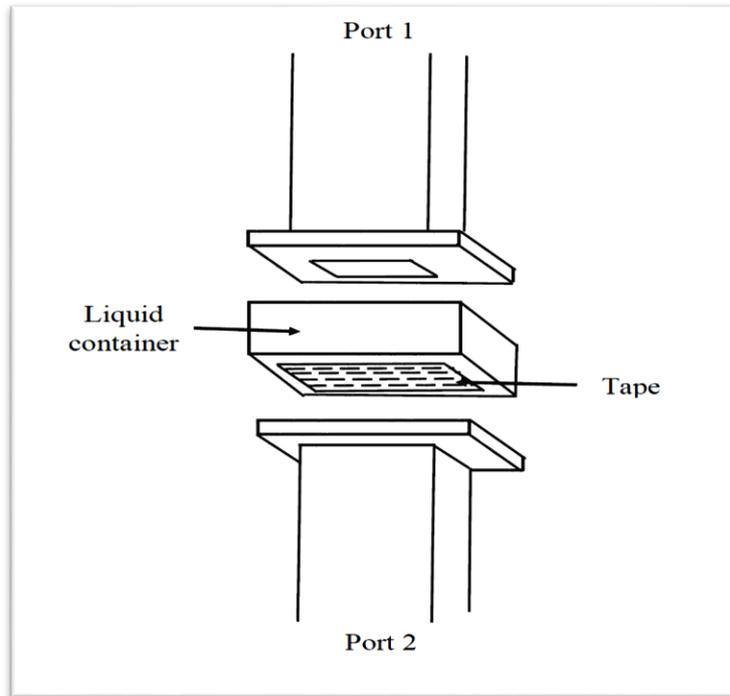
Figure 4-4: Cross section for TR measurement using tape sealed container

A series of frequencies and the corresponding S_{21} readings were recorded and used for tabulating the results. Using equations (3.69) – (3.82) in section 3.7, the various parameters were determined and plotted. The results then were corroborated using the Debye model and verified by comparing with results from a National Physics Laboratory (NPL) report. The complex relative permittivity of methanol was attained using this method, and is shown in table 4.3.

Table 4.3: The complex permittivity of methanol at 20ºC

Material	Dielectric Constant, Ɛ'	Loss factor, Ɛ"
M	21.33	13.89

4.3   Modelling of the Lab Cavity

The cylindrical cavity resonator was used as the sensor to realise all the experiments in the laboratory. The model of the Cavity consists of two cylinders representing the resonator and the sample tube. The heights of both cylinders are aligned with the *z*-axis. The radius of the resonator is taken to be 6 cm and the height is 10 cm. The cylinder representing the sample tube has the radius of 0.4 cm and the height of 10 cm. Two ports representing input (Port 1) and output (Port 2) ports. Figure 4.5 illustrates the lab model of the cavity resonator used for the computer aided simulation.
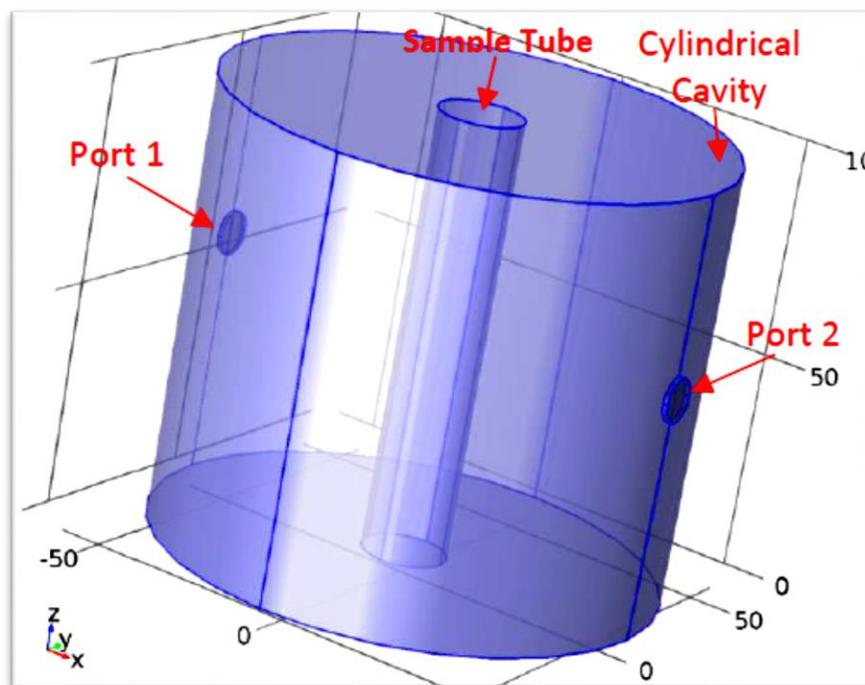
Figure 4-5: model of lab cavity resonator used for the simulation

A total of 3 space dimensions, 6 domains, 32 boundaries, 58 edges and 34 vertices were generated for the model and used for the calculations. Cavity boundaries made of an aluminium conductor and that of the sample tube of a non-conductive polyvinyl (PVC) material were declared in the software.

4.3.1   Mesh Selection

Similar to the standard cavity model, the industry model of the cavity uses an auto generated mesh to enhance the refinement of its elements. Table 4.4 shows the mesh set-up for the lab model using the free tetrahedral.

Table 4.4: Mesh set-up for lab model

Element	Size
maximum element size	6.66
minimum element size	0.484
curvature factor	0.4
resolution	0.7
growth rate	1.4

For the selection of the mesh a free tetrahedral was selected to allow for finer but not too complicated resolution. Figure 4.6 illustrates the mesh set-up for the study of the lab model.
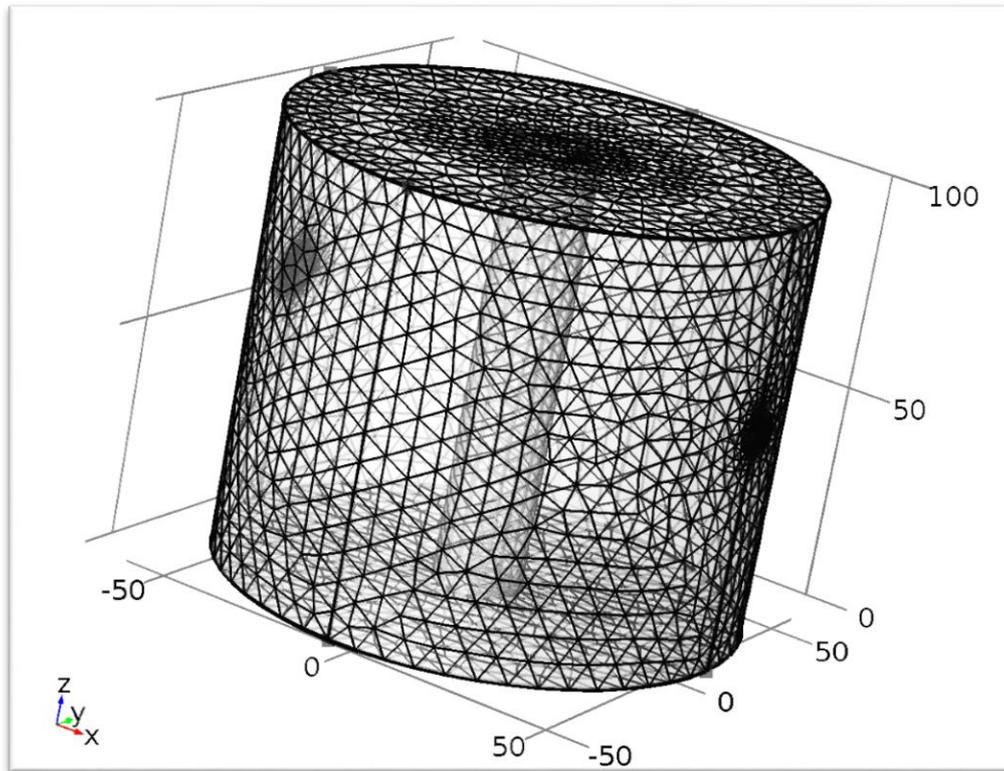
Figure 4-6: Mesh for the study of the lab cavity model

4.3.2 Sample domains

When relative permittivity is selected, the default relative permittivity takes values from the material used. The inbuilt refractive index, remnant electric displacement, relative permeability, flux density, magnetisation, resistivity, and conductivity of the material have all been preselected in the software. For the air sample domain, the inbuilt relative permittivity, $\varepsilon = 1$ was utilised. Figure 4.7 illustrates the normalised electric field distribution of the air sample domain.
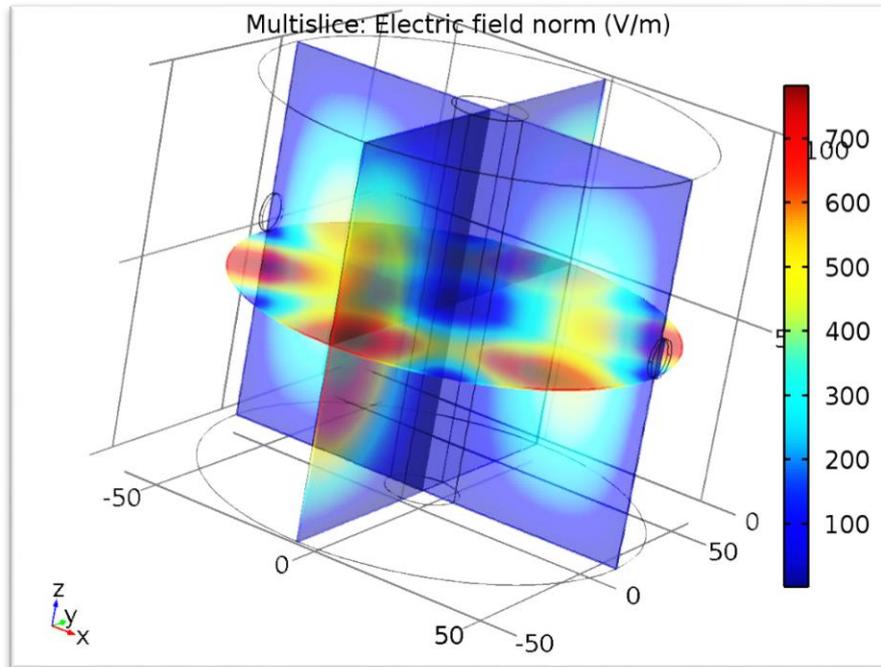
Figure 4-7: Electric field distribution in air sample domain

For the VO sample the main cavity domain area remained air, instead, the sample domain area was changed to reflect the sample material, in this case vegetable oil. The mesh settings remain the same, and for vegetable oil sample domain the relative permittivity used is Ɛ=2.3859+j0.1151, as determined in the laboratory and at the normalised frequency of 2.3887GHz.

For the FFA sample the main cavity domain area remained air, instead the sample domain area was changed to reflect the sample material of FFA. The relative permittivity used for FFA is Ɛ=2.2708+j0.0445 and at the normalised frequency of 2.3924 GHz.

For the methanol sample domain, the relative permittivity used is Ɛ=21.33-j13.89 at the normalised frequency of 2.313 GHz.

4.3.3 S-Parameter Plots

In this model, there are two ports with the numbers 1 and 2, and Port 1 is the input port, the software generates the variables S_{11} for the reflected power. For expediency, the variables for the S-parameters on a dB scale, S_{11}dB, is also defined using the following relation:

$$S_{11(dB)} = 20 \log 10 \left(|S_{11}|\right) \tag{4.1}$$

The S-parameter variables are inserted to the predefined quantities in applicable plot lists.

$$S_{11} = \sqrt{\frac{Power\ reflected\ from\ port\ 1}{Power\ incident\ on\ port\ 2}} \tag{4.2}$$

4.4   Modelling for Industry

Having obtained significant values from the experiments, having used those values to simulate the lab and having ascertained the validity of the model in comparison to the experiments, it is in order to model the industry system using these values. Conditions imposed here include, but are not limited to, the adjustment of volume, and addition of flow system capability.

The system is to enable the monitoring of the pre-esterification part of the process. The amount of free fatty acids in the oil, the amount of methanol used to leach out the fatty acids in the oil, and the amount of fatty acids mixed in the methanol. Figure 4.8 illustrates the process flow diagram of the industry sensor system.
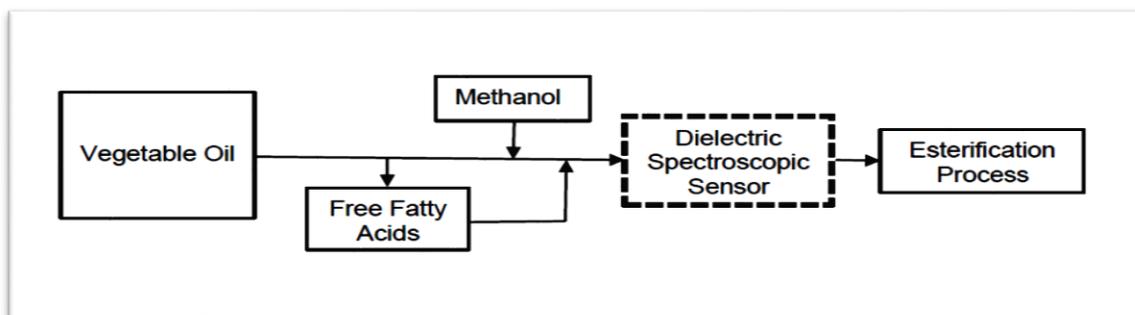
Figure 4-8: Process flow diagram for industry sensor system

The question of the dimensions of the cavity could be addressed in two ways; one is to take into consideration the actual dimensions of the pipeline and build a cavity proportional to it. The other alternative is a flexible system that could continuously draw samples from the pipeline, supply the cavity sensor and feedback into the system. The second alternative was chosen since it is much more adaptable and can be implemented everywhere. It allows for the laboratory system to be scaled using existing dimensions. Figure 4.9 illustrates the design concept for the industry cavity resonator system.
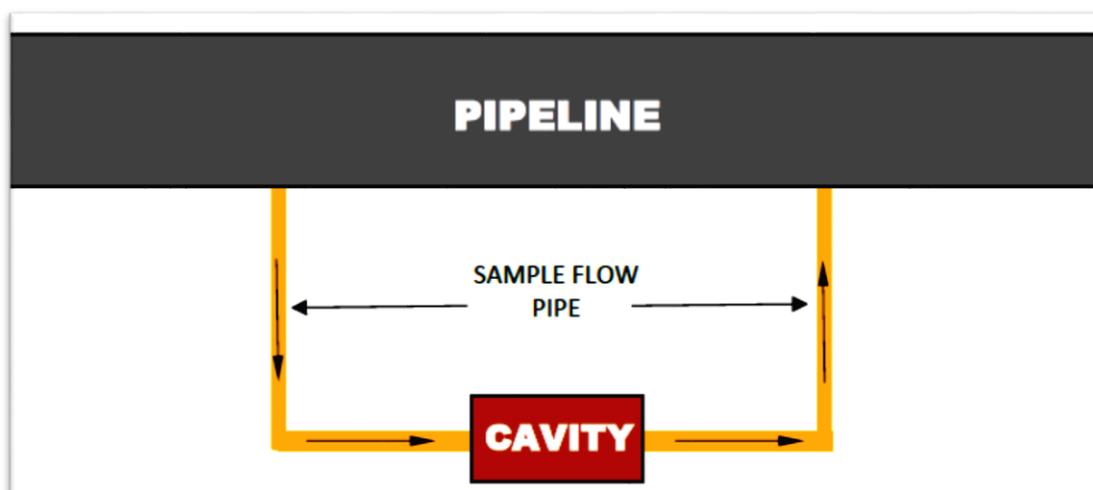
Figure 4-9: Concept design of industry resonant cavity sensor system

For the flow, a smaller pipeline would draw the sample to be measured, from the main pipeline through into the midsection of the cavity and return the sample back to the line without any influence on the content. This would allow the system to perform just as the test tube does in the lab system, but at the same time allowing for a continuous flow. The real-time feature of microwave technology is herein applied. Microwave spectroscopy allows for real-time readings at the same time as the continuous flow takes place.
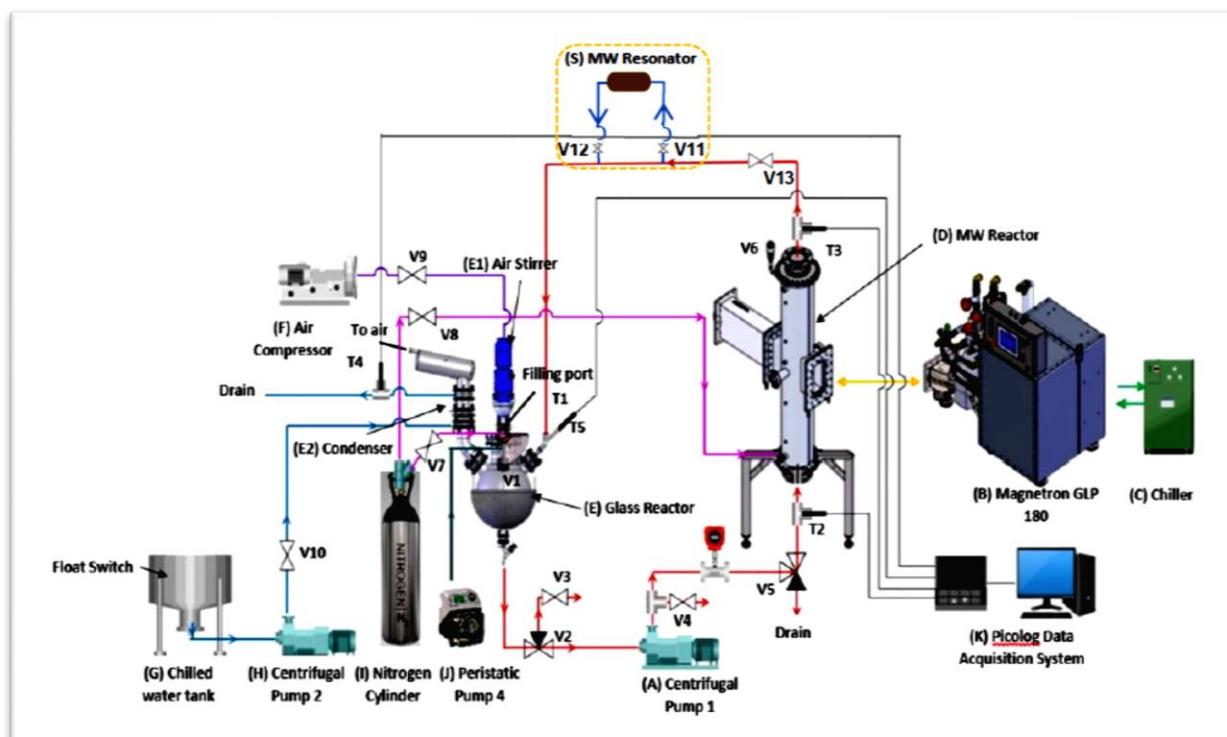
Figure 4-10: P&ID of Biodiesel Process showing how sensor system will fit in industry

Figure 4-10 illustrates the P&ID of a biodiesel plant indicating where the sensor will fit in the industry. The microwave sensor (S) is in the dotted yellow square. Connected after the reactor (D). A differential measurement would allow the microwave impact to be assessed. The flow is $1m^3$/hr and the temperature is maintained at 73°C. As this is a pumped system, the valves V11 and V12 will allow a small sample to flow through the sensor whilst the main flow stays in the full pipe.

4.4.1 The Scale of the model

The industrial model of the cavity sensor was scaled based on Bessel functions and using equations 3.45-3.54 of section 3.4.9.1. The essence of the design of a cylindrical cavity is to determine the Q-factor and resonant frequency for which the dominant mode is requisite. The mode applied here is TM_{010} because the ratio between the height and radius is $1 < 2.03$, for which the Q-factor is determined by

$$Q_{TM_{010}} = \frac{\eta}{R_S\left(1+\frac{a}{h}\right)}.$$

(4.3)

Where

a is the radius

h is the height

R_S is surface resistance

η is the characteristic impedance of free space

the resonant frequency is determined by

$$f_{TM_{010}} = \frac{1}{2\pi\sqrt{\mu\varepsilon}} \sqrt{\left(\frac{2}{a}\right)^2}$$

(4.4)

The resonant frequency of 2.3562 GHz was attained and the Q-factor value of 7856 was attained using equation 3.67 and 3.68 respectively of section 3.61. Table 4.5 displays the values of the Q-factor and the resonant frequency of the model.

Table 4.5: Values attained for Industry model of the cavity resonator

Resonant Frequency	Q-Factor
2.3562 GHz	7856

Since, the developed sensor and proposed flexible design arrangement only draws a sample from the main line, the dimensions and subsequently the measurement frequencies, i.e. resonant frequencies, will effectively remain the same. The benefit being the sensor will maintain the performance of the original sensor.

4.4.2 Geometry of the industry model

The dimensions of the interior part of the cylinder that constitutes the main cavity, after scaling should measure, radius of 300mm and height of 300mm. the sample pipe should measure 26mm radius and run across the total length of the main cylinder. The geometry has 3 dimensions, 2 domains, 40 boundaries, 74 edges and 42 vertices. It has been oriented on the x-axis to go with the flow system. Figure 4.11 illustrates the AutoCAD drawing of the proposed prototype industry-based cavity with the assigned dimensions.
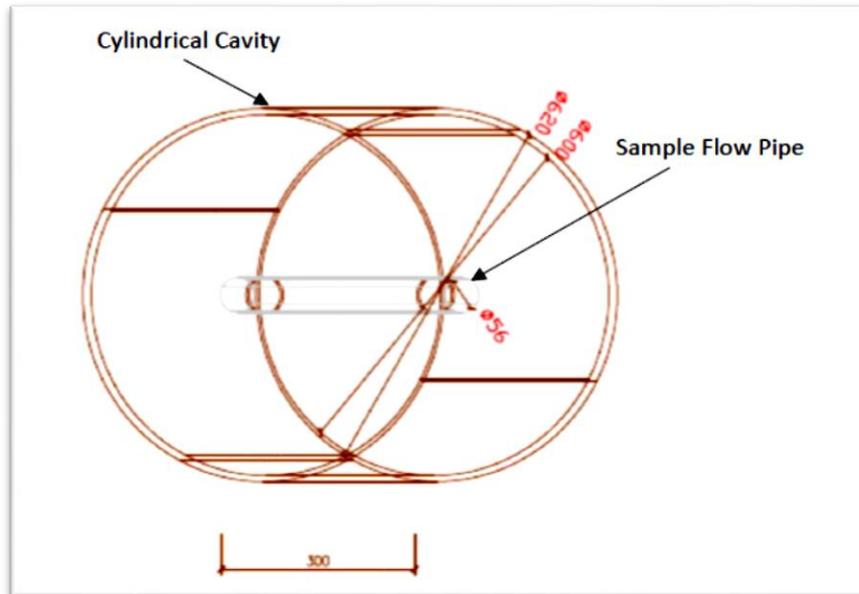
Figure 4-11: AutoCAD design of industry-based prototype cavity with dimensions

Conditions followed for the physics of this work were the same as preparations done with the laboratory work. The only change here is the axis, which now lays in the x-axis. This horizontal orientation is necessary because the design takes recognition of the flow of the fluid through the pipe. In the experimental work test tubes were utilised and had to stand upright inside the cavity, hence the vertical orientation. Figure 4.12 illustrates the 3D geometry as inputted for the model simulation showing the different parts of the cavity, the sample pipe and the input and output ports.
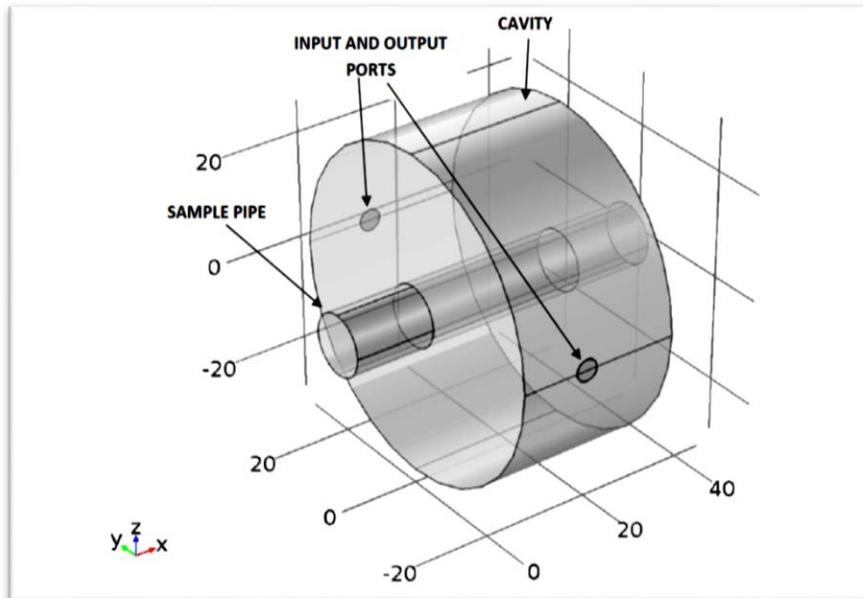
Figure 4-12: COMSOL® generated geometry of industry cavity model

4.4.3 Mesh creation of the industry model

For the selection of the mesh a free tetrahedral mesh option was selected to allow for finer yet processing efficient resolution. Table 4.6 shows the proposed mesh set-up parameters and their values for the industry model using the free tetrahedral option. Figure 4.13 illustrates the outcome of the finer mesh set-up.

Table 4.6: Mesh set-up for industry model

ELEMENT	SIZE
maximum element size	4.5
minimum element size	0.81
curvature factor	0.6
resolution	0.5
growth rate	1.5
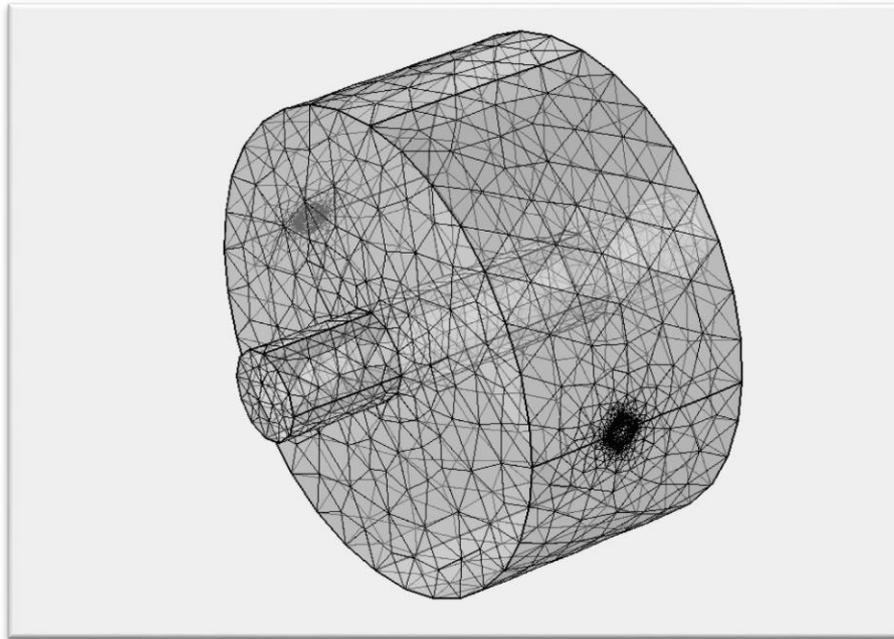
Figure 4-13: Mesh setup for model simulation

4.4.4 Physics of the model

The frequency domain electromagnetic wave study was utilised with allocated frequencies ranging from 2.4 to 3.4 GHz and intervals of 1 MHz in between. The initial results of the laboratory work dictated the chosen frequency range. Table 4.7 shows domain parameter settings using the properties of the copper material (domain).

Table 4.7: Basic settings for copper domain

DESCRIPTION	VALUE
Relative permeability	1
Electrical conductivity	$5.998 \times 10^7 [S/m]$
Coefficient of thermal expansion	17×10^{-6} 1/K
Heat capacity at constant pressure	385[J/(kgK)]

DESCRIPTION	VALUE
Relative permittivity	1
Density	$8700[kg/m^3]$
Thermal conductivity	400W/mK,

5.0 RESULTS

5.1 Introduction

This chapter outlines the results of the work carried out on the various experiments as attained. For clarity of purpose these are subdivided into different formats, beginning with oil verification and culminating in the design for industry. The oil verification has two facets, one is the differentiation and the other is authentication. Then came the formation of the waste oil recovery process, under which different permutations of samples to assimilate the process are evaluated.

Modelling and simulating of lab work gave out some results. The various sample materials were evaluated independently and as a mixture with others. The electromagnetic aspects of all the sample domains were measured and the electric field distribution observed in its different forms. Plots from simulated models were extrapolated and compared with actual plots of the experiments.

The results of the design of the industry model also feature in this chapter. It shows the results of scaling, modelling and simulation of the industry model. Aspects of the electric field distribution and the S-parameter plots were attained using the normalised frequencies used in the lab model.

5.2 Oil Verification

Oil verification was carried out in a two-fold process consisting of differentiation and the dilution of EVOO, and the results are as follows in section 5.2.1 and 5.2.2.

5.2.1 Differentiation of Oil Samples

Different oils from the supermarket were tested to verify their difference. The results indicated that each of the samples displays a distinct character signal spectrum from the rest except the Groundnut oil and the Extra virgin oil showing minor differences. Figure 5.1 shows

the results of the microwave spectra readings between 2 and 5.5 GHz of the different samples of the oils, sunflower, grape seed, groundnut and the 4 different forms of olive oils.
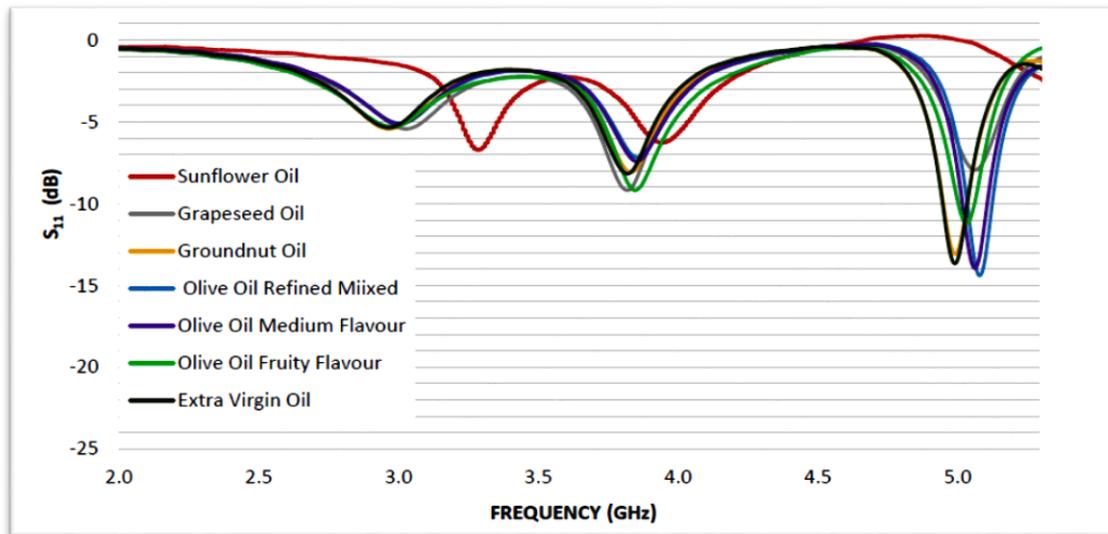

Figure 5-1: Microwave Spectra verifying differences in vegetable oils

The test results (as illustrated in Figure 5.1) show that each sample presented unique signal spectra with some needing advance analysis techniques to provide a clear difference between samples, paving the way for potential identification of different oils with this method. One could see patterns and sequences in the peaks between 3.5 and 4 GHz and around 5GHz zone. The values of frequency associated with these peaks could be valuable analytical tools for further investigations and could be handy when it comes to the development of electronics. It also means that with this capability, the microwave sensor system can verify the differences in supermarket oils.

5.2.2 Dilution of Extra Virgin Oil with Sunflower Oil

The dilution of EVOO was carried using same sample preparation with two different techniques, microwave spectroscopy and spectrophotometry and the results are shown as follows in section 5.2.2.1 and 5.2.2.2.

5.2.2.1   Microwave Spectroscopy Approach

The spectra of the microwave spectroscopic readings show the peaks of the samples with a drop pattern in amplitude as the percentage of the dilution increased of the extra virgin olive oil. Figure 5.2 illustrates the microwave spectra of SFO percentages in EVOO.
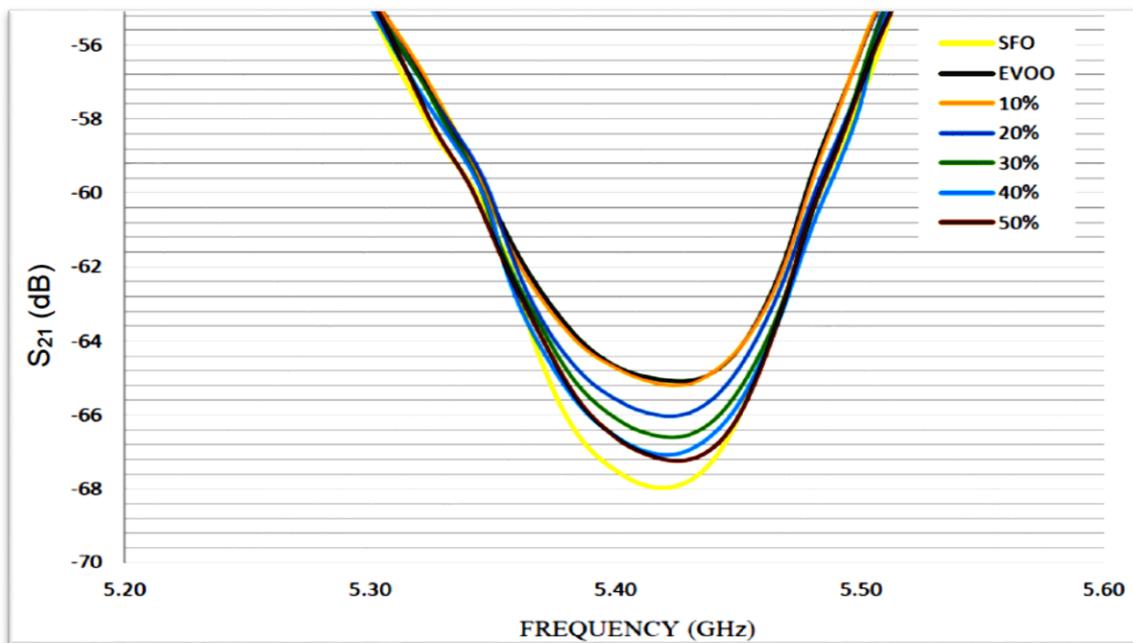

Figure 5-2: Microwave spectra of mixtures of SFO (0-50%) in EVOO

The frequency range from 5.20 GHz to 5.60 GHz was selected from the direct sorting of the peaks with higher amplitude and greater level of activities of interest converging in the area. The frequency of 5.42 GHz is used here, as a reference line in order to regress the values of the amplitudes against the percentages of concentration of the sample mixture. This allows for the establishment of the linear relationship for statistical analysis. Figure 5.3 illustrates the regression plot of SFO in EVOO at 5.42 GHz using microwave.
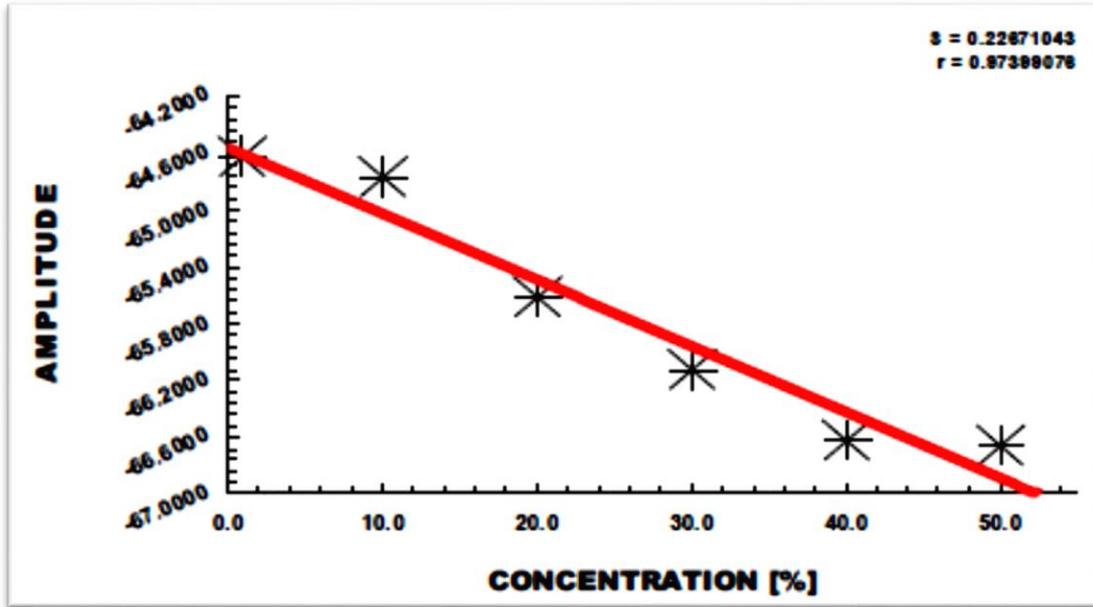
Figure 5-3: Regression plot of concentration of SFO in EVOO 5.42GHz using µW spectroscopy

5.2.2.2 Spectrophotometer Approach

The spectrophotometric readings show a pattern of ascendance in the amplitude of the absorbance with the increase in the percentages of concentration of the mixture. Figure 5.4 illustrates the spectrophotometric readings of the mixture SFO in EVOO.
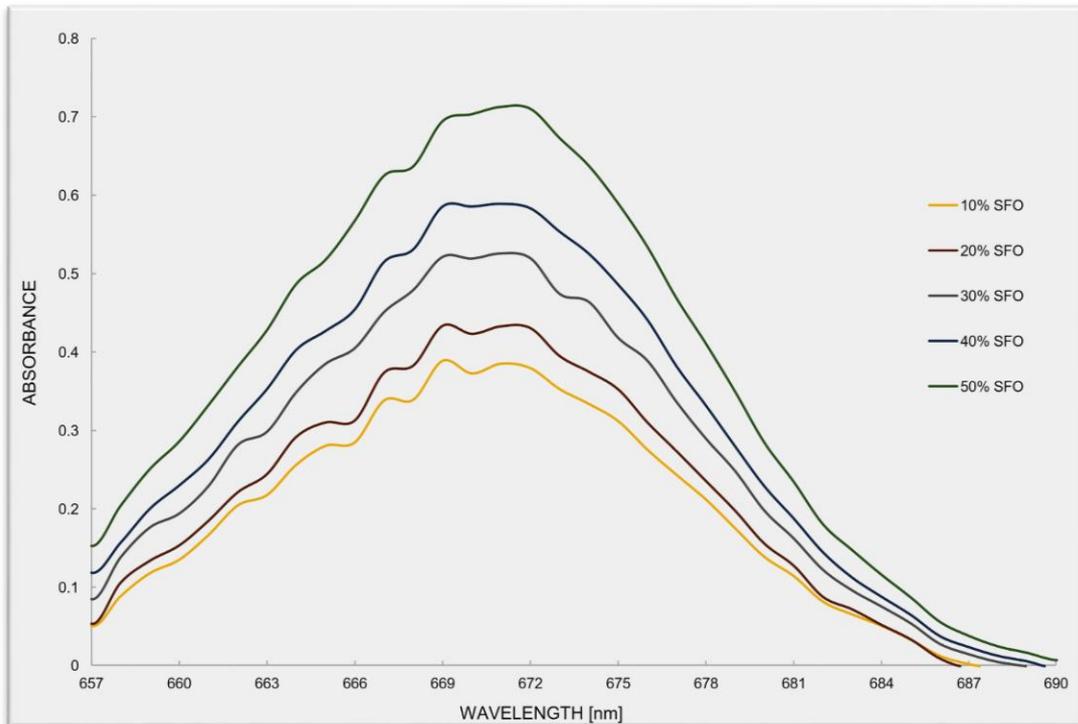

Figure 5-4: Spectrophotometer readings of mixtures of SFO (0-50%) in EVOO

The wavelength of 670nm was utilised as a reference line to regress the percentages of concentration against the amplitude of the absorbance of the sample mixture. Figure 5.5 illustrates regression of percentages of concentration against the amplitude of the mixture using the spectrophotometer.
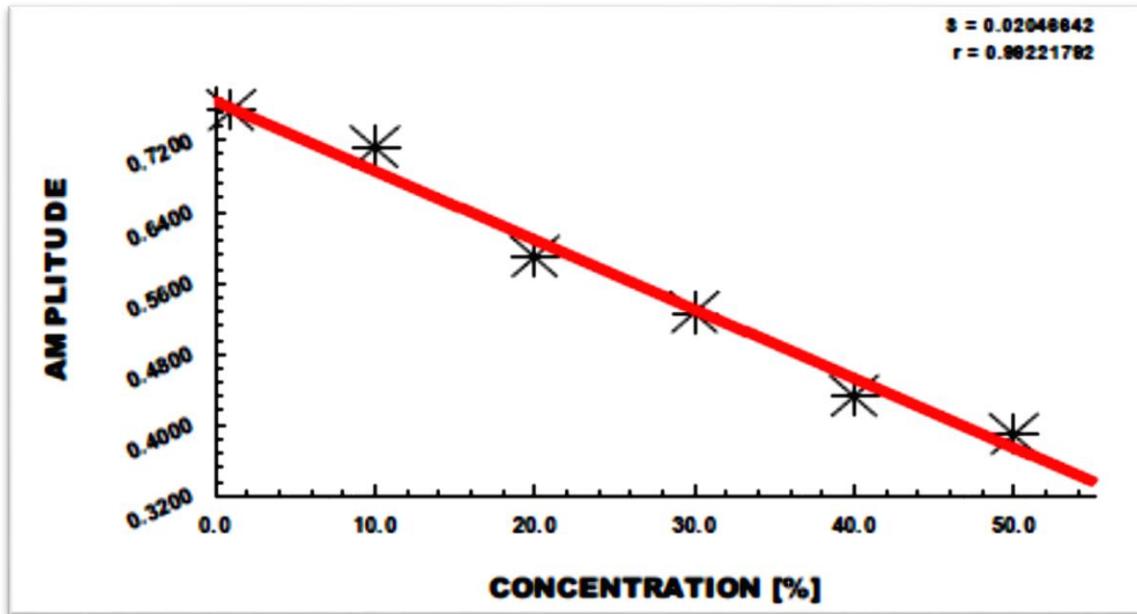

Figure 5-5: Regression plot of concentration of SFO in EVOO at 670nm using spectrophotometer

5.3   Formation of Waste Oil Recovery Process

For the results of the measurements on the formation of the waste oil recovery process, samples were measured of VO, FFA and methanol, after which combinations of their mixtures were carried. Section 5.3.1 to 5.3.6 show the results relating to this. Even though nothing was required out of the results of the individual samples, the spectra of the S_{11}-parameter readings are significant for comparing with the S-parameter plots generated from the simulated model, as.in section 5.5. Section 5.4 is dedicated to the results of the lab cavity model simulation and 5.6 is for the industry model.

5.3.1   Sample of 100% Vegetable Oil

The results from the laboratory work carried on the VO sample gave a peak with amplitude of approximately 25 dB at the frequency of 2.3887 GHz. Figure 5.6 illustrates the signal spectra of the VO sample attained from the lab tests.
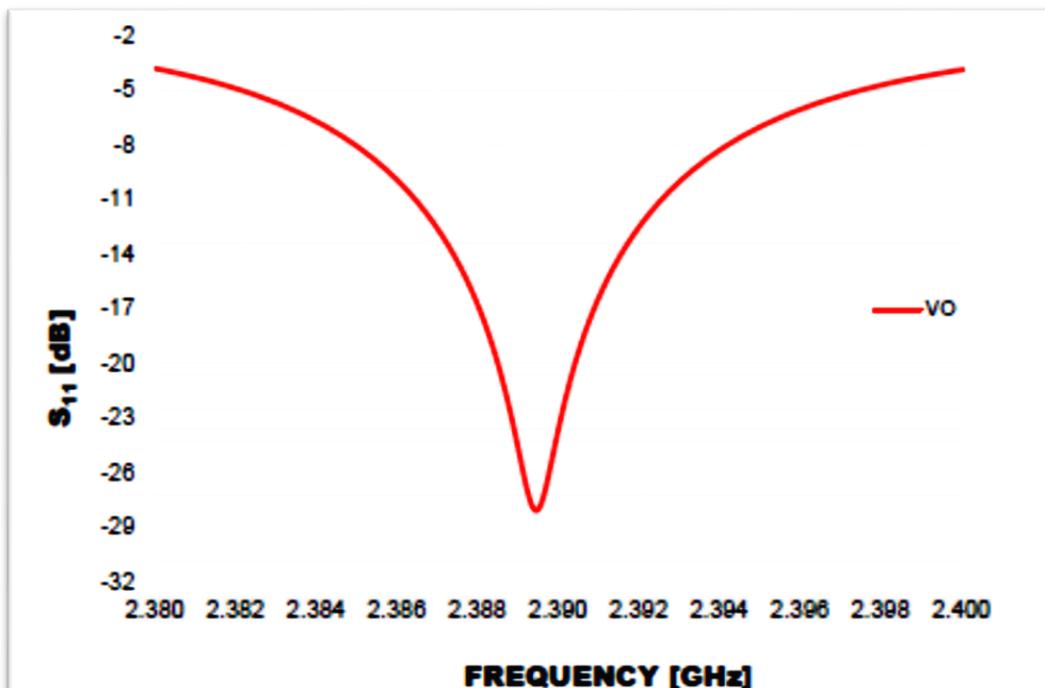

Figure 5-6: S_{11} parameter plot of 100% VO from experiments

5.3.2 Sample of 100% FFA

The results from the laboratory work carried on the FFA sample gave a peak amplitude of about 12 dB at the reference frequency of 2.3924GHz. Figure 5.7 illustrates the signal spectra of the selected peak of FFA sample from the experiments.
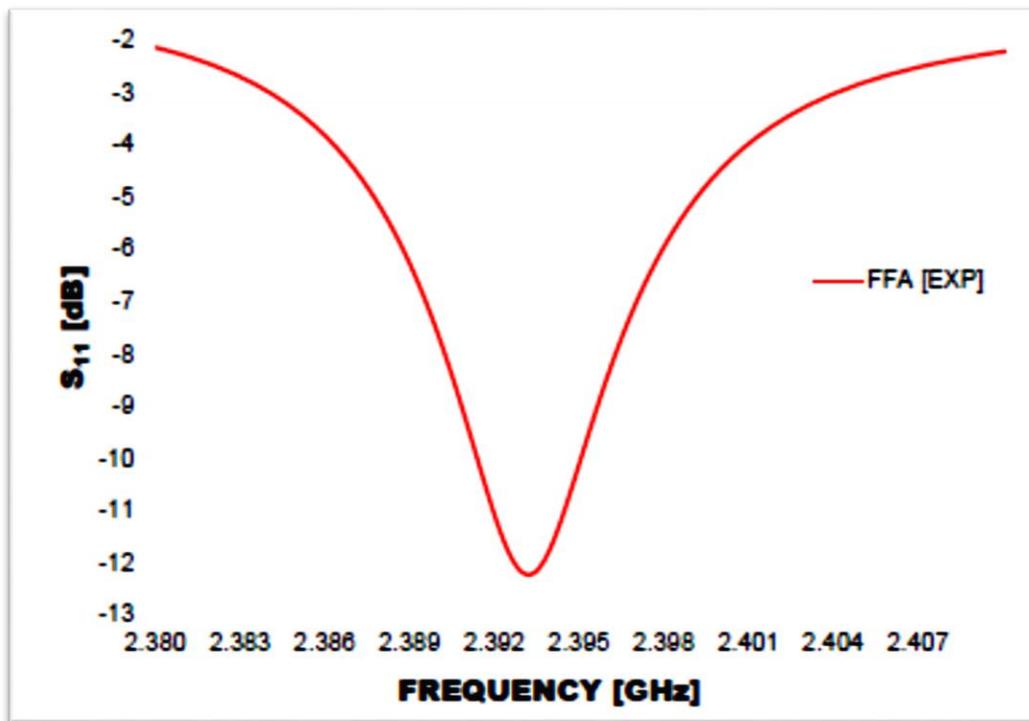

Figure 5-7: S_{11} parameter plot of 100% FFA from experiments

5.3.3 Sample of 100% Methanol

The results from the laboratory work carried on methanol gave a peak of about 1.5 dB at the frequency of 2.313GHz. Figure 5.8 illustrates the signal spectra peak of 100% methanol from the lab experiments.
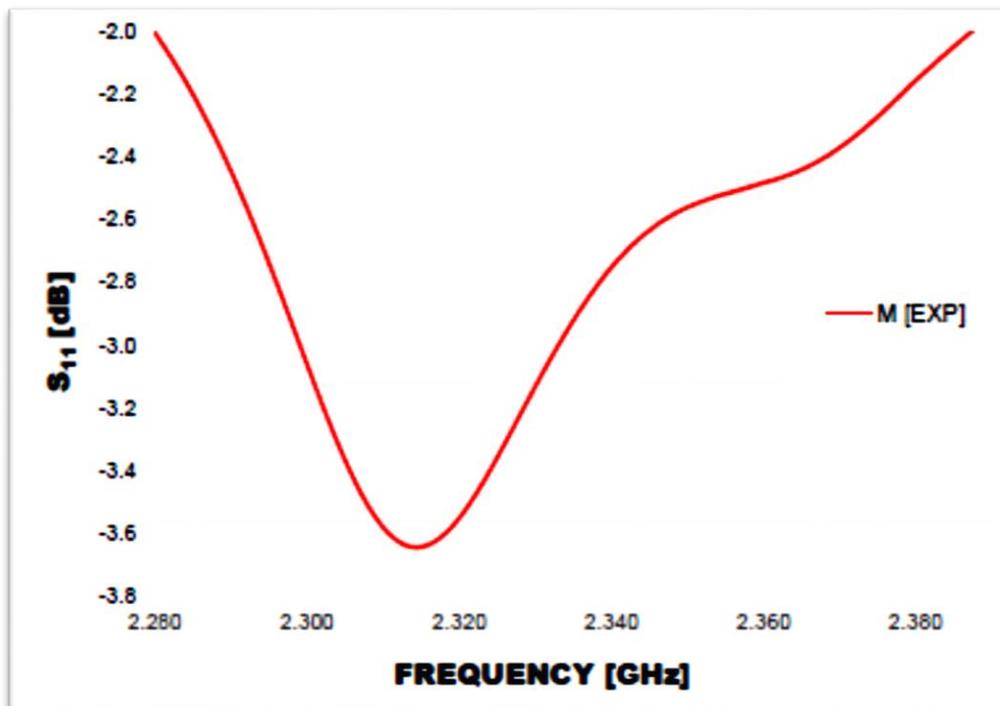
Figure 5-8: S_{11} parameter plot of 100% Methanol from experiments

It is of interest to observe the narrow peak amplitude in the methanol sample. Compared to the samples of VO and FFA, it is quite negligible. This is characteristic of the volatile sample material which tends to flatten in its spectra, The reason for which is that CPM is not performed on it but rather TR. The perturbation method operates on peaks. Figure 5.9 paints the picture of the combined samples, showing the difference in peaks and positions.
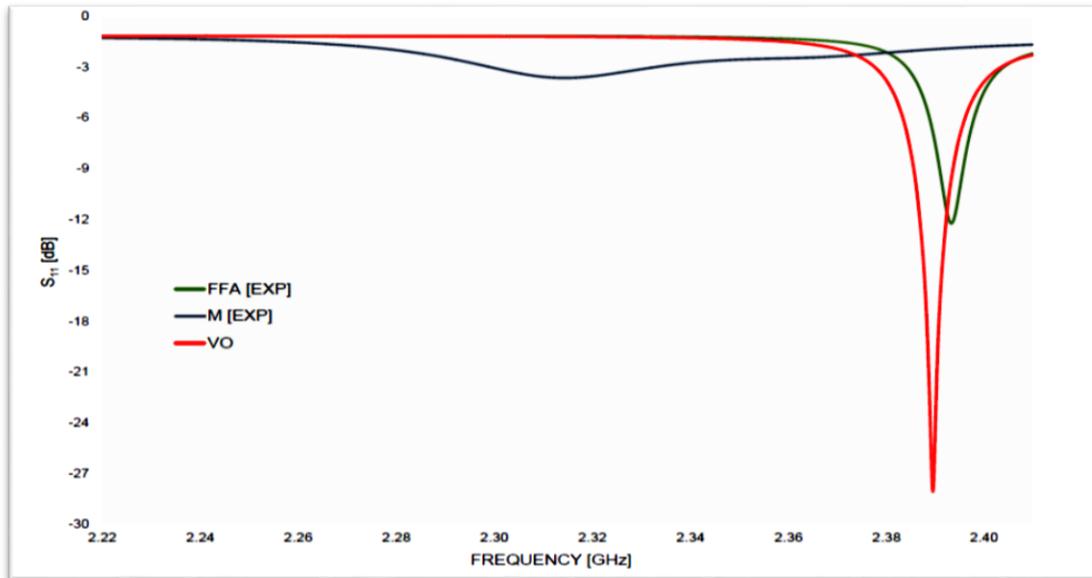
Figure 5-9: The spectra of the combined FFA, M and VO

5.3.4 Mixture of FFA in VO (FO) Sample

At the frequencies of 2.36 to 2.42GHz and at the amplitude of -9.65 to -15.67dB are the peak spectra that represent FO sample. Figure 5.9 illustrates the signature spectra of the sample mixture in percentages of 2.5 to 17.5 of FFA in vegetable oil.
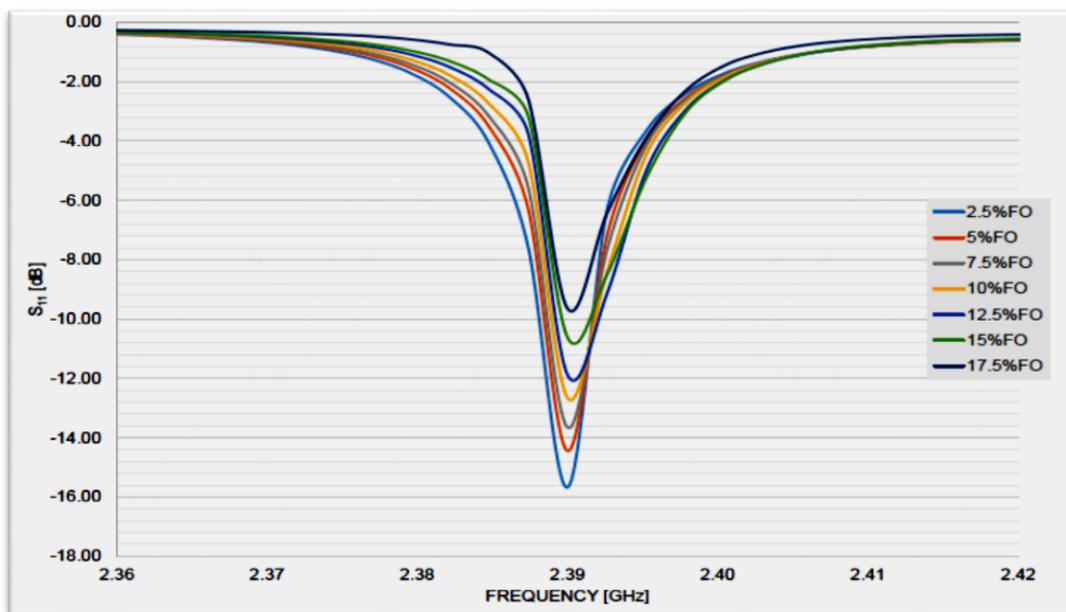

Figure 5-10: Spectra of samples of 2.5 to 17.5 percentages of FO

The regression of the percentages of concentration was realised against the amplitudes of the reflected power, S_{11} of the sample mixtures, using the reference frequency of 2.39 GHz. Figure 5.11 represents the plot of regression of the FO sample.
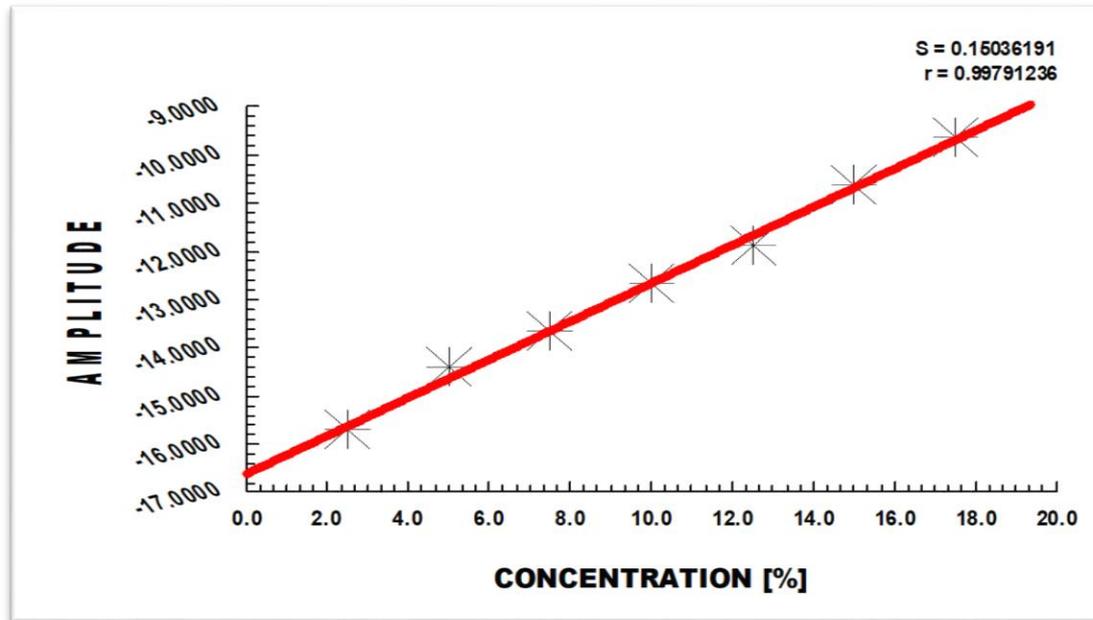

Figure 5-11: Plot of regression of the FO samples at 2.39 GHz

5.3.5   Mixture of FFA in M (FAM) Sample

The spectra of the mixture of FAM sample is shown in Figure 5.12. Frequencies ranging from 4.700 to 4.730 GHz and the relative peak amplitudes of -11.6095 to -13.5459 representing 2.5%, 5%, 7.5%,10%, 12.5%, 15% and 17.5% of FAM are shown.
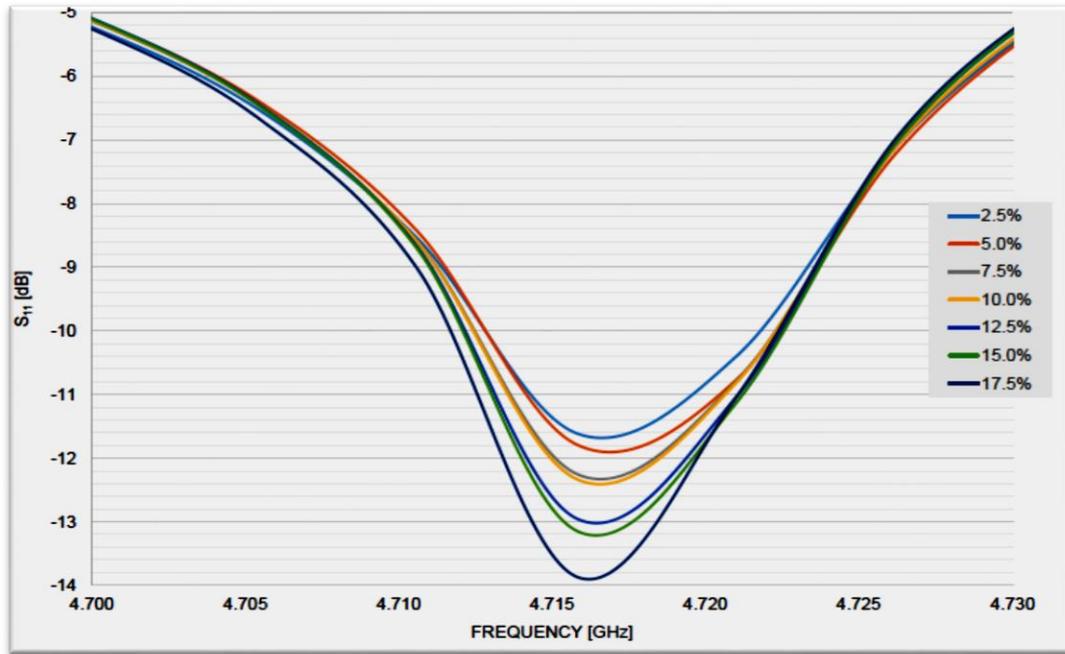
Figure 5-12: Spectra of 2.5 to 17.5 percentages of FAM sample

The correlation of the peak of amplitudes was realised against the percentages of concentration of the mixture sample. The frequency of 4.717 GHz is used as a reference line for the regression using linear fit. Figure 5.13 represents the regression plot of the FAM sample.
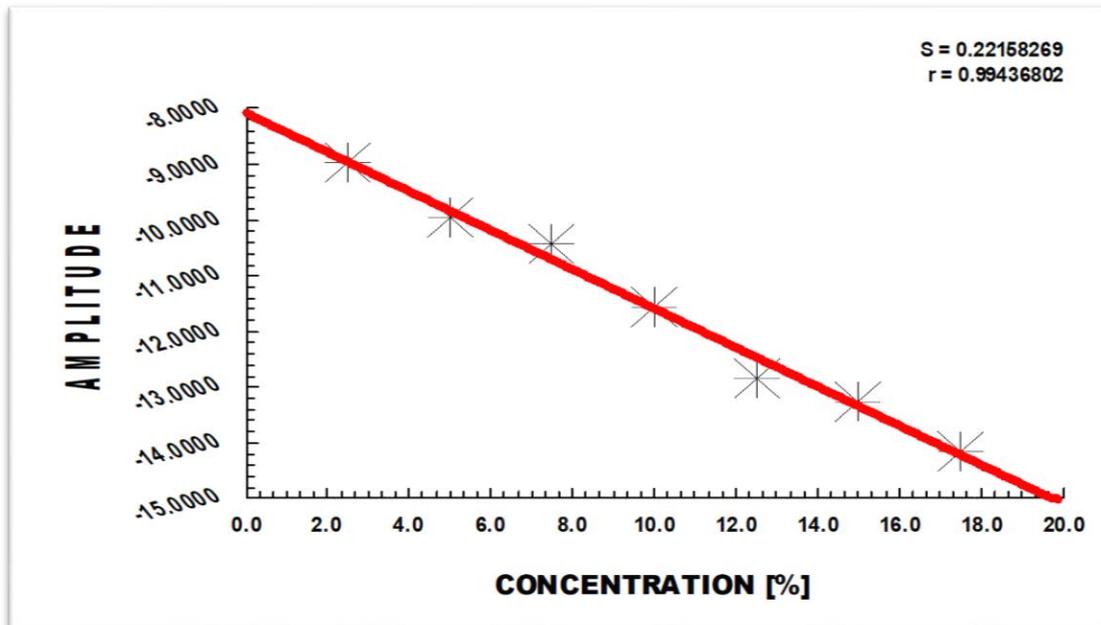

Figure 5-13: Plot of the concentration of the mixture of FFA in M at 4.717 GHz

5.3.6 Mixture of Methanol in Vegetable Oil (MO) Sample

Representing the combination of vegetable oil and methanol and frequencies ranging from 3.63 to 3.65 GHz and -11 to -34 dB peak amplitudes is the selected spectra of 50%, 52.5%,55%, 57.5%, 60%,62.5%,65%,67.5%, and 70% of MO). Figure 5.14 represents the spectra of the MO sample.
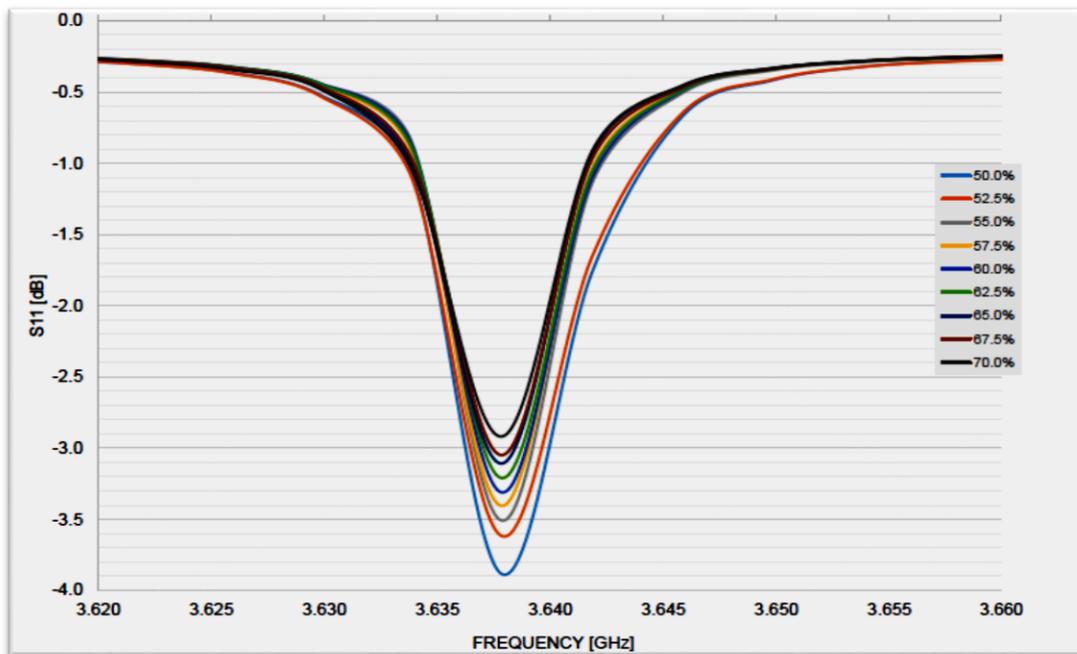

Figure 5-14: Spectra of 50 to 70 percentages of MO sample

The regression of the peak amplitudes was realised against the percentages of concentration of the mixtures. The frequency of 3.628 GHz was used as the reference line to regress the mixture sample using linear fit. Figure 5.15 represents the regression of the amplitudes against the percentages of concentration of MO.
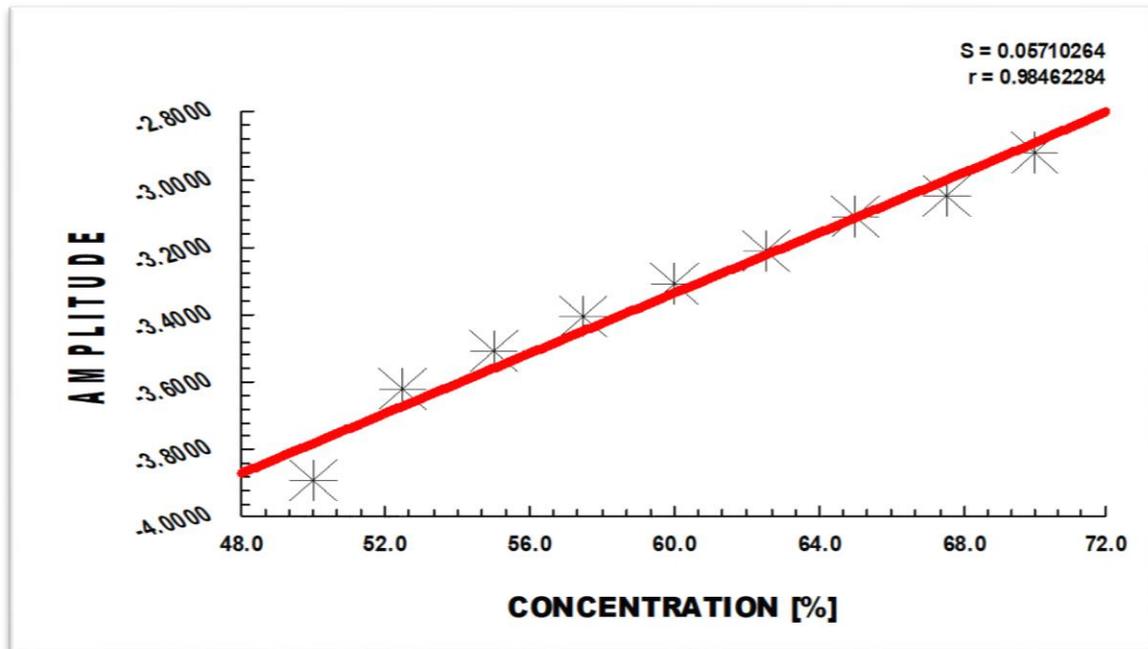
Figure 5-15: Plot of the concentration of the mixture of M in VO at 3.628 GHz

5.4 Model of the Lab Cavity

As a result of simulating the model of the cavity resonator used for the lab, different forms of electromagnetic transactions manifested. The significance of these is the electrical field distributions, which are shown in multi-slice fashion in the following sections.

5.4.1 Sample domains

The simulated model of the cavity using the VO sample showed a domain of active distribution of electric field at the sample tube area. Figure 5.16 illustrates the normalised electric field distribution at frequency of 2.3887 GHz.
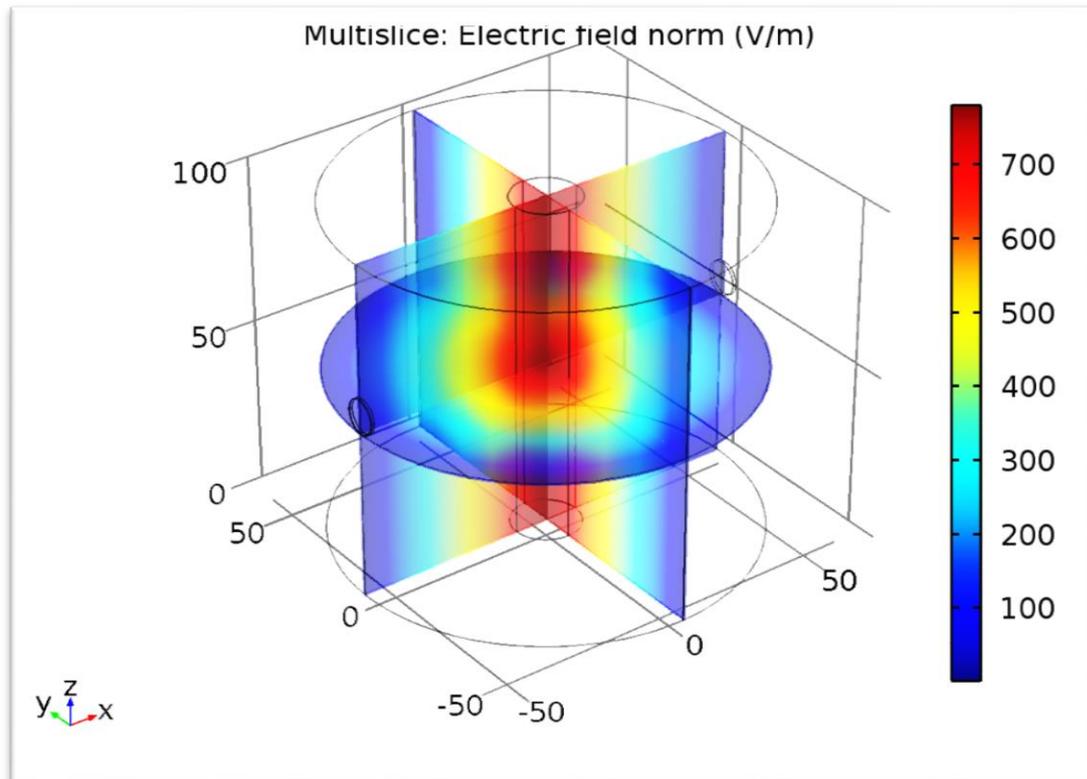
Figure 5-16: Electric field distribution in vegetable oil at 2.3887 GHz

The simulated FFA sample domain showed the normalised electric field distributed along the sample tube area. The electric field distribution of FFA at the normalised frequency is 2.3924 GHz.

For the methanol sample domain, the relative permittivity used has the value of 35.22, the electric field distribution at the normalised frequency is 2.313 GHz.

5.4.2 S-Parameter Plots of Simulated Model

The COMSOL generated S_{11}-parameter in function of frequency plot for the vegetable oil sample domain is illustrated in Figure 5.17.
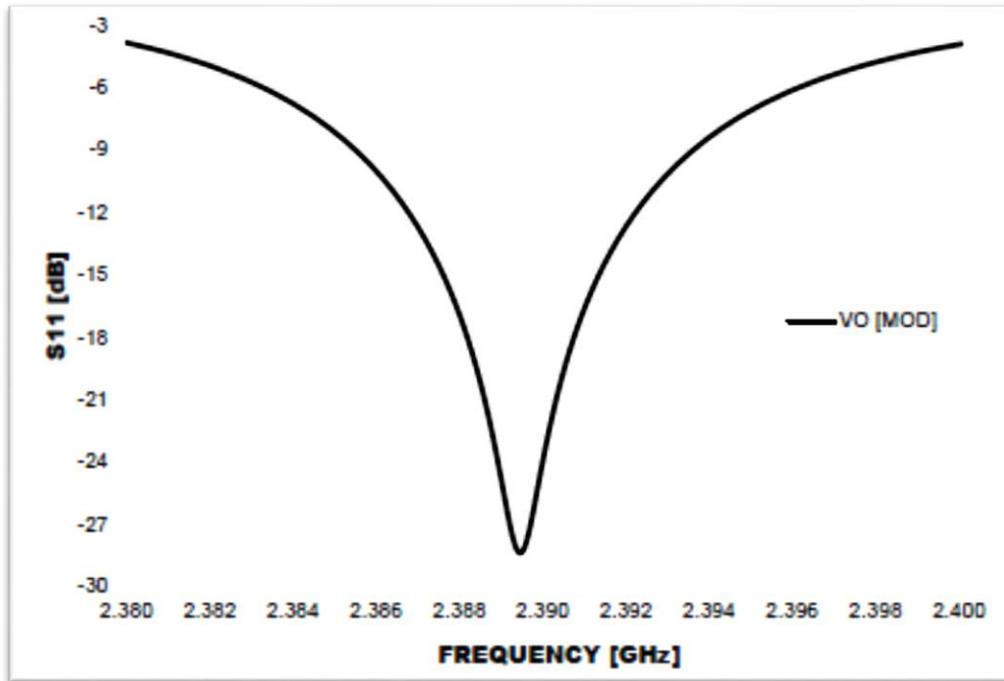
Figure 5-17: S-parameter plot of VO sample domain model

The COMSOL generated S_{11}-parameter in function of frequency plot for the free fatty acid

sample domain is illustrated in Figure 5.18.
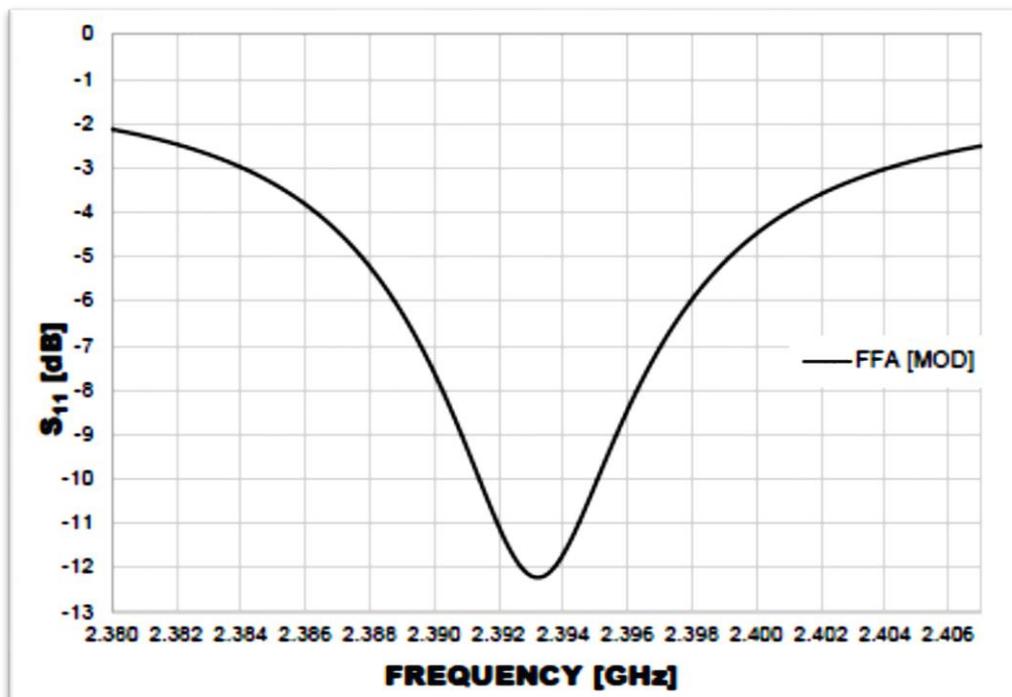
Figure 5-18: S-parameter plot of FFA sample domain model

The COMSOL generated S_{11}-parameter in function of frequency plot for the methanol sample domain is illustrated in Figure 5.19.
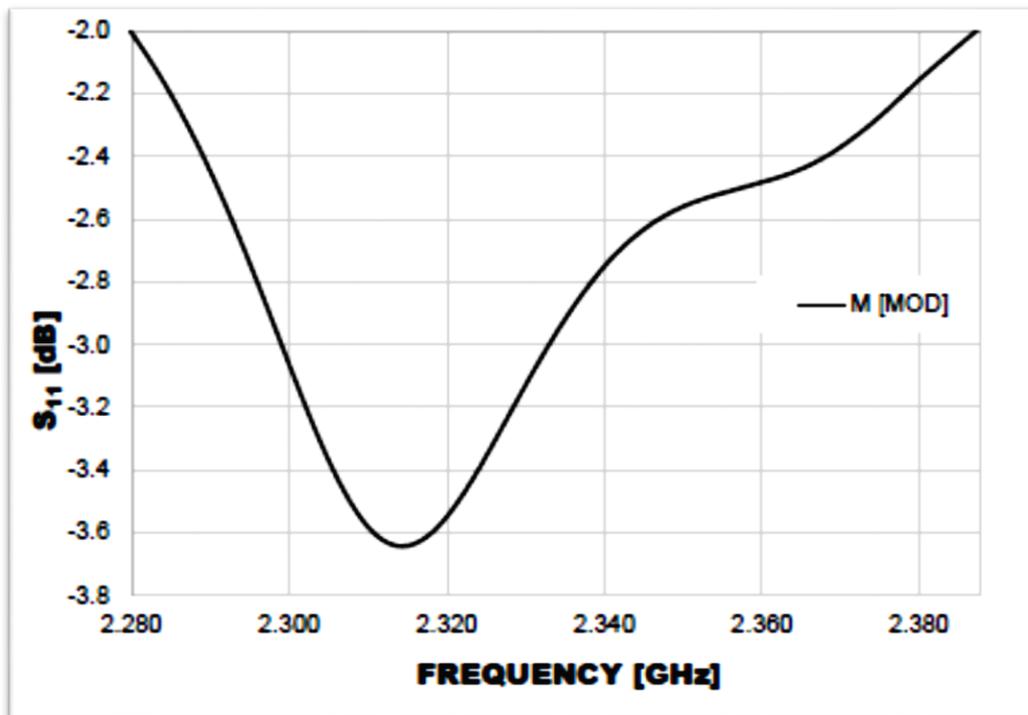
Figure 5-19: S-parameter plot of Methanol domain model

5.5   Comparing Computer Model with Experiments

The S-parameter plots produced by the simulation model of the VO sample domain when superimposed on the experimental plots, showed negligible variation in the signal spectra at the peak area. There is a slight shift of amplitude in favour of the simulated sample. This could be due to minor equipment or measurement errors in the lab work. Figure 5.20 shows the combined plots of the simulated model and experiment of vegetable oil.
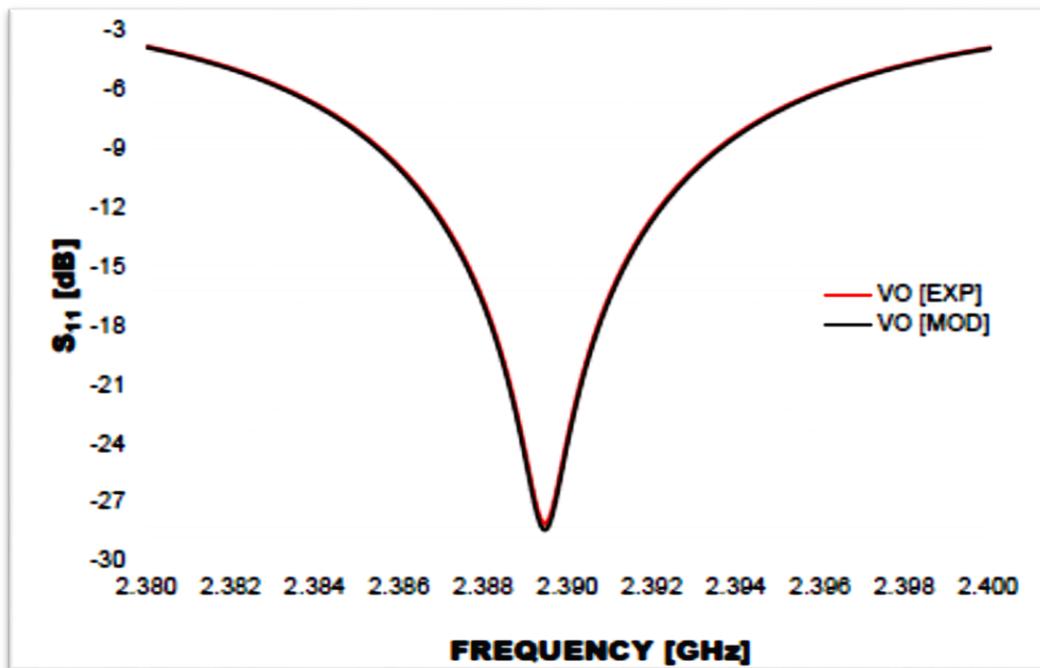
Figure 5-20: S$_{11}$ parameter plot of model and experiment of vegetable oil sample

The S-parameter plots produced by the simulating the model of the FFA sample was superimposed on the experimental plots, and showed tiny variation at the peak area. The pattern follows as the previous situation. There is a slight shift, here also, of amplitude in favour of the simulated sample at peak. This could be due minor equipment or measurement errors in the lab work. Figure 5.21 shows the combined plots of model and experiment of FFA.
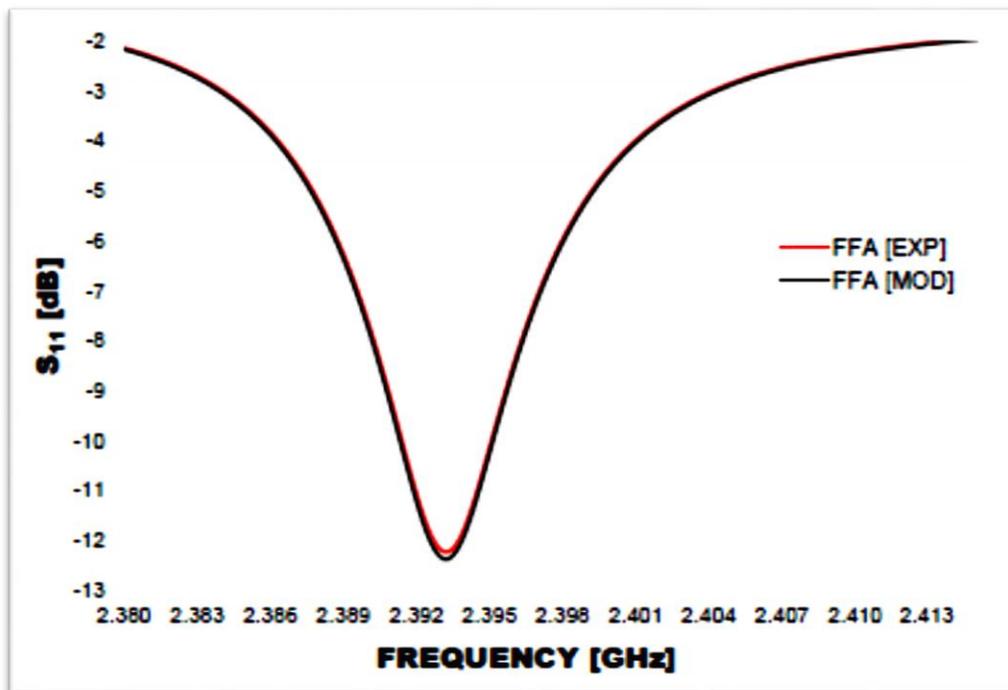
**Figure 5-21: S_{11} parameter plot of model and experiment of FFA sample**

The S-parameter plots produced by the simulating the model of the methanol sample was superimposed on the experimental plots and showed proportional variation along the entire spectra. There is a slight shift of the entire value of the spectra in favour of the simulated sample. This could be attributed to the same equipment or measurement errors associated with the two other samples. Figure 5.22 shows the combined plots of the model and experiment of the methanol sample.
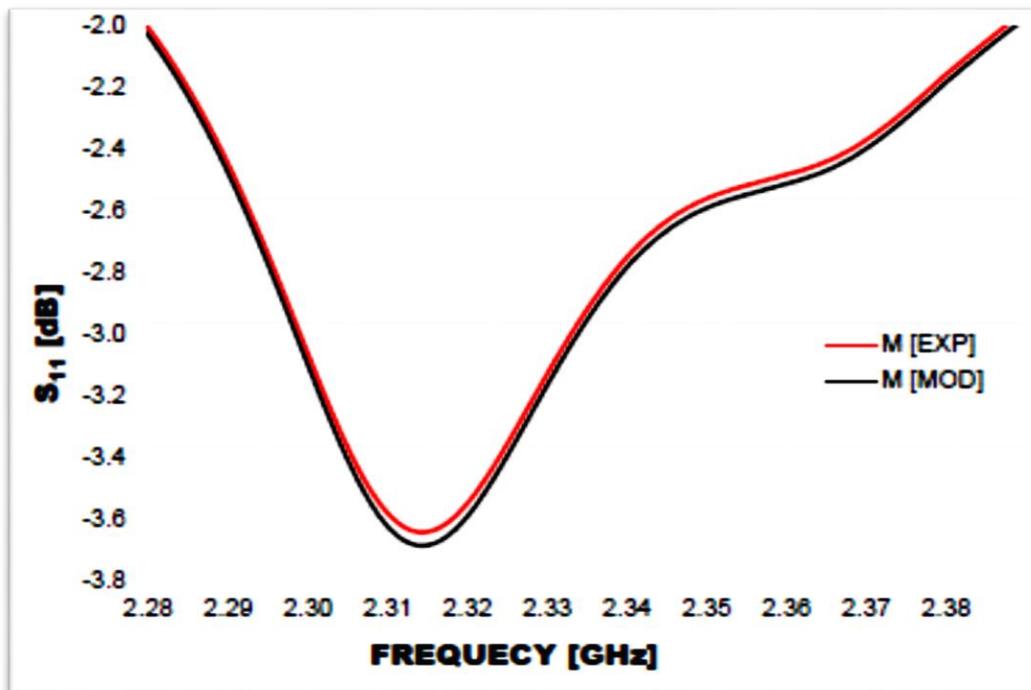
Figure 5-22: S_{11} parameter plot of model and experiment of vegetable oil sample

5.6   Modelling for Industry

After scaling the industry model and determining the Q-factor of 7856 and the resonant frequency of 2.3562 GHz (section 4.5.4), the new model genenerated characteristics that are more industry friendly but yet carried the performance required and adequacy as expected of the lab model.

5.6.1   Electric Field Distribution of Samples

The simulated electric field distribution yielded results that show activity in the flow tube when excited through the ports. Figure 5.23 illustrates the cross section of the normalised electric field of the air sample domain, permittivity, ϵ=1 and using the resonant frequency of 2.3562 GHz.
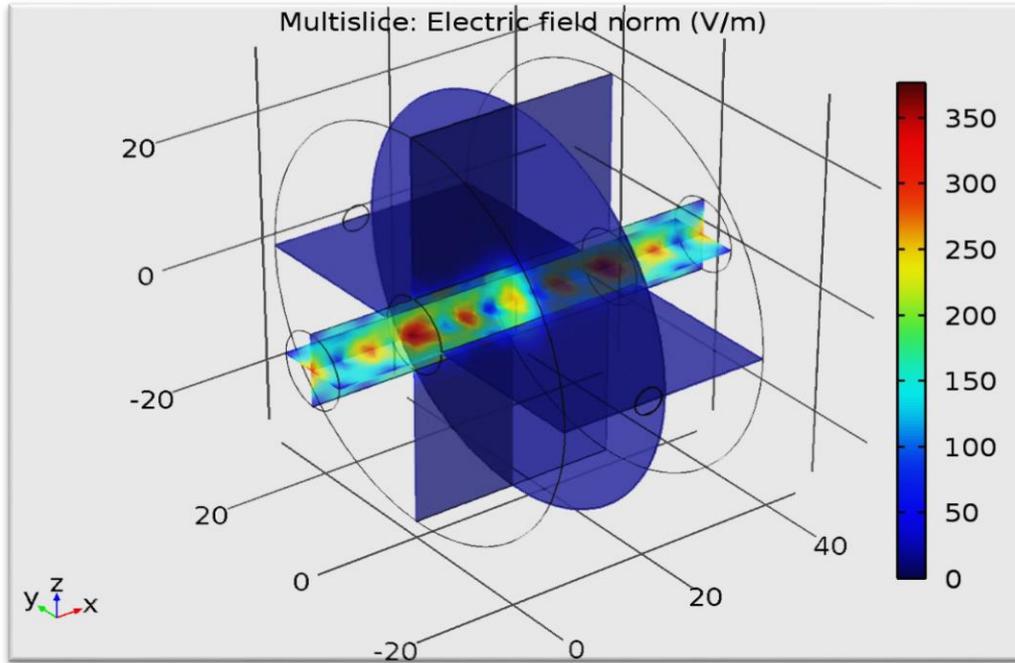
Figure 5-23: Cross section of normalised electric field for air sample domain at 2.3562 GHz

Alternatively, the sample domain and the frequencies as used in the laboratory were inputted

for the simulation of the industry model and the generated results are as predicted. Figure 5.24

illustrates the cross section of the normalised electric field of the VO sample domain, $\varepsilon=2.501$

at the frequency of 2.3887 GHz.
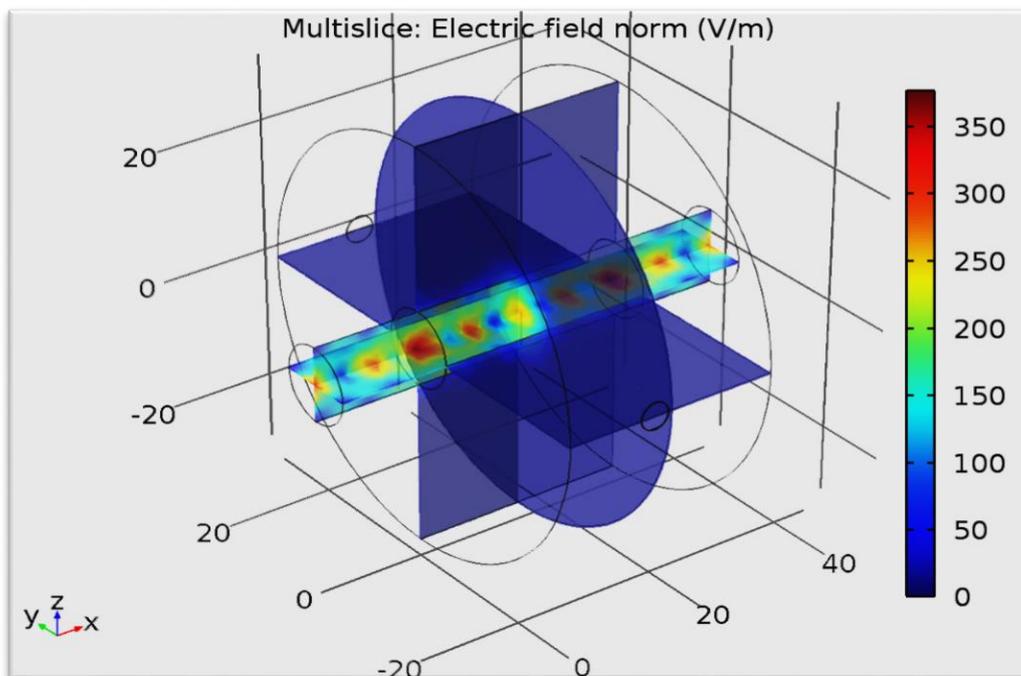
Figure 5-24: Cross section of normalised electric field for VO sample domain at 2.3887 GHz

When inputted Ɛ=2.3153 for the sample domain of FFA and the frequency of 2.3924 GHz the following normalised field was generated (Figure 5.25).
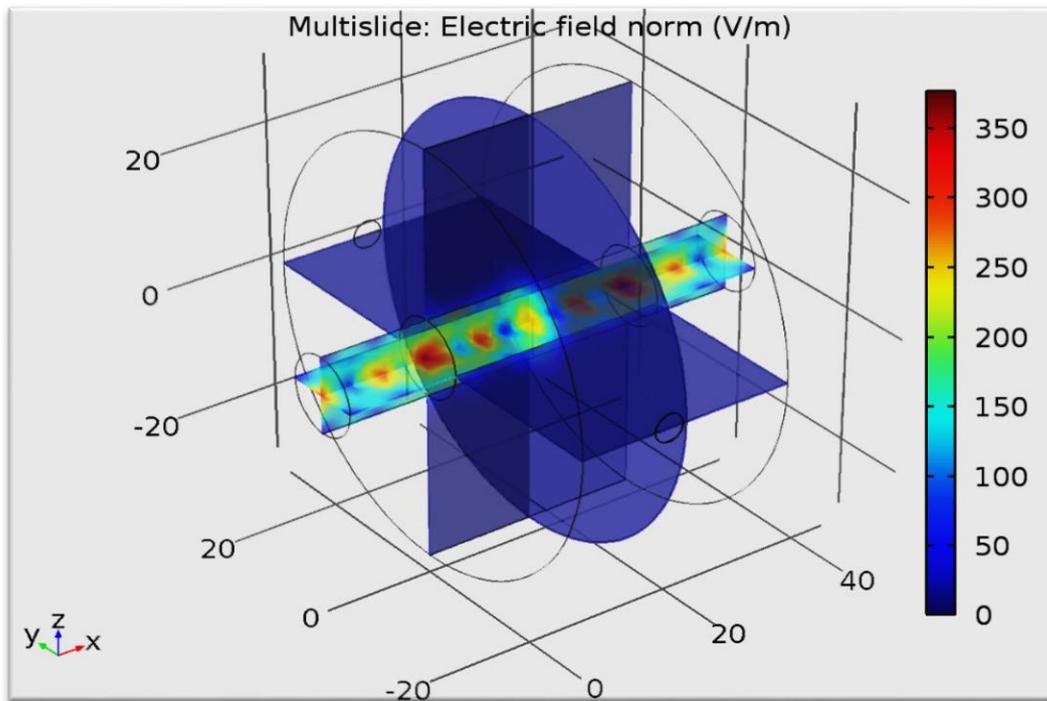
Figure 5-25: Cross section of normalised electric field for FFA sample domain at 2.3924GHz

Moreover, using the transmission /reflection line method, the relative complex permittivity of Ɛ=35.22 was attained for methanol. Figure 5.26 illustrates the normalised electric field of the M sample domain at the frequency of 2.313 GHz for the industry model.
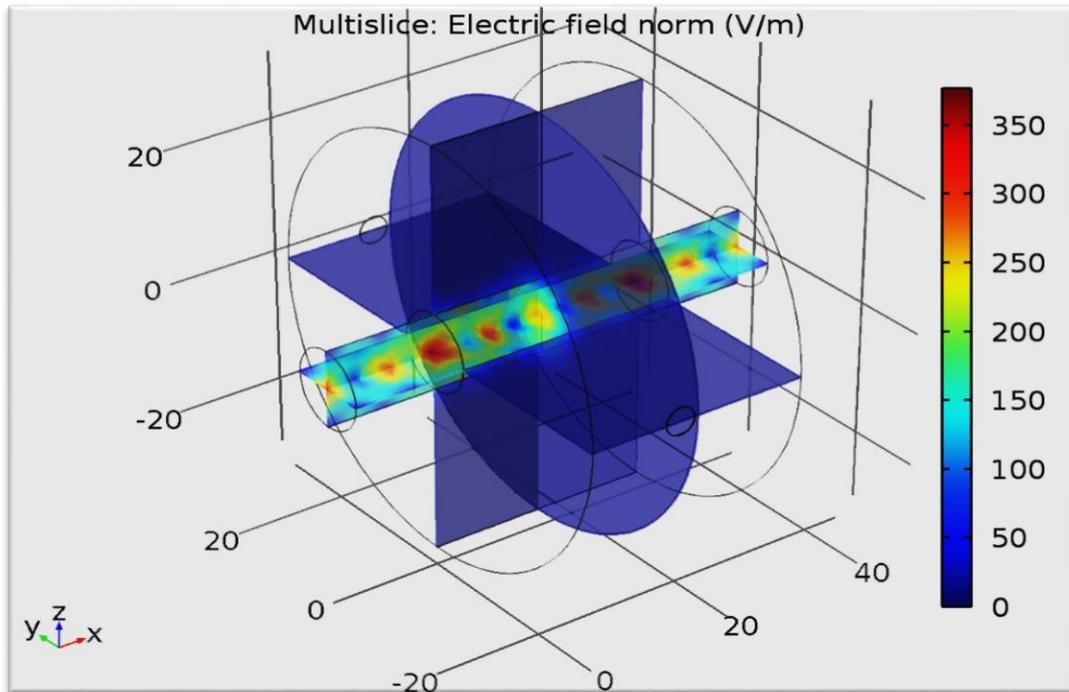
Figure 5-26: Cross section of normalised electric field for M sample domain at 2.313 GHz

5.6.2 S-Parameter Plots of Industry Model

Simulating the industry model with the material properties determined using the CPM and TR methods had enabled the generation of S-parameter vs frequency signal plots. The following figures 5.27 to 5.29 have been generated using the properties of VO, M and FFA for the simulated industry model and demonstrate that a different spectrum is observed with each material and can therefore be used as a sensing system.
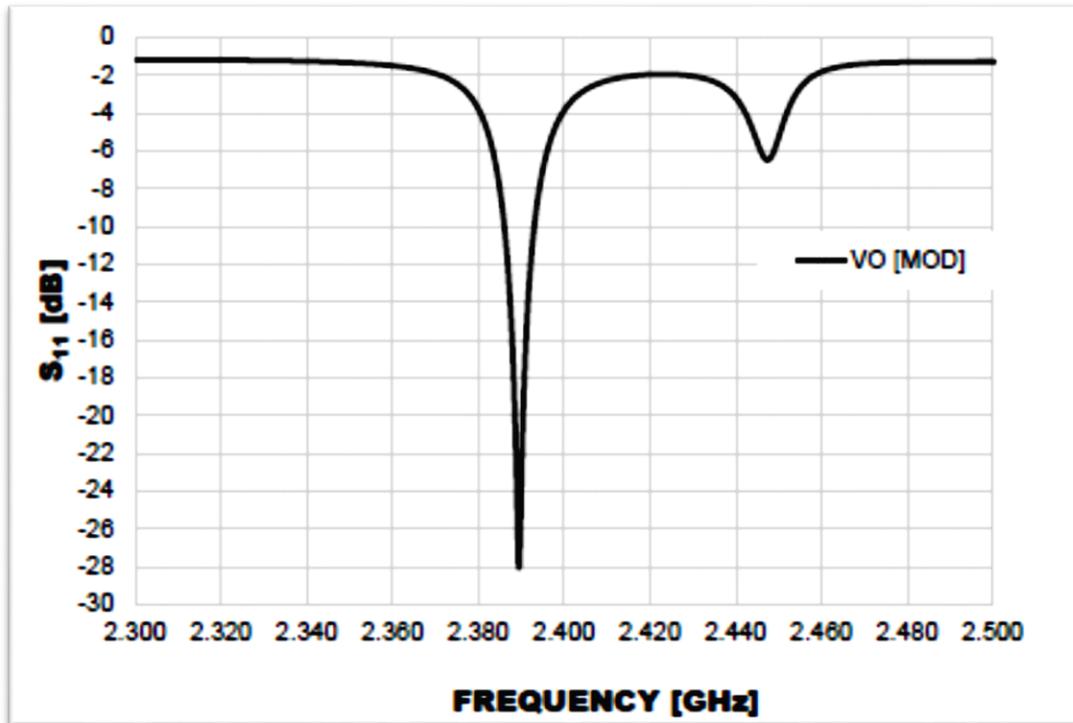
Figure 5-27: S-parameter plot of VO sample domain of industrial model
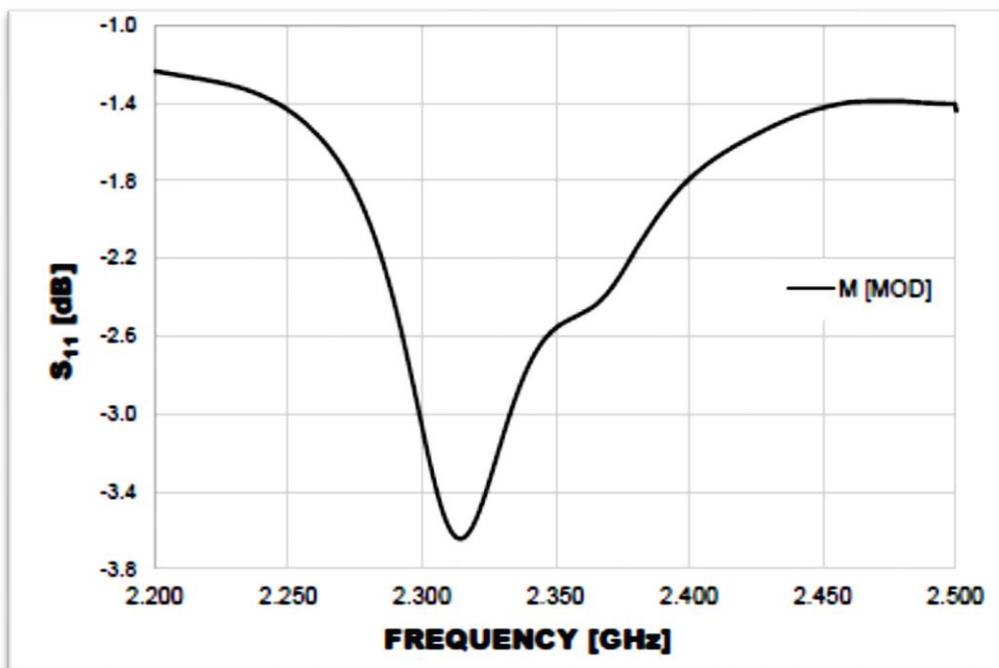
Figure 5-28: S-parameter plot of Methanol sample domain of industrial model
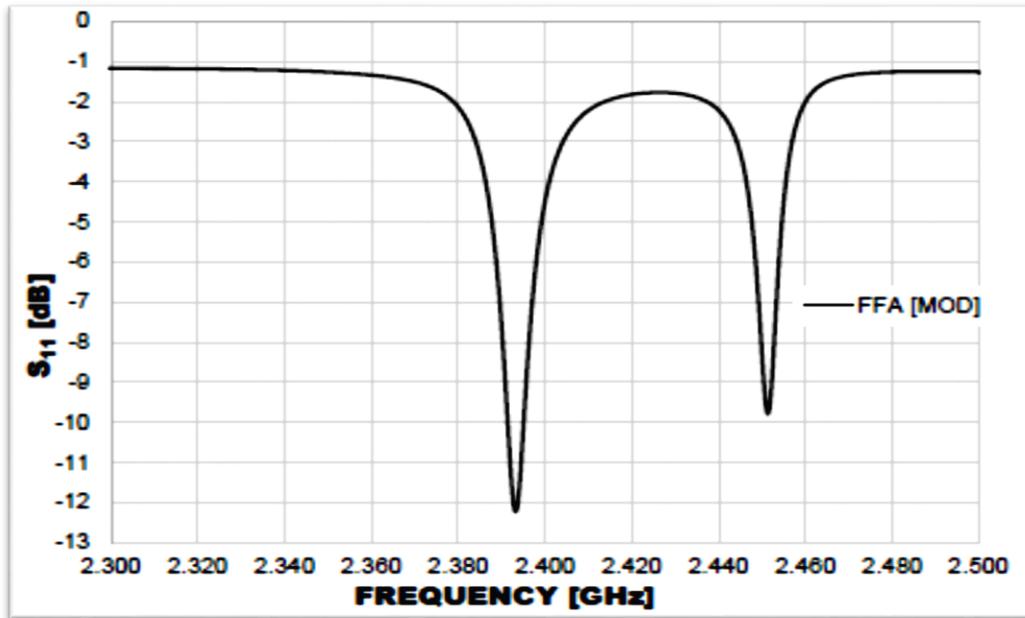
Figure 5-29: S-parameter plot of FFA sample domain of industrial model

6.0 CONCLUSIONS AND FUTURE WORK

6.1 Introduction

Work has been carried out to develop a microwave spectroscopic resonant sensor for the verification of food and waste oils. Edible oil products were sampled as main materials to be used for the measurements with the aim to establish difference and authenticity. Other samples, such as methanol and free fatty acid were used as part of the formation of the waste oil.

A critical understanding of the nature of edible oils, especially the ones in commonplace supermarkets was necessary to start this work. The nature, composition, taste and texture of the oils have played an important role in their characteristics. Oils present different values due to their origin and the way they are produced. While some oils are simple to produce some are really complicated and that affects the value.

Samples have to be prepared according to procedure. Experiments were realised to establish the difference and authenticate some of the oils. Tests were carried out to determine some levels of free fatty acids and methanol in waste oil. Models of sensors were created out of the test results and simulated. Simulated results were used to create a new sensor for the waste oil recovery industry.

6.2   Conclusions

Before providing an overall conclusion, the individual objectives are summarised below:

- Several methods were investigated to analyse edible oils, and the microwave spectroscopy results identified in this thesis were chosen to be used in both cases since they are able to be used in a way that does not result in contamination of the oil (important for food grade oil) and lend themselves to continuous sampling, so the process can be monitored and results generated in near real time. The continuous flow approach means it is suitable for both edible and waste oil industries.

- Edible oil verification was undertaken that showed that the Microwave Spectroscopy approach gave an R^2 value of 0.9485 compared to 0.9845 for an Optical Spectroscopy approach. Even though the correlation coefficient of the optical method is higher than that of the microwave in this case, it is not reliable to use the spectrophotometer alone as a sole technique for authentication of oils. The reason being that it relies mostly on the pigmentation of the material and would be open to falsification by use of dyes or other colorants to achieve similar optical response at the test wavelength. This type of manipulation is not possible with the microwave, which relies on the electrical properties of the material under test, which are impractical to recreate.

- For the determination of levels of FFA in oil and methanol R^2 values in excess of 0.96 were seen, exact figures depended upon the particular parameter that was being investigated. For determining the free fatty acids present in the waste oil, the R^2 value was 0.9884, for free fatty acids in the methanol stream (post separation) it was 0.9888 while the determination of the amount of methanol in the oil (post separation) was slightly lower at 0.9694 these values suggest that they can be used to monitor the consistency of the waste oil plant output, but further verification would need to be undertaken on the output oil at the final output stage.

- Based on the findings of the previous two objectives, subsequent simulations of the cavities showed that the simulation engines matched the real world results. This meant

that the primary problem with the waste oil monitoring system could be overcome. The waste oil incoming the plant is normally either very viscous or is set solid, so the pumping of the oil is difficult. For the initial development small bore sampling was proposed, but this would likely block and render the monitoring ineffective. Since the results of the simulation match the practical results, a cavity system was simulated that would be able to accommodate a larger bore of pipe, thus allowing it to be used with the viscous incoming oil stream.

The overall conclusion can be best summed up with separate consideration of the edible and waste oil analysis methods and requirements separately.

The edible oil analysis methods using field test equipment showed that the accuracy using optical spectroscopy was slightly higher than that using microwave spectroscopy (0.98 compared to 0.95) but the microwave approach has two major benefits, namely the implemented analysis hardware will be smaller and lighter thus more portable and potentially cheaper than the optical approach. More importantly the bulk oil properties are used in the microwave analysis of the oil compared to just its optical absorption when using optical approaches, hence it is harder to fool the sensor.

For the waste oil industry the work has shown for two of the three oil streams (FFA in waste oil, FFA in the wash methanol) encountered in the parameters a very high level of accuracy of the predictions, and the other value is slightly less (Methanol in the final oil stream), but still good enough to monitor the process for consistent performance. The important one of these streams is the incoming to the process stream (FFA in oil), with an R^2 value of 0.9884 shows the level of the contaminant can be monitored accurately and thus the plant process can be optimised to deal with this, thus improving operations.

6.3   Future Work

The testing of vegetable oils in order to verify their differences and authenticity needs further works in laboratory and field environments. The idea was initially to design a system that involved all the electronics, under which the application would have included the building of a hand-held device that probe the oils in real time. That will require more experiments and electronic work to be carried out. That aspect of the work is highly recommended for further scrutiny.

Tests performed to evaluate the authenticity of extra virgin olive oil could trigger additional work using other cheaper oils and the results could be compared with what has been achieved thus far. For example, other cheaper oils like palm nut oil, rapeseed oil, or groundnut oil could be mixed with the extra virgin olive oil and be evaluated for more results and for additional comparative analysis. This could go further to prove the authenticity of the product even more. In addition, a circuitry combination of the electronics of microwave plus spectrometry could go far to offer a suitable formula to address the problem of testing adulteration of oils and this is recommended for further study.

Industry samples of the waste oil recovery process have to be sorted out into their elements to enable further tests to compliment the works carried out using vegetable oil, methanol and free fatty acids. This would allow for further tests to compare with what has been carried out so far. An existing case study should be included in the way forward. This will move the work from being just conceptual into much more practical in nature.

The industry model of the sensor for monitoring waste oil recovery was successful through lab experiments and computer modelling and simulation. The next step would be to have a prototype of this model built to allow for more tests, especially in the field environment to be

carried out, even though this will require further scrutiny and certifications to meet regulation and standards of the industry, for which reason it must be recommended for further work. Simulated work carried out thus far must be taken into consideration and will therefore serve as a guide.

6.4   Research Limitations

The work carried out is mainly of a conceptual basis and is arrived at using theoretical definitions, experiments and computer aided simulations. Even though tests and trials are reliable, it was carried out devoid of field visits or tests. There are so many establishments in the waste oil recovery industry, which could serve as a case study of sorts, if resources and time were to permit. Samples used, especially of waste oil, were not derived from any actual plant or depot of such nature.

The design of the industry model of microwave spectroscopic resonant sensor, even though demonstrated by the results carried in the lab and modelled through mathematical and physical simulations, have not been tried and tested in an established field to probe actual industry conditions. Due to typical site safety requirements and commercial confidentiality, it was not possible to visit sites to see how this system could be implemented in reality.

Samples used in the lab for the process of waste oil recovery are made of combinations of vegetable oil, free fatty acids and methanol. This method is accurate for the fact that it allows for the testing and simulation of the process leading to the esterification of waste oil. The lack of use of real waste oil, which contains much more impurities, would have been much more realistic. Further tests should be able to use them and would prove a good method for comparative analyses.

REFERENCES

ABO-DIEF, H. M., ALTALHI, A. A. & MOHAMED, A. T. 2014. Waste Oil Recycling Using Microwave Pyrolysis Reactors. *Journal of Industrial and Intelligent Information,* 2.

AKOH, C. C. 2017. *Food Lipids: Chemistry, Nutrition, and Biotechnology, Fourth Edition*, CRC Press.

AMIET, A., ELECTRICAL, M. U. D. O. & ENGINEERING, C. S. 2003. *Free Space Permittivity and Permeability Measurements at Microwave Frequencies*, Monash University.

APARICIO, R. & HARWOOD, J. 2013. *Handbook of Olive Oil: Analysis and Properties*, Springer US.

BADDAY, A. S., ABDULLAH, A. Z., LEE, K. T. & KHAYOON, M. S. 2012. Intensification of biodiesel production via ultrasonic-assisted process: A critical review on fundamentals and recent development. *Renewable and Sustainable Energy Reviews,* 16**,** 4574-4587.

BAGAD, V. S. 2009. *Microwave Engineering*, Technical Publications.

BAJPAI, R. P. & CHANDRASEKHAR, U. 2016. *Innovative Design and Development Practices in Aerospace and Automotive Engineering: I-DAD, February 22 - 24, 2016*, Springer Singapore.

BAKER-JARVIS, J., VANZURA, E. J. & KISSICK, W. A. 1990. Improved Technique for Determining permittivity with transmission reflexion method. *IEEE Transactions on Microwave Theory and Techniques,* 38**,** 1096-1103.

BAKSHI, A. V. 2009. *Transmission Lines And Waveguide*, Technical Publications.

BAKSHI, A. V. B. U. A. 2008. *Network Theory*, Technical Publications.

REFERENCES

BAO, X. & XU, Y. 2004. *Natural Gas Conversion VII: Proceedings of the 7th Natural Gas Conversion Symposium, Dalian, China, 6 - 10 June 2004*, Elsevier Science.

BARANSKA, M. 2013. *Optical Spectroscopy and Computational Methods in Biology and Medicine*, Springer Netherlands.

BARTIROMO, R. & DE VINCENZI, M. 2016. *Electrical Measurements in the Laboratory Practice*, Springer International Publishing.

BEHRENS, D. 1991. *DECHEMA Corrosion Handbook, Methanol, Sulfur Dioxide*, Wiley.

BERRIOS, M., SILES, J., MARTIN, M. & MARTIN, A. 2007. A kinetic study of the esterification of free fatty acids (FFA) in sunflower oil. *Fuel,* 86**,** 2383-2388.

BEWLEY, L. V. 1963. *Traveling waves on transmission systems*, Dover.

BOSHIER, J. F. & MOY, M. 1982. *Alternative Uses of Methanol in Liquid Fuels Supply*, The Authors.

BRYANT, G. H. & ENGINEERS, I. O. E. 1993. *Principles of Microwave Measurements*, P. Peregrinus Limited.

BRYANT, L. 1965. Rudolf Diesel: Pioneeer of the Age of Power.W. Robert Nitske and Charles Morrow Wilson. University of Oklahoma Press, Norman, 1965. x + 318 pp. Illus. $5.95. *Science,* 148**,** 211-a.

CALOZ, C. & ITOH, T. 2005. *Electromagnetic Metamaterials: Transmission Line Theory and Microwave Applications*, Wiley.

CARROLL, J. 2014. *Natural Gas Hydrates: A Guide for Engineers*, Elsevier Science.

CASE, C., KIKKAWA, T., KOHL, P. & LEE, W. W. 1998. *Low-Dielectric Constant Materials III*, Materials Research Society.

CHAI, M., TU, Q., LU, M. & YANG, Y. J. 2014. Esterification pretreatment of free fatty acid in biodiesel production, from laboratory to industry. *Fuel Processing Technology,* 125**,** 106-113.

CHANG, C. D. 1983. Hydrocarbons from Methanol. *Catalysis Reviews,* 25**,** 1-118.

CHEN, L. F., ONG, C. K., NEO, C. P., VARADAN, V. V. & VARADAN, V. K. 2004. *Microwave Electronics: Measurement and Materials Characterization*, Wiley.

CHENG, W. H. 1994. *Methanol Production and Use*, Taylor & Francis.

CHEREMISINOFF, P. 1997. *Handbook of Engineering Polymeric Materials*, Taylor & Francis.

CHESTER, R., HARRISON, R. M., SLATER, D. H., EDULJEE, G., HEWITT, C. N., MANSFIELD, T. A., LUCAS, P. W., PRESTON, M. R., HARRAD, S. J. & HOLMAN, C. 2007. *Pollution: Causes, Effects and Control*, Royal Society of Chemistry.

CLARY, J. J. 2013. *The Toxicology of Methanol*, Wiley.

CVENGROŠ, J. & CVENGROŠOVÁ, Z. 2004. Used frying oils and fats and their utilization in the production of methyl esters of higher fatty acids. *Biomass and Bioenergy,* 27**,** 173-181.

DA SILVA, F. F. & BAK, C. L. 2013. *Electromagnetic Transients in Power Cables*, Springer London.

DE BONI, L. A. B. & LIMA DA SILVA, I. N. 2011. Monitoring the transesterification reaction with laser spectroscopy. *Fuel Processing Technology,* 92**,** 1001-1006.

DE REUCK, K. M. & CRAVEN, R. J. B. 1993. *Methanol*, Blackwell Scientific.

DEMIRBAS, A. 2009. Biodiesel from waste cooking oil via base-catalytic and supercritical methanol transesterification. *Energy Conversion and Management,* 50**,** 923-927.

DIJKSTRA, A. J., HAMILTON, R. J. & HAMM, W. 2008. *Trans Fatty Acids*, Wiley.

DYSON, J. D., GINYOVSZKY, R., LABORATORY, A. F. A. & ENGINEERING, U. O. I. A. U.-C. D. O. E. 1970. *The measurement of balanced impedances with a coaxial transmission line system*, Air Force Avionics Laboratory, Air Force Systems Command.

REFERENCES

EDWARDS, M. 2014. Pysical contamination methods. 20**,** 30-35.

EUROPE, W. H. O. R. O. F. 1992. *Toxic Oil Syndrome: Current Knowledge and Future Perspectives*, World Health Organization, Regional Office for Europe.

FINKENZELLER, K. 2003. RFID handbook : fundamentals and applications in contactless smart cards and identification.

FLEISCH, D. 2008. *A Student's Guide to Maxwell's Equations*, Cambridge University Press.

FOLKSON, R. 2014. *Alternative Fuels and Advanced Vehicle Technologies for Improved Environmental Performance: Towards Zero Carbon Transportation*, Elsevier Science.

FUSCO, V. F. 2005. *Foundations of Antenna Theory and Techniques*, Pearson.

GARVERICK, L. 1994. *Corrosion in the Petrochemical Industry*, ASM International.

GRIMM, B., PORRA, R. J., RÜDIGER, W. & SCHEER, H. 2007. *Chlorophylls and Bacteriochlorophylls: Biochemistry, Biophysics, Functions and Applications*, Springer Netherlands.

GUNSTONE, F. D. 2004. *Rapeseed and Canola Oil: Production, Processing, Properties and Uses*, Blackwell Pub.

GUPTA, R. G. 2005. *Television Engineering and Video Systems*, Tata McGraw-Hill.

HOLCAPEK, M., JANDERA, P., FISCHER, J. & PROKES, B. 1999. Analytical monitoring of the production of biodiesel by high-performance liquid chromatography with various detection methods. *JouRNAL OF CHROMATOGRAPHY***,** 13-31.

HURAY, P. G. 2011. *Maxwell's Equations*, Wiley-IEEE Press, ISBN: 978-0-470-54990-2

IDA, N. 2015. *Engineering Electromagnetics*, Springer International Publishing. Edition 3, 978-3-319-07806-9

JACOBSEN, N. E. 2007. *NMR Spectroscopy Explained: Simplified Theory, Applications and Examples for Organic Chemistry and Structural Biology*, Wiley.

JENSEN, P. R. 1994. *Early Radio: In Marconi's Footsteps, 1894 to 1920*, Kangaroo Press.

REFERENCES

JERINIC, G. 1966. *Microwave Cavity Method for Measuring Dielectric Constants and Plasma Properties*, University of Wisconsin--Madison.

KEELER, J. 2011. *Understanding NMR Spectroscopy*, Wiley.

KHARKOVVSKY, S. & ZOUGHI, R. 2007. Microwave and millimeter wave nondestructive testing and evaluation - Overview and recent advances. *EEE Instrumentation & Measurement Magazine,* 07**,** 1094-6969.

KIRITSAKIS, A. & SHAHIDI, F. 2017. *Olives and Olive Oil as Functional Foods: Bioactivity, Chemistry and Processing*, Wiley.

KIZER, G. 2013. *Digital Microwave Communication: Engineering Point-to-Point Microwave Systems*, Wiley.

KNEIPP, K., MOSKOVITS, M. & KNEIPP, H. 2006. *Surface-Enhanced Raman Scattering: Physics and Applications*, Springer Berlin Heidelberg.

KNOTHE, G. 1999. Rapid monitoring of transesterification and assessing biodiesel fuel quality by near-infrared spectroscopy using a fiber-optic probe. *JAOCS,* 76**,** 795-800.

KNOTHE, G. 2000. Monitoring a progressing transesterification reaction by fiber-optic near infrared spectroscopy with correlation to 1H nuclear magnetic resonance spectroscopy. *JAOCS,* 77**,** 489-493.

KNOTHE, G. 2001. Determining the blend level of mixtures of biodiesel with conventional diesel fuel by fiber-optic near-infrared spectroscopy and 1H nuclear magnetic resonance spectro. *JAOCS,* 78**,** 1025-1028.

KNOTHE, G. 2006. Analyzing biodiesel_standards and other methods. *JAOCS,* 83**,** 823-833.

KNOTHE, G. & KENAR, J. A. 2004. Determination of the fatty acid profile by1H-NMR spectroscopy. *European Journal of Lipid Science and Technology,* 106**,** 88-96.

KOGURE, H., KOGURE, Y. & RAUTIO, J. 2011. *Introduction to RF Design Using EM Simulators*, Artech House.

KOROSTYNSKA, O., BLAKEY, R., MASON, A. & AL-SHAMMA'A, A. 2013. Novel method for vegetable oil type verification based on real-time microwave sensing. *Sensors and Actuators A: Physical,* 202**,** 211-216.

KUMAR, A. 2003. *Microwave Techniques :Transmission Lines*, New Age International.

KUMAR, A. & SHARMA, S. Measurement Of Dielectric Constant And Loss Factor Of The Dielectric Material At Microwave Frequencies. *Progress In Electromagnetics Research,* 69**,** 47-54.

KUZNETSOV, Y. I. 2013. *Organic Inhibitors of Corrosion of Metals*, Springer US.

LEE, S. 1989. *Methanol Synthesis Technology*, Taylor & Francis. 9533074809, 9789533074801

LEES, M. 2003. *Food Authenticity and Traceability*, Elsevier Science.

LEWIS, I. R. & EDWARDS, H. 2001. *Handbook of Raman Spectroscopy: From the Research Laboratory to the Process Line*, CRC Press.

LI-CHAN, E., CHALMERS, J. & GRIFFITHS, P. 2011. *Applications of Vibrational Spectroscopy in Food Science*, John Wiley & Sons.

LI, S., AKYEL, C. & BOSISIO, R. G. 1981a. Precise Calculations and Measurements on the Complex Dielectric Constant of Lossy Materials Using TM_sub 010- Cavity Perturbation Techniques. *IEEE Transactions on Microwave Theory and Techniques,* 29**,** 1041-1047.

LI, S., AKYEL, C. & BOSISIO, R. G. 1981b. Precise Calculations and Measurements on the Complex Dielectric Constant of Lossy Materials Using TM_sub 010- Cavity Perturbation Techniques. *iEEE Transactions on Microwave Theory and Techniques,* 29**,** 1041-1048.

LIN, M., WANG, Y. & AFSAR, M. N. 2005. Precision measurement of complex permittivity and permeability by microwave cavity perturbation technique. *Spectroscopy and Material Properties,* M82**,** 62-63.

REFERENCES

LINFENG CHEN, ONG, C. K. & TAN, B. T. G. 1999. Cavity perturbation technique for the measurement of permittivity tensor of uniaxially anisotropic dielectrics. *IEEE Transactions on Instrumentation and Measurement,* 48**,** 1023-1030.

LODODA, M. J., SCIENCE, E. S. D., DIVISION, T., DIVISION, E. S. H. T. M. & MEETING, E. S. 2000. *Low and High Dielectric Constant Materials: Materials Science, Processing, and Reliability Issues : Proceedings of the Fifth International Symposium*, Electrochemical Society.

LUQUE, R., LIN, C. S. K., WILSON, K. & CLARK, J. 2016. *Handbook of Biofuels Production*, Elsevier Science.

LUQUE, R. & MELERO, J. A. 2011. *Advances in Biodiesel Production: Processes and Technologies*, Woodhead Pub Limited.

MAGGIO, R. M., CERRETANI, L., CHIAVARO, E., KAUFMAN, T. S. & BENDINI, A. 2010. A novel chemometric strategy for the estimation of extra virgin olive oil adulteration with edible oils. *Food Control,* 21**,** 890-895.

MAHMOUD, S. F. 1991. *Electromagnetic Waveguides: Theory and Applications*, Peregrinus.

MARCUVITZ, N. 1951. *Waveguide Handbook*, McGraw-Hill.

MASTERTON, W. L. & HURLEY, C. N. 2015. *Chemistry: Principles and Reactions*, Cengage Learning.

MCDONALD, R. E. & MOSSOBA, M. M. 1997. *New Techniques and Applications in Lipid Analysis*, AOCS Press.

MEHER, L., VIDYASAGAR, D. & NAIK, S. 2006. Technical aspects of biodiesel production by transesterification—a review. *Renewable and Sustainable Energy Reviews,* 10**,** 248-268.

MENG, B., BOOSKE, J. & COOPER, R. 1995. Extended cavity perturbation technique to determine the complex permittivity of dielectric materials. *IEEE Transactions on Microwave Theory and Techniques,* 43**,** 2633.

MEREDITH, R. J. 1998. *Engineers' Handbook of Industrial Microwave Heating*, Institution of Electrical Engineers.

MILLER, F. P., VANDOME, A. F. & MCBREWSTER, J. 2009. *Gauss's Law*, VDM Publishing.

MILLER, F. P., VANDOME, A. F. & MCBREWSTER, J. 2010. *Gauss's Law for Magnetism*, Alphascript Publishing.

MITRA, M. 2005. *SATELLITE COMMUNICATION*, PHI Learning.

MONTEIRO, M., AMBROZIN, A., LIAO, L. & FERREIRA, A. 2008. Critical review on analytical methods for biodiesel characterization. *Talanta,* 77**,** 593-605.

MUELLER, T. 2014. *Extra Virginity: The Sublime and Scandalous World of Olive Oil*, Atlantic Books.

OLYSLAGER, F. 1999. *Electromagnetic Waveguides and Transmission Lines*, OUP Oxford.

OSMAN, S. B., KOROSTYNKA, O., MASON, A., CULLEN, J. D. & AL-SHAMMA'A, A. I. Application of microwave spectroscopy analysis on determining quality of vegetable oil. 2014 / 01 / 01 / 2014. IEEE Computer Society, 556-559.

OSMAN, S. B., KOROSTYNKA, O., MASON, A., CULLEN, J. D. & AL-SHAMMA'A, A. I. Development of a sensor system for vegetable oil authentication. Ninth International Conference on Sensing Technology, 24 March 2016 2015 Auckland, New Zealand. IEEE, 104-109.

OZAKI, Y., MCCLURE, W. F. & CHRISTY, A. A. 2006. *Near-Infrared Spectroscopy in Food Science and Technology*, Wiley.

REFERENCES

PAILLET, F. L., SAUNDERS, W. R., SOIL, A. C. D.-O. & ROCK 1990. *Geophysical Applications for Geotechnical Investigations*, ASTM.

PANKOV, A. 2005. *Travelling Waves and Periodic Oscillations in Fermi-Pasta-Ulam Lattices*.

PREEDY, V. R. & WATSON, R. R. 2010. *Olives and Olive Oil in Health and Disease Prevention*, Elsevier Science.

RACHIDI, F. & TKACHENKO, S. 2008. *Electromagnetic Field Interaction with Transmission Lines: From Classical Theory to HF Radiation Effects*, WIT.

RACHMANTO, T., ALLANSON, D. D., MATTHEWS, C. & JENKINSON, I. 2014. Monitoring of Biodiesel Transesterification Process Using Impedance Measurement. *International Journal of Materials, Mechanics and Manufacturing,* 2**,** 265-271.

RAMESH, V. 2016. *Nuclear Magnetic Resonance: Volume 45*, Royal Society of Chemistry.

RAO, R. S. 2015. *MICROWAVE ENGINEERING*, Prentice Hall India Pvt., Limited.

RINCO, J., CANIZARES, P. & GARCıA, M. T. 2005. Waste Oil Recycling Using Mixtures of Polar Solvents. *Ind. Eng. Chem. Res,* 44**,** 7854-7859.

RINCON, J., CANIZARES, P. & GARCıA, M. 2007. Improvement of the Waste-Oil Vacuum-Distillation Recycling by Continuous Extraction with Dense Propane. *Ind. Eng. Chem. Res,* 46**,** 266-272.

RINGLE, E. C. 1974. *Measuring electric field distribution in a microwave oven*, University of Wisconsin--Madison.

ROHMAN, A. & MAN, Y. B. C. 2010. Fourier transform infrared (FTIR) spectroscopy for analysis of extra virgin olive oil adulterated with palm oil. *Food Research International,* 43**,** 886-892.

ROMANO, S. D. & SORICHETTI, P. A. 2010. Introduction to Biodiesel Production. 7-27.

SARIN, A. 2012. *Biodiesel: Production and Properties*, Royal Society of Chemistry.

SCRAGG, A. H. 2009. *Biofuels: Production, Application and Development*, CABI.

SHEEN, J. 2009. Measurements of microwave dielectric properties by an amended cavity perturbation technique. *Measurement,* 42**,** 57-61.

SHELDON, R. A. 2013. *Chemicals from Synthesis Gas: Catalytic Reactions of CO and*, Springer Netherlands.

SIESLER, H. W., OZAKI, Y., KAWATA, S. & HEISE, H. M. 2008. *Near-Infrared Spectroscopy: Principles, Instruments, Applications*, Wiley.

SINGH, G. 2010. *The Soybean: Botany, Production and Uses*, CABI.

SINGH, R. 2000. *Low and High Dielectric Constant Materials: Materials Science, Processing, and Reliability Issues : Proceedings of the Fourth International Symposium : And, Thin Film Materials for Advanced Packaging Technologies : Proceedings of the Second International Symposium*, Electrochemical Society.

SMITH, B. C. 2011. *Fundamentals of Fourier Transform Infrared Spectroscopy, Second Edition*, CRC Press.

SOBEY, E. 2010. *The Way Kitchens Work: The Science Behind the Microwave, Teflon Pan, Garbage Disposal, and More*, Chicago Review Press, Incorporated.

STERLING, C. H. 2004. *Encyclopedia of Radio 3-Volume Set*, Taylor & Francis.

STEWART, J. V. 2001. *Intermediate Electromagnetic Theory*, World Scientific.

STROBEL, O. 2016. *Optical and Microwave Technologies for Telecommunication Networks*, Wiley.

STUART, P. R. & EL-HALWAGI, M. M. 2012. *Integrated Biorefineries: Design, Analysis, and Optimization*, CRC Press.

TOMASEVIC, A. V. & SILER-MARINKOVIC, S. S. 2003. Methanolysis of used frying oil. *Fuel Processing Technology,* 81**,** 1-6.

REFERENCES

UMASHANKAR, K. 1989. *Introduction to Engineering Electromagnetic Fields*, World Scientific.

VAN BLADEL, J. G. 2007. *Electromagnetic Fields*, John Wiley & Sons.

VENKATESH M S, R. G. S. V. 2005. overview of dielectric materials measuring techniques. *Researchgate*, 7.15-7.30.

VIGLI, G., PHILIPPIDIS, A., SPYROS, A. & DAI, P. 2003. Classification of Edible Oils by Employing 31P and 1H NMR Spectroscopy in Combination with Multivariate Statistical Analysis. A Proposal for the Detection of Seed Oil Adulteration in Virgin Olive Oils. *Agricultural and food chemistry,* 51, 5715-5722.

VINZI, V. E., CHIN, W. W., HENSELER, J. & WANG, H. 2010. *Handbook of Partial Least Squares: Concepts, Methods and Applications*, Springer Berlin Heidelberg.

VOLDMAN, S. H. 2005. *ESD Physics and Devices*, Wiley.

WADELL, B. C. 1991. *Transmission Line Design Handbook*, Artech House.

WEBER, W. H. & MERLIN, R. 2000. *Raman Scattering in Materials Science*, Springer Berlin Heidelberg.

WELTON, D. M. 2011. *Transmission Lines: Theory, Types, and Applications*, Nova Science Publishers.

WHITE, J. F. 2016. *High Frequency Techniques: An Introduction to RF and Microwave Design and Computer Simulation*, Wiley.

WIESEL, W. E. & TECHNOLOGY, A. F. I. O. 2003. *Modern Astrodynamics*, Aphelion Press.

WILSON, K. & LEE, A. F. 2013. *Heterogeneous Catalysts for Clean Technology: Spectroscopy, Design, and Monitoring*, Wiley.

YEH, C. & SHIMABUKURO, F. 2008. *The Essence of Dielectric Waveguides*, Springer US.

YU, P. & CARDONA, M. 2005. *Fundamentals of Semiconductors: Physics and Materials Properties*, Springer Berlin Heidelberg.

ZHU, D., TUDOR, M. J. & BEEBY, S. P. 2010. Strategies for increasing the operating frequency range of vibration energy harvesters: a review. *Measurement Science and Technology,* 21**,** 022001.

PUBLICATIONS

1. Osman, S. B., Korostynka, O., Mason, A., Cullen, J. D. and Al-Shamma'a, A. I. (2014) **'Application of microwave spectroscopy analysis on determining quality of vegetable oil'**, in 2014 / 01 / 01 /, IEEE Computer Society, 556-559.

2. Osman, S. B., Korostynka, O., Mason, A., Cullen, J. D. and Al-Shamma'a, A. I. (2015) **'Development of a sensor system for vegetable oil authentication'**, in *Ninth International Conference on Sensing Technology*, Auckland, New Zealand, 24 March 2016, IEEE, 104-109.

3. Osman SB, Korostynska O, Mason A, Cullen JD, Al-Shamma'a AI. 2015. **Comparative Analysis of Microwave Spectroscopy and Spectrophotometry on Determining Olive Oil Authenticity** Faculty of Engineering and Technology Research Day